FIELD TRANSPORT OF *CRYPTOSPORIDIUM* SURROGATE IN A GRAZED CATCHMENT

Prepared by:

Appiah Amirtharajah, Michael H. Young, Kurt D. Pennell

School of Civil and Environmental Engineering

Georgia Institute of Technology

Atlanta, GA 30332-0512

and

Jean L. Steiner, Dwight S. Fisher, Dinku M. Endale

USDA, Agricultural Research Service

J. Phil Campbell, Sr., Natural Resource Conservation Center

Watkinsville, GA 30677-2373

Sponsored by:

Awwa Research Foundation

6666 West Quincy Avenue

Denver, CO 80235-3098

Published by the

Awwa Research Foundation

American Water Works Association

Page missing from thesis

DISCLAIMER

This study is funded by the Awwa Research Foundation (AwwaRF). AwwaRF assumes no responsibility for the content of the research study reported in this publication or for the opinions or statements of fact expressed in the report. The mention of trade names for commercial products does not represent or imply the approval or endorsement of AwwaRF. This report is presented solely for informational purposes.

ISBN 0-00000-000-0

CONTENTS

TABLES

FIGURES

FOREWORD

The Awwa Research Foundation is a nonprofit corporation that is dedicated to the implementation of a research effort to help utilities respond to regulatory requirements and traditional high-priority concerns of the industry. The research agenda is developed through a process of consultation with subscribers and drinking water professionals. Under the umbrella of a Strategic Research Plan, the Research Advisory Council prioritizes the suggested projects based upon current and future needs, applicability, and past work; the recommendations are forwarded to the Board of Trustees for final selection. The foundation also sponsors research projects through the unsolicited proposal process; the Collaborative Research, Research Applications, and Tailored Collaboration programs; and various joint research efforts with organizations such as the U.S. Environmental Protection Agency, the U.S. Bureau of Reclamation, and the Association of California Water Agencies.

This publication is a result of one of these sponsored studies, and it is hoped that its findings will be applied in communities throughout the world. The following report serves not only as a means of communicating the results of the water industry's centralized research program but also as a tool to enlist the further support of the nonmember utilities and individuals.

Projects are managed closely from their inception to the final report by the foundation's staff and large cadre of volunteers who willingly contribute their time and expertise. The foundation serves a planning and management function and awards contracts to other institutions such as water utilities, universities, and engineering firms. The funding for this research effort comes primarily from the subscription program, through which water utilities subscribe to the research program and make an annual payment proportionate to the volume of water they deliver and consultants and manufacturers subscribe based on their annual billings. The program offers a cost-effective and fair method for funding research in the public interest.

A broad spectrum of water supply issues is addressed by the foundation's research agenda: resources, treatment and operations, distribution and storage, water quality and analysis, toxicology, economics, and management. The ultimate purpose of the coordinated effort is to assist water suppliers to provide the highest possible quality of water economically and reliably.

The true benefits are realized when the results are implemented at the utility level. The foundation's trustees are pleased to offer this publication as a contribution toward that end.

Edmund G. Archuleta, P.E.
Chair, Board of Trustees
Awwa Research Foundation

James F. Manwaring, P.E.
Executive Director
Awwa Research Foundation

ACKNOWLEDGEMENTS

The authors acknowledge the advice and help of the Project Advisory Committee (PAC) including, Edward (Rob) Atwill, DVM, MPVM, Ph.D., University of California, Davis, Jon Standridge, Wisconsin State Lab of Hygiene and Wolfe Tone, formerly with New York State Department of Environmental Protection. The help of the AwwaRF project manager, Linda Reekie is appreciated.

The authors wish to acknowledge the assistance of Curt Boke and Stephen Norris, for collecting and preserving water and soil samples at the Field Site in Watkinsville, GA and Lingjun Kong for completion of the column studies at Georgia Tech.

The authors also acknowledge the assistance of A.J. Horowitz , Ph.D., of the U.S. Geological Survey in collecting colloids from large volumes of water using a flow-through centrifuge and Carolyn Ruppel, Ph.D., School of Earth and Atmospheric Sciences, Georgia Institute of Technology, for her contribution in the geophysical survey and analysis.

Andrea Bé, Administrative Coordinator for the Environmental Engineering Program, who provided assistance during the research program and in the production of the final report, is also acknowledged.

EXECUTIVE SUMMARY

SUMMARY

The project is the first study to investigate the transport of a *Cryptosporidium* surrogate under field conditions. Polystyrene microspheres of similar size (4-6 μm) as *Cryptosporidium* oocysts were used to spike a defined area in a cattle grazing field site with borehole wells instrumented with zero-tension lysimeters and pressure transducers. The polystyrene microspheres were detected and counted using epiflorescence microscopy. The groundwater flow at the field site was characterized using state of the art geophysical surveys and the hydrology (rainfall, soil water, groundwater flow and evapo-transpiration) was followed for a period of approximately one year. The transport of the surrogate microspheres was followed by periodic sampling at the zero-tension lysimeters, monitoring wells and a perennial spring.

The field study was complemented by column studies in the laboratory under controlled conditions. The column studies focused on transport of surrogate microspheres through well characterized sand media and soil media from the field site. The column studies produced numerical values for parameters used for a one-dimensional transport model. The model was tested for the column configuration and the field site.

RESEARCH OBJECTIVES

This project focuses on field studies of colloidal-sized particle transport (similar to *C. parvum*) through unsaturated soils at a small catchment used for cattle production. Known quantities of polystyrene microspheres, manufactured with properties similar to *C. parvum*, and a bromide tracer were applied in specific areas of a small catchment and monitored for breakthrough at an on-site perennial spring. Microspheres were used as surrogates of microorganisms in this field study. The focus on cattle grazing areas stems from the findings that many large-scale outbreaks of *Cryptosporidiosis* have been attributed, at least in part, to contamination of surface waters by cattle excreta. Though previous work has been done to characterize the surface water pathway, the intent of this study is to focus on subsurface transport of oocysts at the field scale. This is a topic which is not well researched or understood.

The overall goal of the proposed research is to investigate the near-surface transport of *C. parvum* surrogates in the vadose zone of cattle production systems. This project is designed to improve our knowledge of the mechanisms and processes that contribute to contamination of small streams and shallow groundwater from these microorganisms using surrogate particles. The following specific objectives are designed to couple field-scale studies, with mathematical modeling.

Field Characterization Studies

1. Instrument specific areas of a small catchment used for cattle grazing and quantify shallow subsurface flow.
2. Conduct tracer experiments at the catchment using microspheres, and a second non-reactive tracer, placed beneath the soil surface to promote interflow transport.
3. Conduct post-tracer sampling of soil at the field site for mass balance estimates.

Modeling Studies

1. Improve approaches to modeling the transport of oocysts in unsaturated soils using existing water flow and transport models, and incorporating concepts of trajectory theory. Results of the modeling studies can be used to simulate microsphere transport at the field site.

The study is a first step in assessing the transport of *Cryptosporidium* oocysts in watersheds under field conditions.

APPROACH

The project included a literature review and gathering of background information of the field site and a preliminary geophysical survey conducted at the base of the catchment area used as the field site. The project was divided into four tasks: site characterization, field tracer studies, laboratory column studies, and numerical simulation of microsphere transport. The site characterization task required the installation of monitoring devices, so that components of the hydrologic water budget (e.g., soil water storage, ground water flow, etc.) were quantified. The field

tracer studies involved the use of a non-invasive, bromide tracer to better understand dispersion and pore water velocity at the site, and the use of latex polystyrene microspheres as a surrogate to *Cryptosporidium* oocysts. A sequential water sampler was installed at the mouth of a perennial spring and a flow-through centrifuge was used to collect the colloids including the microspheres from large volumes of water. Column studies were used to develop numerical values for parameters used in the simulation models for microsphere transport. The numerical simulation task included incorporation of concepts of trajectory theory into an existing, variably saturated flow model. Results of the field tests were used as input to the one-dimensional simulation model.

RESULTS AND CONCLUSIONS

The major contribution and conclusions of the project are:

1. Improvements in field sampling and measurements for a surrogate used for *Cryptosporidium parvum* have been developed for field transport studies and laboratory column studies.
2. The vertical migration of polystyrene microspheres in the column studies was minimal. This suggests that migration of *Cryptosporidium parvum* oocysts through fine-textured soils is likely to be minimal.
3. Since a few microspheres were detected on a few occasions at sampling sites of the field, especially after rainfall events, the data suggests that a very small number of these surrogate particles travel through preferential flow paths at field sites.
4. The parameters measured from column studies were used as input variables in a 1-D hydrological (HYDRUS-ID) transport model, and indicated that reasonable predictions could be made on soil water content and the limited movement and depth penetration of solutes (surrogate particles) would occur based on antecedent water storage and precipitation.

CHAPTER 1
INTRODUCTION AND BACKGROUND

INTRODUCTION

The focus of the new drinking water regulations in the U.S.A over the last decade of the last millennium has been to minimize and balance the health risks associated with the microbial pathogen, *Cryptosporidium*, and the cancer causing risks of disinfectants and disinfection-by products, such as the trihalomethanes and haloacetic acids. One of the significant regulations derived from the 1996 Amendments of the Safe Drinking Water Act was the Enhanced Surface Water Treatment Rule (ESWTR), which seeks to provide protection against *Cryptosporidium*. The rule has progressed through three stages, interim, long-term 1 and long-term 2 (LT2 ESWTR) and the final LT2 ESWTR is expected to be promulgated in 2002. The requirements of the LT2 ESWTR will apply to all public water systems that use surface water or groundwater under the direct influence of surface water. The Federal Advisory Committee that negotiated the proposed regulation, recognized the importance of providing additional protection against *Cryptosporidium,* based on the results of a monitoring program to determine the concentration of this organism in source waters (Pontius, 2001).

One of the viable options of meeting the provisions of the LT2 ESWTR and minimizing the risk associated with *Cryptosporidium* in drinking water is to use a multiple barrier approach in water treatment process trains including watershed protection and filtration. There has been little or no published literature on a quantitative approach to assess the transport of this organism through soil under real world field conditions. Transport can occur in surface runoff, via the vadose zone in unsaturated flow and in groundwater. It is also important to determine the extent of transmission of this organism in a variety of geological formations such as sand, fine-grained soils and formations having preferential flow paths. Thus, the research has to integrate knowledge from hydrology, soil science and mathematical transport analysis. The overall goal of this project is to initiate this fundamental understanding of the process that leads to transport of this organism through surface and groundwater under field conditions, so that a significant impact can be made in protecting the public health of communities.

SIGNIFICANCE OF *CRYPTOSPORIDIUM*

The presence of microbial pathogens, specifically *Cryptosporidium parvum (C. parvum),* has been recognized as a significant health hazard when found in drinking water supplies. In the last two decades, several cases of waterborne gastroenteritis have been attributed to *C. parvum*. Toward the late 1980's, the occurrence and size of outbreaks attributed to *C. parvum* began to increase. In 1987, an estimated 13,000 people in western Georgia were afflicted with gastroenteritis caused by *C. parvum* (Hayes, et al., 1989b). In April, 1993, the largest reported *C. parvum* outbreak occurred in Milwaukee, Wisconsin, where 400,000 people were sickened, and over 100 persons died as a result of contamination of the public drinking water supply (MacKenzie et al., 1994). Other, smaller outbreaks have been attributed to insufficient treatment of contaminated surface water and the contamination of groundwater wells by sewage effluent.

These pathogens are a major concern of water treatment because they are considered ubiquitous in surface waters in the U.S. (LeChevallier et al., 1991). In one survey of water in the Western U.S., Rose (1988) found *C. parvum* oocysts in more than 75% of lakes and rivers. Another study by Hancock et al. (1997) used samples collected from a variety of subsurface environments to show that *C. parvum* and *Giardia lamblia* were present in 20% and 14% of springs, respectively. Higher percentages were recorded in horizontal wells and infiltration galleries. The surface properties of the oocysts, such as zeta potential and hydrophobicity affect their adhesion on filter media and soil particles in subsurface flow (Drozd and Schwartzbrod 1996). However, these pathogens are extremely difficult to inactivate by disinfection with chlorination. Conventional water treatment technologies which rely on coagulation, sedimentation, and filtration followed by disinfection, provide several barriers to transmission of oocysts.

In rural areas where sophisticated treatment technologies are not always used to treat drinking water, humans can more frequently be exposed to these organisms leading to gastroenteritis. This may be especially true if cattle grazing is practiced in these rural areas, given that high density agricultural areas with cattle pastures have been shown to contain high levels of *C. parvum* oocysts (Madore et al., 1987). In several cases, direct causal links were made between the presence of cattle and illness in humans (Miron et al., 1991; Lengerich, et al.,

areas, where cattle paddocks and winter calving areas are penned at high stocking rates, often exceeding the ability of the pasture to provide forage. These heavy use areas represent a possible source of stream contamination, and possibly a pathway for human contact. These cases indicate that ingestion by humans of inadequately treated water, contaminated by run-off from cattle manure, can increase the risk of these waterborne diseases.

It is commonly understood that leaching by water is the primary mechanism of material translocation through the soil profile. Dissolved constituents, colloidal particles in suspension and larger particles not in suspension are carried downward through the soil fabric following precipitation events. The rate of translocation depends on a number of factors, including precipitation and infiltration rates, topography, presence of root holes or other preferential flow paths, and the characteristics of the migrating constituents, to name a few (Powelson and Gerba 1995). Under higher flux conditions, such as those that occur during precipitation events, flood irrigation of agricultural fields or periodic disposal of waste water in an evaporation basin, a larger portion of water will travel through larger pores, where a significantly higher number of microorganisms will also travel through the soil profile (Jury, Gardener and Gardener 1991). As the flux rate decreases, larger pores cease transmitting water first, and straining leads to decreased transport rates (Jacobsen et al. 1997). This transient phenomenon could be responsible for deeper penetration of microorganisms into the soil profile, especially, if flooding occurs or if preferential flow pathways exist in the profile.

PROJECT RATIONALE

Studies have identified the presence of *C. parvum* in ground water environments (wells, springs, seeps, etc). It is generally assumed that shallow saturated water environments are greatly influenced by the hydrologic processes in the vadose zone. Moreover, the diversity of environments where *C. parvum* was shown to be present raises the question of whether and under what conditions these parasites can travel through soil material, and toward the water table or directly into discharge points. Conducting a field experiment at a site with a dynamic subsurface flow system could provide information on conditions that would promote, discourage or prevent the deep penetration of *C. parvum* into ground water environments.

The overall rationale of this research was to study the movement of *C. parvum* surrogates (e.g., latex polystyrene microspheres) through undisturbed soil material in the vadose zone of a small catchment. The catchment was characterized using a variety of techniques that included high intensity data collection of water fluxes into and out of well defined catchment boundaries. Using these techniques and the data collected, a full water balance was developed, so that the significance of soil water flow and transport on ground water discharge could be ascertained. Samples collected from the field were also used in column studies under more controlled conditions to characterize the filtration and detachment properties of the flow system, allowing these parameters to be used in 1-D and 2-D numerical models of water flow and particle transport. Both the site-specific data collection and transport experiments, coupled with the more general laboratory experiments, provide a data set under which the transport phenomena of *Cryptosporidium* surrogates can be studied.

RESEARCH OBJECTIVES

This project focuses on field studies of colloidal-sized particle transport (similar to *C. parvum*) through unsaturated soils at a small catchment used for cattle production. Known quantities of polystyrene microspheres, manufactured with properties similar to *C. parvum*, and a bromide tracer were applied in specific areas of a small catchment and monitored for breakthrough at an on-site perennial spring. Microspheres were used as surrogates of microorganisms in this field study. The focus on cattle grazing areas stems from the findings that many large-scale outbreaks of *Cryptosporidiosis* have been attributed, at least in part, to contamination of surface waters by cattle effluent. Though previous work has been done to characterize the surface water pathway, the intent of this study is to focus on subsurface transport of oocysts at the field scale. This is a topic which is not well researched or understood.

The overall goal of the proposed research is to investigate the near-surface transport of *C. parvum* in the vadose zone of cattle production systems. This project is designed to improve our knowledge of the mechanisms and processes that contribute to contamination of small streams and shallow groundwater from these microorganisms. The following specific objectives are designed to couple field-scale studies, with mathematical modeling.

Field Characterization Studies

1. Instrument specific areas of a small catchment used for cattle grazing and quantify shallow subsurface flow.
2. Conduct tracer experiments at the catchment using microspheres, and a second non-reactive tracer, placed beneath the soil surface to promote interflow transport.
3. Conduct post-tracer sampling of soil at the field site for mass balance estimates.

Modeling Studies

1. Improve approaches to modeling the transport of oocysts in unsaturated soils using existing water flow and transport models, and incorporating concepts of trajectory theory. Results of the modeling studies can be used to simulate microsphere transport at the field site.

The study is a first step in assessing the transport of *Cryptosporidium* oocysts in watersheds under field conditions.

Page intentionally left blank

CHAPTER 2
MATERIALS AND METHODS

FIELD SITE DESCRIPTION

Location and Land Use

Field research was performed at the J. Phil Campbell, Sr., Natural Resource Conservation Center, in Watkinsville, Georgia. The laboratory and center are operated by the Agricultural Research Service (ARS) of the U.S. Dept. of Agriculture. The site is located within the Upper Oconee River Basin, in the Southern Piedmont region, which has been identified through the Unified Watershed Assessment process as being a high priority watershed in the state of Georgia, based primarily on high fecal coliform counts. The Southern Piedmont region is characterized by rolling topography with abundant precipitation and surface water resources, and a landscape of forest, woods, pasture, cropland, creeks, streams and urban sprawl.

The research location consists of a 10-hectare (ha) catchment designated as W2, within the North Unit Watershed of the ARS facility (Figure 2.1). The catchment is used for rotational grazing of a pure-bred Angus herd to maintain the soils and hydrology in a state representative of Southern Piedmont grazing lands. The Conservation Center has maintained a research cattle herd for over 25 years. The current herd consists of 250 breeding cows and a total of 500-700 cattle at any given time. The calving season is in late winter (February-March). Calves are weaned in the fall and most of the heifer calves are sold. The steer calves are retained for experiments during the subsequent year and are sold at about 20 months of age. The retained heifers are developed as replacement heifers for culled cows. The Conservation Center uses its own bulls for breeding. No more than 200 head of cattle (cows + calves) are expected to graze in the W2 catchment at one time. Scheduling allows the cattle to be moved to the W2 catchment approximately every six weeks, where they graze for approximately one week before moving to other pastures. The grazing interval and duration depends on the forage growth. The catchment is not used for calving or weaning.

Physiography, Soils and Geology

Topographic slopes at W2 generally range from 2-10%. Soils are predominately Cecil and Pacolet sandy loam and sandy clay loam, derived from underlying and weathered schist, gneiss and granite. Bedrock depth varies from approximately 3 to 30 meters below ground surface; however, some outcroppings of saprolite (weathered crystalline rock) are visible in the area. Bruce et al. (1983) characterized the hydraulic properties of the soil in the West Unit, which includes the W2 catchment. Their characterization included the determination of soil water retention curves and saturated hydraulic conductivity.

Hydrology

The average annual precipitation is 125 centimeters (cm) (49.2 inches), and mean annual temperature is 16.5°C. The rainfall is distributed throughout the year, but greatly exceeds evaporation in the winter months, leading to saturated soils with a high probability of runoff/or drainage through the profile. The summer time precipitation is characterized by higher intensity, convective thunderstorms. Variable dry periods occur in most summers, where soils are depleted of stored water. Recharge occurs rapidly to depths exceeding one meter (m). Ground water level in calendar year 2000 varied from about seven meters below ground surface at the higher elevation of W2, to within one meter below ground surface near the spring.

The North Unit Watershed includes headwaters of a first-order stream that originates on the property, with water coming from different ecosystems including pastures, crop land, farm roads, and woods. The stream flows into and out of a pond, near the outlet of the property, then into a residential area less than 1 kilometer (km) away increasing in order as other streams join from the surrounding areas. It eventually enters into Lake Oconee, a large hydroelectric and recreational reservoir. A unique characteristic of the W2 catchment is the presence of numerous seeps. Three of these seeps are large enough to form measurable and largely perennial spring flow. The strongest of these springs has been monitored by ARS for *E. coli* and was selected for continuous monitoring in this project. An approximately 40- by 30-m site just above this spring was intensely instrumented to quantify the hydrologic balance, and was used for the nonreactive tracer and microsphere bead field transport studies.

FIELD CHARACTERIZATION STUDIES

Geophysical Surveys

Background and Methods

On November 29, 1998, a surface geophysical survey was conducted to obtain preliminary estimates of depths to the water table and underlying bedrock. The survey was conducted under the direction of Dr. Carolyn Ruppel (School of Earth and Atmospheric Sciences, Georgia Tech). Drs. Young and Endale, along with two graduate students from Georgia Tech, and other technical personnel from USDA-ARS, participated in the survey. Three geophysical methods were chosen: Terrain conductivity measurements with instrument no. EM-31, ground-penetrating radar (GPR), and DC resistivity. The EM-31 (Geonics Ltd., Mississauga, Ontario, Canada) method is a non-invasive, surface geophysical technique, which uses electromagnetic energy to measure the apparent electrical conductivity (ECa) of earthen materials. It can be used to infer changes in soil water content (Sheets and Hendrickx 1995) under specific field conditions (e.g., uniformity in clay content and salinity). The effective depth of penetration is approximately 3.0- and 6.0-m for horizontal and vertical orientations (McNeill 1992), depending mostly on the height of the unit above the soil surface. Conductivity data were collected in both vertical and horizontal dipole modes on two grids with 5-m spacing between nodes. The data were inverted to obtain the depth to the critically saturated layer using the exact inversion technique of McNeill (1980):

$$z_v = \frac{s}{2}\left[\left(\frac{\sigma_2 - \sigma_1}{\sigma_a - \sigma_1}\right)^2 - 1\right]^{1/2} \tag{2.1}$$

$$z_h = \frac{s}{4}\left[\left(\frac{\sigma_2 - \sigma_1}{\sigma_a - \sigma_1}\right) - \left(\frac{\sigma_a - \sigma_1}{\sigma_2 - \sigma_1}\right)\right] \tag{2.2}$$

where z = depth to a subsurface interface between unsaturated and saturated material;

v = vertical dipole modes h = horizontal dipole mode

σ = apparent electrical conductivity (ECa)

sub-scripts a, 1, and 2 = ECa values measured with the EM-31 and assumed for layers 1 and 2, respectively

s = distance between source and detector (3.7m for EM-31)

The parameters assumed were two-layer model and σ_1 = 1 mS/m (obtained using the GPR). The ECa value for the lower layer (σ_2) was changed until the root mean square error (RMSE) of the difference between Z_v and Z_h was minimized, at which point both horizontal and vertical modes were assumed to converge to the same value of interface depth:

$$RMSE = \left(\sum_{i=1}^{n} \frac{(z_v - z_h)^2}{n-1} \right)^{1/2} \tag{2.3}$$

Ground-penetrating radar involves the introduction of radar waves directly into the ground through a transmitting antenna and reception of the returned signal through a receiving antenna. GPR has proven to be a powerful tool for defining soil stratigraphy, locating the water table, and constraining shallow drainage features. For this work, 50 MHz and 100 MHz antenna configurations were the most useful and will nominally yield 8 to10-m and 5-m penetration, respectively. GPR data are collected in bistatic mode, which produces an image of the subsurface similar to that generated by reflection seismic methods. GPR data collection is fast and completely nondestructive, requiring only that the antenna be moved by the operator over relatively cleared areas at even increments.

The DC resistivity survey was implemented as a Schlumberger vertical electrical sounding (VES). The VES method provides constraints on simplified layered structure to depths of tens of meters (e.g., possibly up to 30-m based on preliminary surveys at some Piedmont sites). The method uses four electrodes (1.25-cm diameter) driven 15- to 20-cm into the ground. Small currents are introduced and the resulting potential differences between the electrodes are measured digitally. The electrode configuration is then shifted and the test is rerun. Inversion of

Schlumberger data yields information about depth to bedrock (overburden thickness), soil stratigraphy, and water table depth. The Schlumberger survey was conducted along a ~175-m N-S line at the east side of the study area.

Instrumentation

Figure 2.2 shows an idealized, 2-dimensional cross-section of the area in the immediate vicinity of the spring with instrumentation. The figure shows three instrumentation clusters, each with monitoring wells, TDR probes and tensiometers. Zero tension lysimeters were located beneath the injection ring for sampling both bromide and microspheres. The suite of instruments allowed for monitoring of soil water flow direction, soil water storage and the presence of tracers during those experiments.

Earthworks

Early in the location's history, ARS had developed a pond immediately downstream of the springs and seeps by excavating an area of approximately 0.5-ha and using it as a water source for cattle and perhaps irrigation. In time, the pond filled in, and now acts as a wetland. The discharge point is a culvert under the access road immediately west of this pond. It was first necessary, therefore, to excavate a channel through the wetland to allow free flow at and from the main spring and install a flume that would not become submerged, and hence bias spring flow measurement.

Runoff from W2 flowed over the springs into the wetland and subsequently through the culvert. It was necessary to remove the influence of runoff on spring flow and potential surface transfer mechanism from the selected small research plot. A berm was, therefore, constructed using material from the channel excavation to allow runoff from about 90% of W2 to bypass the springs and wet land, and discharge just upstream of the culvert. This would permit measurement and better characterization of runoff from 90% of W2 as it enters the culvert. Runoff from about 10% of W2 still entered the wetland but did not affect flow measurement at the main spring nor overland flow patterns at the selected 40- by 30-m research plot. The berm, springs and wetland area were then fenced off from cattle.

Flume, Logging and Sampling Equipment

The next phase of the site work consisted of installation of a measuring flume, data logging equipment and a water sampler. Figure 2.3 shows a front view of this apparatus. The data logger (model CR-10X, Campbell Scientific, Inc., Logan, UT), mounted on a pole and secured using a padlock, was used for storing discharge measurements, and for controlling the water sampler. A battery and solar charging system (model SM10, Atlantic Solar Products, Baltimore, MD), was used to power the data logger. Just below the pole, a concrete pad was constructed as base for a wooden shelter built to house the water sampler (model 900 MAX, American Sigma, Medina, NY). The shelter was bolted to the concrete pad, providing a level and secure location for the water sampler. The sampler was completely automated and could be programmed to collect water samples at any time interval desired, initiated by rainfall, flow exceeding a preset rate, or dates. Water volume collection ranges from one composite sample of up to 10 liters, to 24 separate composite samples from 300 ml to one liter, for each event. Samples were collected through a 0.95-cm (3/8 inch) diameter 9.15-m (30 foot) teflon tubing, at the outlet of the flume and stored in 300 ml bottles. The water sampler accounts for "dead volume" in the tubing by purging the line before and after collection of the actual sample.

A 0.33-m (1-ft) H flume was then installed to monitor spring flow. The supporting structure was built from a series of aluminum I-beams, pressure treated lumber, sheet metal and concrete blocks. A retaining wall constructed of treated timber protected the flume and sampler from soil slumps immediately upstream. A cover, consisting of wood and screen material, was added to prevent intrusion of animals into the flume. A pressure transducer (model PDCR-1830-8388, Druck, Inc. New Fairfield, CT) inserted in the flume stilling well and wired to the data logger was used to measure the spring flow depth above the flume base. Calibration procedures (head versus flow) for the flume were developed according to the Field Manual for Research in Agricultural Hydrology (U.S. Department of Agriculture, 1979) for higher flows. Calibration of low flows was refined with independent flow measurements using 10-liter buckets and a timer. The data logger was programmed to execute every 10 seconds and record the average flow depth and flow rate every 5 minutes. These data were then used to develop the spring hydrograph. All of the wiring for the data logger, pressure transducer, solar panel, and water sampler was placed in conduit to prevent damage from animals.

Instrumentation for Measuring Components of the Water Budget

The instruments used to measure components of the water budget are listed in Table 2.1. These measurements included precipitation, evapotranspiration, soil water and potential, and ground water table, and are described below.

Table 2.1

Breakdown of instruments for measuring components of the water budget

Component	Device	Vendor	Number and Location
Rainfall	Rain gauges	CSI, Logan, UT	3;< 400m
Evapotranspiration	Weather station	CSI, Logan, UT	1;< 2km
Spring flow	0.3-m H flume	Leather Inc, Athens, GA	1, base of watershed
Interflow	0.3-m H flume	Leather Inc, Athens, GA	1, base of watershed
Groundwater level	Wells	Tweedell and Van Buren, Inc., Athens, GA	16; upgradient of spring
Soil water content	MoisturePoint	Environ. Sensor, Inc., Victoria, BC, Canada	5; onsite in vicinity of subplot
Soil water tension	Tensiometers	Soil Measure. Systems, Tucson, AZ	13; onsite in vicinity of subplot

Precipitation and evapotranspiration

Precipitation was initially measured at two nearby locations using rain gauges (model TR525M, Texas Electronic, Inc.). One measurement site was approximately 160-m SE of the spring, and the second site was approximately 800-m west of the spring. The rain gauges were used for an unrelated study, but the precipitation rates were transferable to W2 with little error. For more accurate water budgeting of the research subplot, however, a similar gauge was added closer to the site, so that data could be collected directly by the data logger. The data logger program was modified to include total precipitation, collected at 5-minute intervals. Daily potential evapotranspiration was calculated by the Penman-Monteith method using the Reference

Evaporation Calculator (Allen, 1994). Evapotranspiration data were obtained from a standard weather station operated by the University of Georgia, approximately 2 km west of the site.

Soil water content

Soil water content was measured at 5 locations using the MoisturePoint system (model MP-917, ESI, Victoria, British Columbia, Canada). Each probe is 1.2-m long and measures soil water content in 5 segments: 0-15, 15-30, 30-60, 60-90, 90-120 cm. The system measures the soil capacitance, which is calibrated for soil water content. Measurements are made through a portable interface and then downloaded to a computer. These sensors were used to estimate soil water storage, possibly indicating when saturated conditions occurred in the shallow soil. Probes are installed by advancing a solid steel rod template (1-cm diameter) to the target depth using a tractor mounted hydraulic soil sampling, coring and drilling machine (model GSR-T-S, Giddings Machine Company, Ft. Collins, CO). The machine is powered by tractor PTO through a pump and drive assembly. The rod is removed and the probe is pushed into place, ensuring that air gaps around the probe are minimized.

Soil water potential

Soil water potential was measured using tensiometers (models SW-031 through SW-036, Soil Measurement Systems, Tucson, AZ). Tensiometers varied in length between 23, 46 and 107 cm (0.75, 1.5, 3.5 ft). One cluster of up to three tensiometers (13 total) was installed close to each ESI probe so that simultaneous measurements of soil water content and soil water potential could be obtained. The 23-cm-long tensiometers were installed at only three locations. The tensiometers were installed approximately 10-cm apart from one another in a triangular pattern to facilitate protection of the units with a cover. The triangular pattern also allows the tensiometers to be equidistant apart, improving the determination of hydraulic gradient. Tensiometer tops were positioned about 3 cm above ground surface and covered with 15-cm PVC cap.

Tensiometers were installed by first augering (1.25-cm diameter) a borehole to the completion depth. Second, a heavy slurry composed of sieved native material was placed at the

bottom of the borehole. Third, tensiometers were lowered into the borehole and backfilled with cuttings to reduce the potential for preferential flow along the tensiometer body. A portable pressure transducer connected to a digital readout screen (tensimeter, Soil Measurement Systems, Tucson, AZ) was used to measure soil water tension at each tensiometer. When the transducer probe is placed over a tensiometer, a needle penetrates a stopper at the tensiometer and the vacuum inside the tensiometer is measured and digitally displayed in millibars (1 millibar $\approx$1 cm).

Ground water level

A total of sixteen wells were installed during two field campaigns to obtain ground water level and hydraulic gradient information in the vicinity of the spring. Eleven wells were installed during the first campaign and five during the second. Table 2.2 provides well construction details, and Figure 2.4 shows the well locations.

Table 2.2

Details for the sixteen 1-inch and two 2-inch wells installed at the monitoring site.

Well #†	Length of Screen (cm)	Length of Solid (cm)	Total Length (cm)	Length Cut off † (cm)	Total Well Depth (cm)	Total Well Depth (ft)
1	457.2	0	457.2	9.7	447.5	14.68
2	304.8	152.4	457.2	134.5	322.7	10.59
3	457.2	0	457.2	86.8	370.4	12.15
4	304.8	152.4	457.2	103.5	353.7	11.60
5	304.8	152.4	457.2	11.4	445.8	14.63
6	304.8	304.8	609.6	12.5	597.1	19.59
7	304.8	304.8	609.6	23.2	586.4	19.24
8	304.8	304.8	609.6	64.8	544.8	17.87
9	304.8	304.8	609.6	31.5	578.1	18.97
10	304.8	152.4	457.2	48.0	409.2	13.43
11	304.8	304.8	609.6	33.7	575.9	18.89
12	457.2	0	457.2	2.0	455.2	14.9
13	457.2	0	457.2	2.0	455.2	14.9
14	457.2	0	457.2	2.0	455.2	14.9
15	457.2	0	457.2	2.0	455.2	14.9
16	609.6	0	609.6	91.0	518.6	17.0
MW1††	131.1	63.5	194.6	0	274.5	9.0
MW2††	131.1	116.9	248.0	248.0	254.2	8.3

† PVC screens and solids came in standard length of 5 or 10 ft. This is what was sticking above ground after initial installation, which was then cut off to keep the well tops at ground level.

†† These monitoring wells had 2-inch solid, screened and solid PVC sections. Length of solids refers to that above screen.

The wells were installed at a spacing of approximately 9 m, covering a total area of about 31 m (west to east) by 38 m (north to south). All wells were installed by Tweedell and Van Buren, Inc. (Athens, GA) using a direct-push drilling rig. Borehole diameter was 3.81 cm (1.5 inches), into which were placed 2.54-cm (1-inch) diameter, schedule 40 PVC well pipes consisting of a machine drilled screen (#0.001) 305- to 610-cm (10 to 20 ft) length at the bottom attached to solid riser pipe that reached the surface. Given the very small annular space between the outside of the well pipe and the inside wall of the borehole, only a small amount of graded sand was used for backfill. The solid pipe extending above ground was then cutoff and the well-head was secured with concrete and a 15-cm PVC well cover. The wells were not developed because they were used only to monitor water level and not the concentration of either bromide or microspheres. Water level measurements were obtained using an electronic indicator (model WLT, Ben Meadows, Atlanta, GA). All wells were GPS surveyed and referenced to the state-wide coordinate system. Depth to the water table was taken from and referenced to the well tops.

After monitoring water levels in the first set of 11 wells located on the north side for several months, is was determined that the source of the spring water was predominantly from the southern portion of this subplot. Consequently, five additional wells (2.54-cm (1-inch) diameter) were installed along the southern edge of the plot boundary. After studying the direction and magnitude of the gradient using data from all 16 wells, it appeared that ground water flowing beneath the original southern boundary of the monitored plot was most likely the source of the main spring.

Instrumentation for Tracer Studies

Several instruments were installed in the field to directly support the conservative tracer (bromide) and microspheres transport experiments. These devices included two monitoring wells, six zero-tension lysimeters, a bromide specific ion electrode, and a flow-through centrifuge.

Monitoring wells

Based on the measurements of ground water level obtained from the 16 wells, the injection area for the study was chosen approximately 10-m upgradient of the spring. Two conventional 5.08-cm ID (2-inch) monitoring wells were then constructed along the southern boundary of the subplot, for subsequent water sampling and analysis during the tracer study (see bottom, Table 2.2). These wells were constructed according to EPA procedures for water sampling wells (U.S. EPA 1986). Installation consisted of drilling a 15-cm diameter borehole using a solid-stem auger to the desired depth. PVC well pipe (5-cm diameter) with slotted screens was then lowered into the hole. The hole was back filled with fine sand to approximately 60 cm above the screen, and then sealed to the ground surface with bentonite and concrete. A circular concrete pad was constructed around the well-head to prevent potential contamination by surface water. The PVC pipe was also capped to protect of the well. Both monitoring wells were developed using a mechanical surging technique described by Driscoll (1986) to reduce turbidity levels in the well water. The 5.08-cm monitoring wells are shallower with shorter screened intervals than the 2.54-cm wells. The intent of this design was to monitor ground water in the immediate vicinity of the water table, rather than focusing on deeper ground water. Microsphere beads and dissolved solutes that migrate through the soil profile at this site are likely to be transported near the water table, because a low-permeability layer approximately 1.3-m below the water table should prevent transport into deeper regions of the saturated zone.

Zero Tension Lysimeter

Thompson and Scharf (1994) described a zero-tension lysimeter (ZTL) that is inexpensive, easy to install and capable of sampling colloidal sized particles in soils. The research team decided to use these devices to collect microspheres directly under and adjacent to the injection area as they migrate through the soil profile. The basic design was modified, however, by sloping the floor of the lysimeter at an angle of 30° rather than close to 0° as in the original design, thereby ensuring that water collected by the sampler can be withdrawn. The 3-mm (1/8 inch) tubing that penetrates the outside of the sampler did not need to be sealed because the upper chamber was now completely isolated from the lower chamber. The design provided

additional security from shear of the sampling tubing during installation. The ZTLs incorporating the new design were assembled at a machine shop at the University of Georgia. Figure 2.5 shows detailed schematic diagram of the ZTLs and their field installation.

A total of six ZTLs were installed, three inside and three outside (down gradient) the microsphere injection area. Each cluster of three ZTLs was spaced laterally approximately 30 cm from one another. Within each area, a ZTL was installed at 30, 60, and 90 cm below ground surface. The units were installed by first removing an "undisturbed" soil core to the appropriate depth using the tractor mounted Giddings hydraulic soil sampling, coring and drilling machine. After the core was removed from the soil profile, the ZTL was carefully lowered to the base of the hole and centered. Fine-grained sand was poured into the top ring until the open space was completely filled with sand. The undisturbed soil core was then carefully lowered into the borehole, on top of the ZTL, making sure that the polystyrene pressure and return lines were taut. Soil material that extended above ground surface was removed. Finally sieved native soil material was packed into any air gaps between the soil core and the soil profile to minimize preferential flow around the ZTL. The soil surface was cleared of any debris, returning it to approximately original condition. The tips of the polystyrene tubes were then sealed.

Bromide Specific Ion Electrode

A bromide specific ion electrode (SIE, model M-12-BR-AMP-1Tz, Innovative Sensors, Inc., Anaheim, CA), which measures the difference in bromide ion concentration between a closed reference cell and the sensing tip, was installed at the site on December 11, 1999. The probe was installed so that spring water would be funneled through 2.54-cm (1in.) diameter PVC pipe, into which the sensing tip of the probe was inserted horizontally. The advantage of using the SIE was that the bromide readings could be used to remotely trigger the Sigma auto sampler, reducing personnel time and cost. All water entering the flume could then be subject to sampling. The data logger records the output in millivolts (mv). Elevated mv readings indicate low bromide concentration, and vice versa. The probe was factory calibrated, but became suspect after the first bromide tracer experiment when it became apparent that the measured mass recovery was almost two orders-of-magnitude greater than the amount of bromide applied. The formation of air bubbles around the probe tip was suspected of reducing voltage response,

which in turn would lead to elevated bromide concentration values. Reinstallation of the probe in a vertical orientation did not solve this problem. As a result, the SIE probe was of little value during the project, and was replaced by conventional ion chromatography analysis of collected water samples. Bromide analysis and results are further discussed in the *Bromide Transport Experiment* section of this chapter and in Chapter 3, respectively.

Flow-Through Centrifuge

The methodology used to collect microspheres from the spring water was of paramount importance to the research team. It was recognized that collecting relatively small volumes of spring water might, or might not, yield measurable quantities of particles, yet collection of large volumes of spring water would be logistically difficult due to site access and water storage requirements. To address these countervailing issues, a flow-through centrifuge (FTC), as described by Hayes et al. (1989a), was used to sample virtually all spring water without the consequent problems of water storage. Continuous flow-through centrifuges process all water samples placed in line, as opposed to the collection of subsamples. Power is transmitted to the centrifuge via a liquid coupling (clutch), and the bowl spins at about 10,000 rpm. Water samples continuously pumped into the device are centrifuged, so that system retains solids (material denser than water) while discharging the clarified effluent. Use of the FTC (Westfalia Separator, Inc., Northvale, NJ) was courtesy of the Dr. Art Horowitz of the U.S. Geological Survey, Atlanta, GA.

Water samples are pumped through the top of the bowl assembly and evenly distributed by the vane insert. The centrifugally separated solids accumulate in the various bowl chambers, the most dense or largest particles tend to collect in the inner bowls while the lighter or smaller particles tend to collect in the outer bowls. The clarified effluent is discharged via a centripetal pump, which is an integral part of the bowl assembly.

Prior to field implementation, the efficacy of the FTC to separate the microspheres from water was tested. Duplicate water samples containing three concentrations of the microspheres to be used in the experiment were prepared in 4 L glass containers and transported to the USGS. Samples were introduced into the centrifuge with a peristaltic pump at the rate of 2 L/minute. The clarified effluent was collected at the exit line of the centrifuge. When completed, the bowl

was removed and each chamber thoroughly rinsed with de-ionized water to remove collected particles. Filtration of both clarified and particle-laden water, and subsequent enumeration of microspheres using an epiflourescent microscope counting methods (described later) was then carried out at Georgia Tech. The results showed positive correlation between particle concentration and percent recovery. Microsphere bead recovery ranged between 79 and 99 percent.

Mr. Kent Elrick (USGS, Atlanta, GA) trained ARS and GT personnel in the field installation and use of the FTC. Soon thereafter, the FTC was transported to the ARS site and installed on a leveled area adjacent to the spring. A peristaltic pump was also installed adjacent to the FTC. The inlet tubing of the peristaltic pump was installed in the outlet side of the 2.54-cm diameter PVC pipe that housed the specific ion electrode. Several test runs of the peristaltic pump/FTC system were conducted to ensure that field personal understood the sampling instrumentation and methodology.

MONITORING DATA and ANALYSIS

Site conditions were monitored automatically and manually, primarily to establish the water budget at and around the spring. The data logger was programmed to automatically monitor rainfall and spring flow every 10 seconds and then process these data, storing average readings over 5 minutes. The equivalent average flow rate in liters per minute was obtained from flume head measurements. Automatic monitoring of rainfall at the spring began in early September 1999. Prior to that time, 5 similar rainfall gauges located from SE to N of the spring at distances varying from 200-m to 2-km were used to record rainfall. Monitoring of spring flow began on June 28, 1999.

Monitoring data were downloaded from the data logger approximately every two weeks into a storage module, transferred into a computer and then imported into Microsoft Excel. Graphs were prepared to show cumulative rainfall and corresponding spring response with time. The monthly total rainfall was compared to monthly long-term average values. The Excel data files were also exported to the project file transfer protocol (ftp) site at Georgia Tech, making them available to all research team members. To facilitate the management of the potentially large amount of records, the data were compiled into a database using Microsoft Access 97.

Spring flow data, for example, was collected at 288 records a day, which translated to 105,000 records per year.

Soil water, soil water potential and ground water levels were recorded manually two to three time a week and entered into an Excel spreadsheet. These time series data were also graphed. Contours of ground water elevations were prepared at 5-cm intervals using a Surfer32 (v6.01, Golden Software, Golden, CO) kriging technique to determine variations in flow direction with time and in response to wet and dry conditions.

TRANSPORT EXPERIMENTS

Bromide Transport Experiments

A preliminary bromide tracer study was conducted at the field site, prior to microsphere spiking, to provide data and information on subsurface flow paths and characteristics (e.g., dispersivity and tracer velocity). Bromide is a very common anionic tracer, which is known not to interact with solid material to any great extent, though minor reactions can occur. Sodium bromide (NaBr) was used as the bromide ion source, with calcium chloride ($CaCl_2$) added to maintain the same ratio of cations/anions as measured in the spring water. This ratio, known as the Sodium Adsorption Ratio (SAR) is an important parameter that governs potential swelling of clay constituents in the soil. Therefore, the tracer solution was prepared so that the SAR was identical to that of spring water. The tracer solution contained 6.4 grams NaBr and 18.4 grams $CaCl_2 \cdot 2H_2O$ in 1 L of de-ionized water, providing a concentration of 5.0 g/L bromide ion.

Field Methodology

The first conservative tracer experiment was initiated on December 11, 1999, at 14:15 hours, by pouring the bromide solution slowly into MW2, the 2-inch monitoring well furthest from the spring. To ensure that significant levels of bromide did not remain on the sides of the borehole, the inside of the borehole was rinsed with approximately two liters of spring water. The bromide solution and spring water were added slowly to the borehole, so that positive gradients would not be created inside the borehole and toward the aquifer unit, thereby ensuring

that bromide would migrate with bulk water under ambient gradient conditions. A second conservative tracer test was initiated on February 10, 2000 using the same concentration of bromide as the first test and the same spiking technique. The second tracer test was performed because the results of the first test were compromised by the failure of the SIE probe to accurately measure bromide concentrations in the spring water. A third and final tracer injection was carried out on February 28, 2000, at the same time as the microsphere spiking (see below). The intent of this tracer experiment was to characterize nonreactive solute transport and water flow relative to the microsphere beads.

Method of Detection

The specific ion electrode (SIE) was used to measure continuous bromide concentrations in spring water following the December 11, 1999 spiking of MW2 with bromide. The data logger program was modified to collect bromide concentration data at 10-sec intervals, averaged every five minutes, and if the bromide concentration exceeded 2.5 mg/L during any single sampling event, to trigger the Sigma 900 sampler every 120 minutes to sample 280 mL of fluid. The mass recovery of bromide, according to the SIE, after the first experiment, was found to be about 75 times more than what was added raising serious questions about the accuracy of the probe calibration. To confirm the high mass recovery, 14 water samples collected with the Sigma sampler were analyzed using the SIE and independently analyzed by ion chromatography at the University of Georgia. All samples yielded bromide below the detection limit by both analytical methods. After a series of checks and counter checks, including sending the probe back to the manufacturer for analysis of the problem, these discrepancies were thought to be a result of attachment of air bubbles to the probe due to its horizontal orientation, which would cause the voltage response to decrease and hence lead to elevated pseudo bromide concentrations. Prior to the second bromide tracer experiment, therefore, the SIE field setup was modified to orient the probe vertically and place it at the bottom of the conveyance pipe, reducing the chance of air bubble attachment. Bromide response in the spring water after the second spiking on February 10, 2000, was monitored from March 2 to March 10 and again from April 21 to May 1, representing early and late periods after spiking. In both periods diurnal periodicity was observed in the SIE bromide data, and the probe became unstable during the latter period. In

summary, the bromide concentration data obtained with the SIE were not suitable for quantitative use.

In subsequent field tests, discrete water samples were collected over time using the Sigma sampler, and were analyzed using ion chromatography (IC). The ion chromatograph (model DX-100, Dionex) was equipped with a separator column (Ion Pac AS4A, 4mm), a suppressor column (ASRS-ULTRA, 4mm) and a low volume, flow through, temperature compensated electrical conductivity detector. The eluent solution consisted of 1.8mM $NaCO_3$ and 1.7mM $NaHCO_3$, operated at a flow rate 1.5 mL/min. Under these conditions, the bromide detection limit was approximately 0.4 mg/L, with an overall retention time of approximately 3.0 minutes. Prior to injection, the water samples passed through 0.2 μm filters to remove particulates. Standard calibration curve were obtained for every batch of samples or whenever the eluent solution was replaced.

Microsphere Spiking Experiments

An important assumption inherent to this research is that the microsphere beads behave in a manner similar to *Cryptosporidium* oocysts. Based on the work of Li et al. (1997), Fluoresbrite YG carboxylated microspheres beads, 4.505 μm diameter, were purchased from Polysciences, Inc. (Warrington, PA). The zeta potential of the microsphere beads was selected to be similar to that of oocysts, as a function of solution pH and ionic strength. Typical zeta potentials of *Cryptosporidium* oocysts range from -30 to -40 mV at a pH = 7.0 (Ongerth and Pecoraro 1996). The spheres are prepared by attaching a pre-specified number of carboxyl groups onto the sphere to make them negatively charged. The suppliers indicated that very little to no pretreatment of the microspheres was needed prior to field spiking (Bangs Laboratories, Fishers, IN. The spheres are supplied in aqueous suspensions containing surfactant, and if desired, an antimicrobial agent. The suspensions were shipped in hydrophobic containers, and were stored in these containers until used for field spiking.

Field Methodology

A site 14-m ESE of the spring was chosen as the spiking location based on analysis of the groundwater movement as determined from the sixteen 2.54-cm well readings. The microsphere

bead field spiking experiment was initiated on February 28, 2000. A 152-cm by 76-cm (5-ft by 2.5-ft) rectangular section of aluminum mesh material with 5.04-cm (2-inch) squares was cut and placed and over the spiking area and secured to the ground using large nails. Based on the dimensions of the mesh section, 450 grid openings were available for microsphere injection. The same mesh had been used earlier at the same location to place three ZTLs directly below the spiking spot.

A stock solution of microsphere beads was prepared on February 27, 2000, by mixing nine vials of the microspheres in 1 L of de-ionized water that contained sodium bromide (NaBr) as a conservative tracer at a concentration of 5 g/L. Each vial nominally contained 5×10^8 microspheres, thus a total of 2.25×10^{10} microspheres were added to the stock solution. A stirring bar was kept in motion during the entire mixing process, including through the evening, to reduce settling of the microspheres. On the morning of February 28, the stock solution, stirring plate and an HPLC pump (model Dynamix SD-200, Varian, Inc., Palo Alto, CA) were transported to the field and setup adjacent to the spiking area (Figure 2.6). The HPLC pump was equipped with a pulse dampener to induce backpressure on the effluent line and to reduce pulsing. Teflon tubing was used throughout the pump setup. At the end of the effluent line, a 16-gauge surgical needle (10-cm length, blunt tip) was used to inject microspheres at a point ~5-cm below ground surface. Guide holes were first advanced using a long nail, and the needle opening was then placed at the bottom of the guide hole. The pump was calibrated in the field using a digital balance, so that approximately 2-mL of fluid was dispensed at each injection point (Figure 2.7). Based on the concentration of the stock solution, approximately 4.5×10^7 microspheres were introduced at each injection point. Microsphere spiking commenced at 1300 hours and was completed at approximately 1500 hours. A total of approximately 2.03×10^{10} microsphere beads (20 billion) were applied at the field site. A sprinkler system was set up the next day and about 1-cm of water was applied to the spiking area to initiate microsphere migration into the soil. This step was taken to reduce the potential for wind erosion of microsphere beads attached to surface soil particles.

Sampling methods

To monitor microsphere transport following the spiking event, periodic fluid samples were collected from four types of locations/samplers: zero-tension lysimeters, 5.08-cm diameter monitoring wells, and the spring (FTC and Sigma sampler). Sampling from the ZTLs was attempted only after rainfall events. Sampling from the ZTLs consisted of first placing the fluid return line into a sample bottle, and then pressurizing the airline using a suitable pump. As the air space inside the ZTL pressurized, fluid inside was pushed upward into the sample bottle. To insure that all microspheres were recovered and to minimize cross-contamination, de-ionized water was pumped into the ZTL through the fluid return line and then recovered in the sample bottle. Each of the six ZTLs was checked for fluid during each sampling event, although samples were not always recovered from all ZTLs. Lack of rainfall at the site reduced the potential number of samples from the ZTLs. Only four ZTL sampling dates produced sufficient fluid for microsphere enumeration: 03/06/2000, 03/21/2000, 11/21/2000, and 02/07/2001. A total of 32 ZTL samples were collected: 15 inside and 17 outside the spiking area; 10 each at 30 and 60-cm depth and 12 at 90-cm depth.

Water samples were also collected from the two monitoring wells using a bailer (2.54-cm OD) equipped with a ball stopper. The bailer was triple-rinsed with de-ionized water between boreholes to minimize cross-contamination. A total of 56 samples from MW1, nearest to the spring, and 46 samples from MW2 were collected from 03/01/2000 to 08/07/2000.

The flow-through centrifuge was operated a total of 35 times from 03/29/2000 to 08/01/2000 for a period of one hour each time. At the end of each sampling period, the centrifuge bowl was removed and transported to an ARS laboratory for processing. The bowl was thoroughly rinsed with de-ionized water, ensuring that any visible particles were removed. Rinsing procedures were deemed effective, since most rinsed samples only contained a few beads and it is unlikely that small numbers of beads in any control samples would have materially modified the findings. The rinsate was collected and stored in glass jars for processing and analysis of microspheres at Georgia Tech.

The Sigma sampler was used to collect discrete spring water samples over time. The sampler was run almost continuously from 3/20/00 to 11/13/00. A six week gap occurred in October and early November 2000 due to a malfunction of the sampler. Another sampling gap

occurred in mid July 2000, when the spring almost stopped flowing. Sampling frequency was usually every 30 minutes, when between 35 and 140-mL of spring water was pumped into each of the twenty-four 300-mL sample bottles. The number of samples per bottle varied from 2 to 8. The total time required to fill all 24 sample bottles ranged from 1 to 4 days. The latter rate was used after March 2000. A total of 999 samples, each just under 300-ml, were collected this manner.

All water samples were labeled and tracked using field sampling sheets and spreadsheets, so that results would not be lost or misidentified during the various processing tasks of fluid collection, fluid filtering, data entry, and transporting.

Destructive soil sampling

To evaluate the distribution of microspheres retained in the soil, destructive soil sampling was conducted on August 10, 2000. Four soil cores were collected inside the spiking area, and two additional cores were collected immediately down gradient (west) of the spiking area. The purpose of the lateral sampling was to evaluate microsphere transport, both vertically and laterally, within the soil profile. Soil samples were collected using a tractor mounted Giddings hydraulic soil sampling, coring and drilling machine, 2.54 cm (1 in.) diameter coring tubes, and butyrate plastic liners (2.2-cm i.d. X 122-cm length).

Due to the large number of microspheres that were originally applied to the site, special precautions were taken to minimize cross-contamination during soil core collection and preservation. Seven coring tubes and tips were first cleaned and wrapped in aluminum foil for transport to the site. Within the spiking area, different sampling tubes were used at each location. During practice drilling, conducted away from the site, only two cutting tips were found to work well with the butyrate plastic liner. Thus, the cutting tips were cleaned between collection of each soil core. The cleaning process included an acetone wash to dissolve residual microsphere beads followed by a water rinse.

The sampling procedure involved inserting the butyrate plastic liner and spacer into the clean (i.e., decontaminated) tube, and securing the cutting tip. The coring unit was then attached to the Giddings push-pull hydraulic mechanism. The sampling tool was advanced into the profile to a depth of approximately 120-cm (Figure 2.8). The sampling tool was then retracted

from the soil, disengaged from the Giddings rig, and laid flat on a sheet of aluminum. The cutting tip was then unscrewed from the core tube, and the liner pushed from the bottom with a push rod that was cleaned before each use (Figure 2.9). The liner containing the undisturbed soil core was then sealed with red (top end) and black (bottom end) caps. The liners were kept in a horizontal position at all times to avoid any redistribution of material between layers. The boreholes were then filled with bentonite to reduce potential preferential flow into the soil profile. The soil cores were initially stored in a walk-in cooler at ARS, and then transferred to Georgia Tech for separation and counting of microsphere beads.

The location of each bore hole was surveyed relative to the SE corner of the spiking area (i.e., benchmark of 0,0 (cm) on the X (N), Y(W) grid). The X, Y coordinates were (20, 18), (73, 47), (100, 19), (141, 30) inside and (52, 133), (92, 142) outside the spiking area (152-cm by 60-cm). Compaction occurred in some of the soil cores, reducing the actual length of the recovered core relative to the drilling depth. The length of core #1 was about 120-cm (100%), core #2 recovery was about 100-cm (83%), while core #3 and #4 were only about 55-cm length (46%). Advancement of the drill bit was resisted until about 75-cm depth, where a texture transition from sandy loam to sand/loamy sand is known to occur based on prior textural analysis.

Laboratory Soil Column Experiments

A series of one-dimensional (1-D) soil column experiments was conducted to investigate transport and retention processes influencing the fate of *Cryptosporidium parvum* oocysts in porous media. As was the case for the field study, fluorescent microsphere beads (Fluoresbrite YG carboxylated microspheres beads, 4.505 μm diameter, Polysciences, Inc., Warrington, PA) were used as a surrogate for *Cryptosporidium* oocysts. The specific objectives of this work were to a) develop analytical methods to count fluorescent microspheres, (b) develop protocols to extract and separate microspheres from the solid phase, (c) quantify conservative tracer and microsphere transport in a 1-D soil column systems as a function of flow rate and soil type, and (d) evaluate the utility of several mathematical models to describe microsphere transport and retention in porous media.

The 1-D column apparatus consisted of a Rainin HPLC pump (model Dynamix SD-200, Varian, Inc., Palo Alto, CA) equipped with a 25 mL pump head and pulse dampener; a Kontes

borosilicate glass column (15 cm in length X 4.8 cm inside diameter), and an ISCO fraction collector (Figure 2.10). The column endplates were fitted with two 40-mesh nylon screens to retain the porous medium and to enhance radial distribution of the influent solution. Two reference sands, Ottawa 20-30 mesh and F-70 Ottawa sand (40-270), and Cecil soil collected at the field site were used as the solid media in the column. The Cecil soil was gently ground to pass a 20-mesh sieve to remove large particles and debris. Air-dry sand or soil was poured into the column in 1-cm increments and packed under gentle vibration. Prior to water saturation, the soil columns were flushed with $C0_2$ gas to enhance dissolution of entrapped gas. De-aired, MilliQ water containing 0.01 M KCl as a background electrolyte was then pumped through the column in an upflow mode at a flow rate of 5 mL/min. Approximately 15 pore volumes were flushed through the soil column to achieve complete water saturation.

For each column, a non-reactive, conservative tracer study was performed using a pulse injection (1.5 pore volumes) of 0.01 M KI solution. Following the tracer experiment, the microsphere transport experiment was conducted. The fluorescent microsphere solution, containing approximately 3,000 microspheres/mL, was injected as a pulse (4.0 pore volumes or 500 mL), followed by continuous flushing with 10.0 pore volumes (1,250 mL) of MilliQ water containing 0.01 M KCl.

The column effluent solution was collected continuously in 20-mL vials, filtered, and counted for microspheres using an epifluorescence microscope. Effluent concentrations of the conservative tracer (KI) were analyzed using an HPLC system at a wavelength of 240 nm. After completion of each microsphere transport experiment, the columns were sectioned into 1.0- to 1.5-cm increments. The microspheres were separated from the soil, filtered, and counted using epifluorescence microscopy as described below.

MICROSPHERE ANALYSIS

Sample Preparation

Water samples collected from the ZTLs at the field site were often just a few milliliters, and thus, the sample vials were rinsed with a known volume of de-ionized water after each sampling event. All fluids were then collected in 125-ml plastic bottles. Sample bottles were

capped and labeled to record the date of collection, ZTL location relative to spiking area (inside or out) and the depth (30, 60,or 90-cm). Solutions were filtered in the laboratory under vacuum through a 3 μm polycarbonated track-etch filter (model #23066, Osmonics Corp.). Since higher sediment loadings tended to clog the filters, it was determined through experience that field-collected samples would need dilution before filtration. The exact volume water added for dilution was also recorded, but it was usually sufficient to increase the sample volume to approximately 200 mL.

Thorough rinsing of the flow-through centrifuge bowls produced about 2200 mL of solution, which was stored in glass jars with proper labeling. Before filtration, a mechanical agitation system was set up to ensure thorough mixing of this solution. About 200 mL was then sub-sampled, while under agitation, into the funnel of the filtration system using an electric pump attached to a 100-mL burette. Samples were then filtered as described above.

Samples collected from the monitoring wells were processed in a similar manner. Occasionally, rather turbid samples were encountered, which were diluted with de-ionized water to avoid clogging the filters. In some cases, samples were split, requiring two filtrations. These samples were sufficiently small that agitation was performed manually by shaking the samples in capped bottles, and transferring the volume to be filtered into a graduated beaker. This solution was then transferred to the filtration system.

Spring water samples obtained from the Sigma sampler were also treated in similar fashion. Since the total volume of each sampling bottle was about 300 mL, the solutions were manually shaken, and then transferred to 300-mL graduated beakers, and then into the filtration system. Turbidity and filter clogging was not encountered with any of the spring water samples collected.

Once filtration was complete, the filtration unit was disassembled and the filters recovered. All filter holders with filters in them were carefully labeled, packaged and shipped to Georgia Tech for microsphere enumeration.

Separation of Microspheres from Soil

To separate the microspheres from 20-30 mesh and F-70 Ottawa sand, approximately 300 mL of MilliQ water was added to each soil sample, which was then sonicated for 30 minutes.

The resulting slurry was filtered through a mesh screen to remove the soil, while the solution that passed through the filter underwent a second filtration process to capture microspheres for counting. For the Cecil soil, which contained a large fraction of fine particles, 200 mL of a concentrated sucrose solution (350 g/L, density of ~1.15 g/mL) was added to the sectioned soil samples. The slurry was then separated by centrifugation, and the resulting supernatent was filtered through a 3.0 μm pore size filter.

Analysis of Microspheres using Epiflourescence Microscopy

Fluorescent microspheres were analyzed using an epifluorescence microscope (model BHS, Olympus America, Inc., Melville, NY), equipped with a reflected light fluorescence attachment (BH2-RFC). The mercury burner light source is filtered so that only wavelengths longer than 455 nm reach the specimen. The microscope was also equipped with a model PM-10ADS photomicrographic system, so that slide or print film can be used to record images of the slide platform. The WHK 10X20L eyepiece (model 2LC-321) and 10X objective combine to provide a 200 magnification. The eyepiece was fitted with a model BLO-509 net grid (10 Xy 10) for improved counting on the filter surface. Using the 10X objective, the grid dimensions are 0.8 mm on a side, or 0.64 mm^2 area. The 47 mm diameter filter yields an area of 1735 mm^2. Figure 2.11 shows a representative view of the fluorescent microspheres on filter #1 (rep 2) obtained from an original microsphere concentration of 1×10^5. Prior to extracting microspheres from soil cores collected from the field site, a series of 1-D soil column experiments was conducted in the laboratory to test and refine the extraction procedure. The columns were packed with Cecil soil, obtained adjacent to the microsphere spiking area. Approximately 500 mL of aqueous solution containing ~2,700 microsphere beads per mL were introduced to the column. The total recovery of microsphere beads from the treated soil columns ranged from 53 to 80% of the injected amount.

The large area of the filter relative to the area under the microscope makes counting the entire filter surface somewhat cumbersome, especially when many microspheres are present. We therefore chose to count microspheres within a representative number of subareas, and then

normalize the microspheres counted on the filter to the total number present, according to the ratio of total filter area to the counted area, or:

$$\text{total spheres} = \left(\frac{A}{a}\right)\frac{\sum_{i=1}^{N}\text{spheres}_i}{N} \qquad (2.4)$$

where A = filter area

a = the area of each subarea

N = number of subareas

The need to count microspheres within subareas opens several questions regarding 1) the distribution of microspheres on the filter surface and 2) the representative number of subareas required to estimate the total population of spheres. These questions were approached by choosing one of the filters used on the 10^5 mixture (filter #1, rep 2), counting the number of spheres in 9, 12, 16, 20 and 24 subareas, and performing a statistical analysis on the results to determine if the distribution on the filter surface was normal. The number of subareas was considered to be a treatment(s) in this analysis. The hypothesis testing was:

H_0: No difference in the sphere counts across the filter surface (i.e., normal distribution)

H_1: Differences in sphere counts across the filter surface greater than can be attributed to randomness (i.e., distribution on filter surface subject to trends)

A verified normal distribution of the microspheres on the filter surface would allow for the use of a stratified random sampling scheme (Gilbert, 1987), so long as the entire filter surface was included in the sampling. The subareas for each of the five treatments were chosen by subdividing the filter into X subareas of approximately equal area, and then counting the number of microspheres within the subarea. The sum, mean and variance were used in the Kolmogorov-Smirnov (K-S) test, which calculates the cumulative probability distribution, and compares that to the distribution of normally distributed population (McBean and Rovers, 1998). SigmaStat (v.2, Jandel Scientific, Inc. San Rafael, CA) was used to run the analyses. Differences between

the cumulative sample distribution and the cumulative normal distribution, which exceed a critical value, indicate non-normality. Table 2.3 provides the results of these tests, and shows that each of the 5 treatments yielded results that indicate a random distribution of the spheres on the filter surface.

Table 2.3

Results of normality testing for microspheres counted on filter surface

# subareas	Mean	Std. Dev.	K-S distance	D_{crit}	P/F†
9	14.11	5.97	0.219	0.432	P
12	15.42	5.89	0.151	0.375	P
16	18.63	5.02	0.205	0.328	P
20	18.45	5.31	0.122	0.298	P
24	19.88	6.00	0.143	0.264	P

† - P/F indicates pass or fail null hypothesis

Data shown in Table 2.3 indicate a possible trend of higher mean counts as a function of the number of subareas. This observation was then checked to determine whether or not such behavior was an artifact of counting the filter a single time or an actual trend. After numerous replicate counting of the filter surface (data not shown), it became apparent that the trend was simply an artifact of sampling a random distribution a single time.

The second question to be answered involved the number of subareas that need to be counted to reduce the variation on the filter surface to a pre-specified level. For example, if only two locations are selected for sampling, where one location yielded no microspheres and the second location yielded 10 microspheres, the coefficient of variation (CV = std deviation / mean) would be 141%. Increasing the number of subareas counted reduces the CV because the extreme values would be averaged. Using the method of Gilbert (1987), the number of subareas required to reduce the standard deviation to a value of two was calculated using the following equation:

$$n_i = \frac{\left(t_{(crit,df,\alpha)} SD / SD_{target}\right)^2}{1 + \left(t_{(crit,df,\alpha)} SD / SD_{target}\right)^2 / N} \qquad (2.5)$$

where n = number of sampling locations needed to reduce the standard deviation (SD) below SD_{target},

i = an iteration counter,

N = the total number of microspheres

The degrees of freedom (df), the original number subareas counted with the microscope, is used for calculating t_{crit} at an $\alpha = 0.05$.

The analysis was iterated by updating t_{crit}, using $n_{i-1} = df$, and recalculating n_i, until it was stable after subsequent iterations. Using the 16 subarea count, which represents the median of the five treatments, 29 subareas would need to be sampled in order to reduce the SD below a value of two. The number of subareas was somewhat dependent on the filter used in the analysis, which admittedly retained a very large number of microspheres. It was found that the target subareas were essentially identical to the 24-subarea count, in terms of the t_{crit}; and thus, a 24-subarea count was deemed necessary to provide a representative sampling of the filter for microspheres.

During the field tracer experiment, it was anticipated that a substantially smaller number of microspheres would be collected and counted on any given filter. For filters that contain a small number of microspheres, the entire filter will be counted for microspheres in the manner described by Standridge (1999). If a large number of microspheres are present, such that scanning the entire filter is not realistic, the 24-subarea count will be employed to determine a statistically valid estimate of the microspheres.

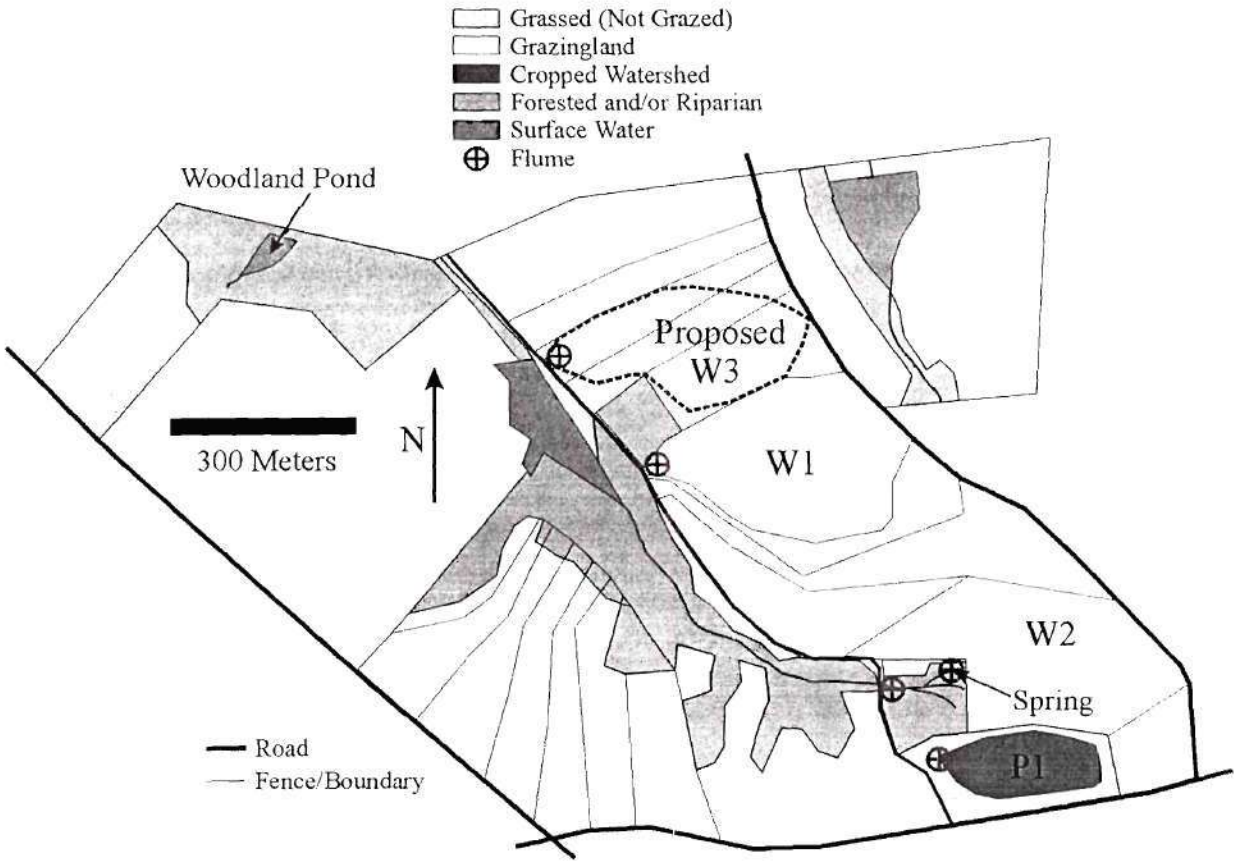

Figure 2.1 Location of W2 catchment within the North Unit Watershed at the USDA-ARS, J. Phil Campbell, Sr., Natural Resource Conservation Center.

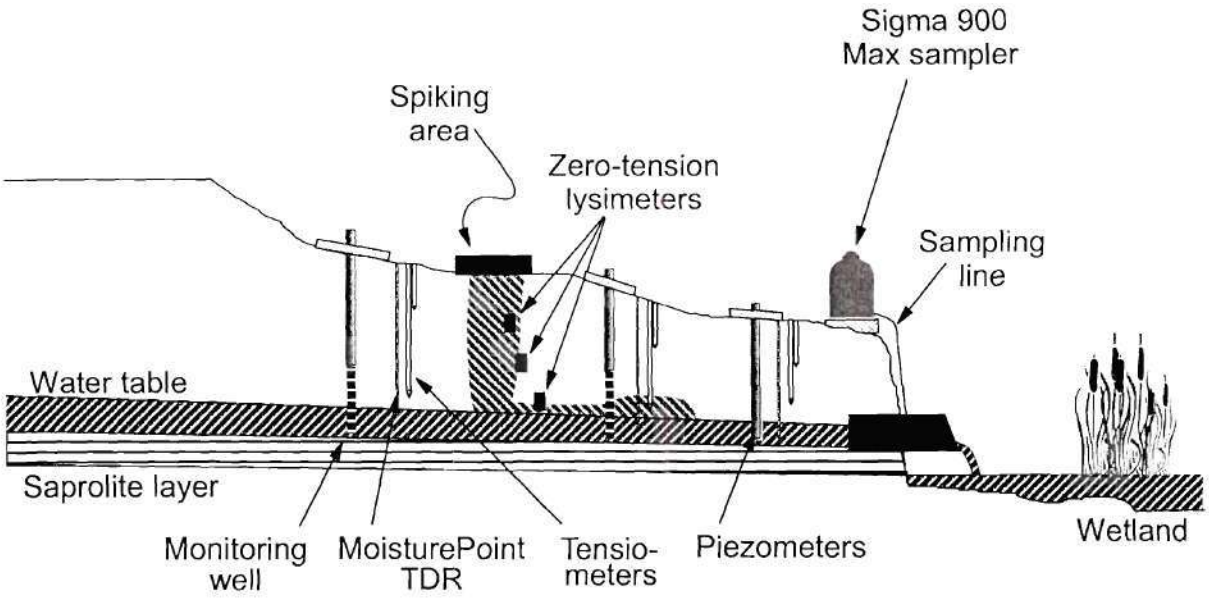

Notes:
1. Schematic not to scale.
2. Assumes water table depth of ~1.3 m near spiking area.
3. Completion depths of instruments site dependent.

Figure 2.2 Idealized, two-dimensional cross section of area adjacent to wetland, including instrument clusters, W2 catchment.

Figure 2.3 View looking east from the wetland showing monitoring and sampling instrumentation at the spring. Left to right are: flow-through centrifuge and peristaltic pump assembly, flume protected from animals, data logger, and housing for SIGMA sampler.

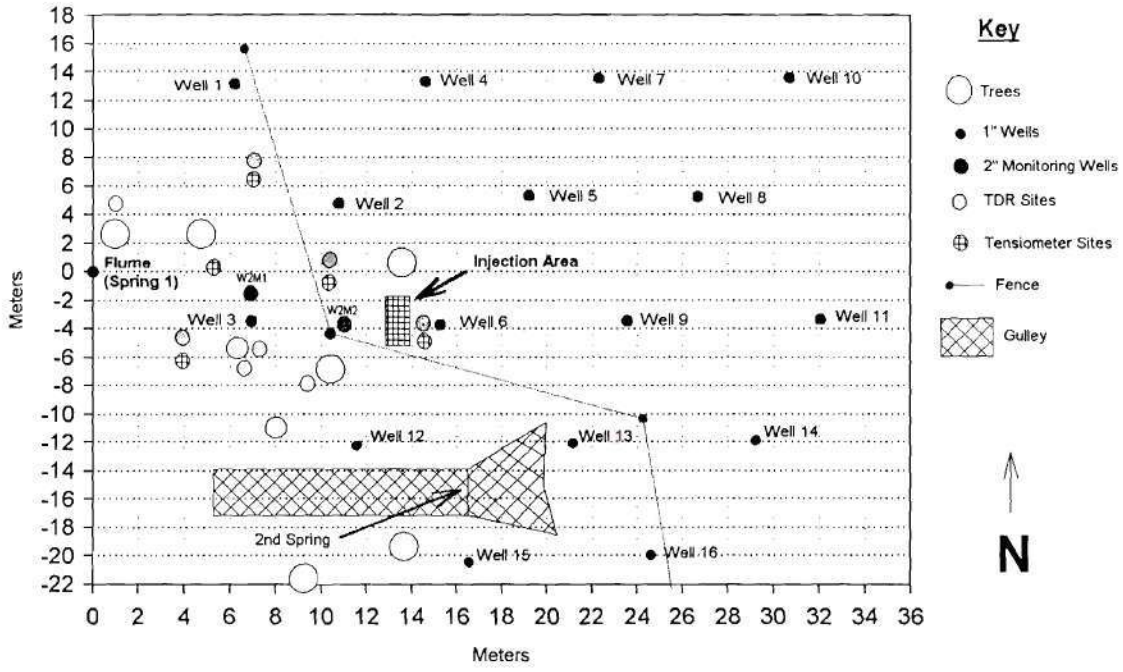

Figure 2.4 Locations of the flume, monitoring sites for soil water, soil water potential, and ground water, and the microsphere and bromide injection site by the main spring

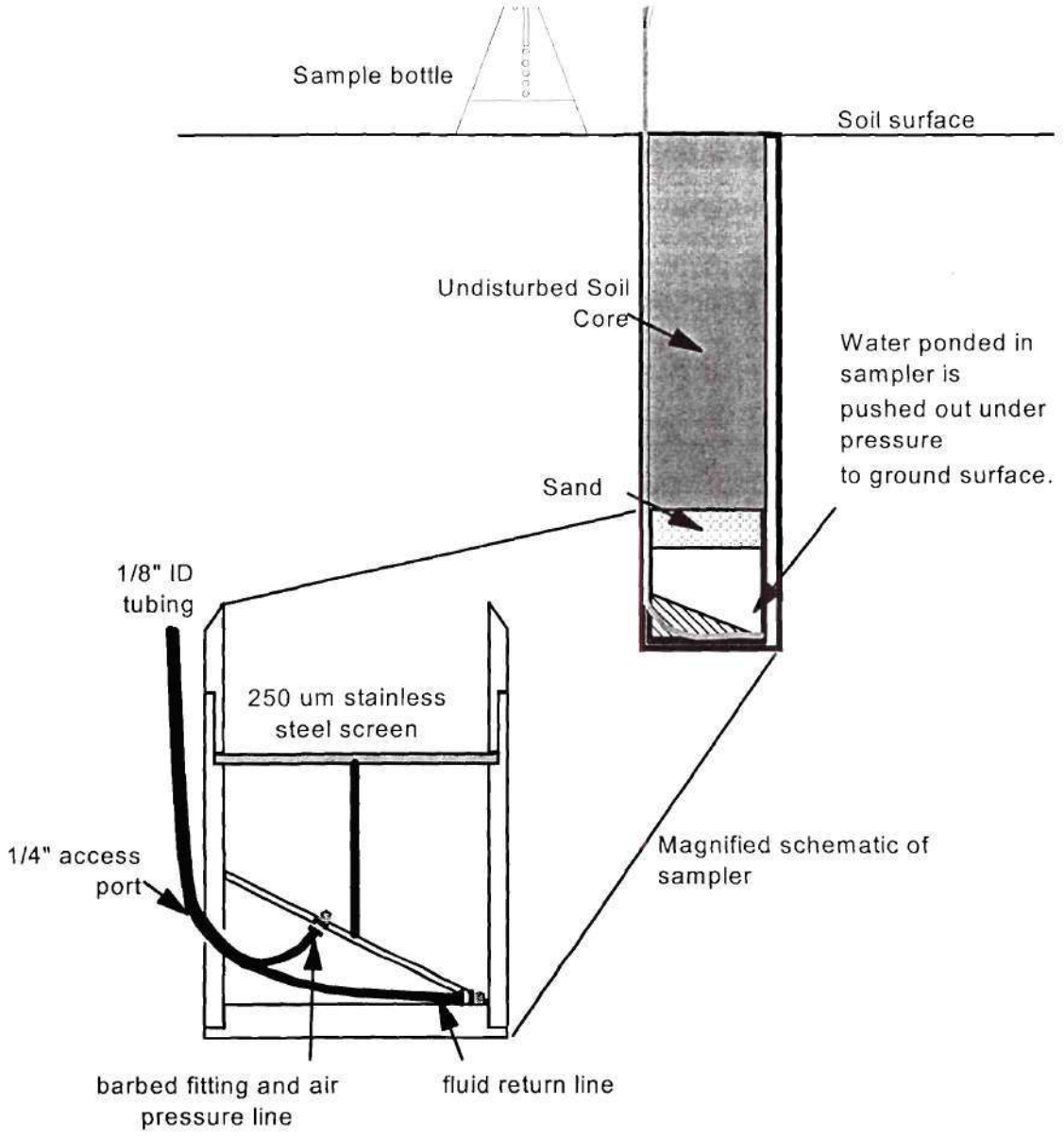

Figure 2.5. Schematic diagram of zero-tension lysimeter installed in a borehole, and a magnified view showing individual components of the collection apparatus

Figure 2.6. Picture of microsphere injection apparatus

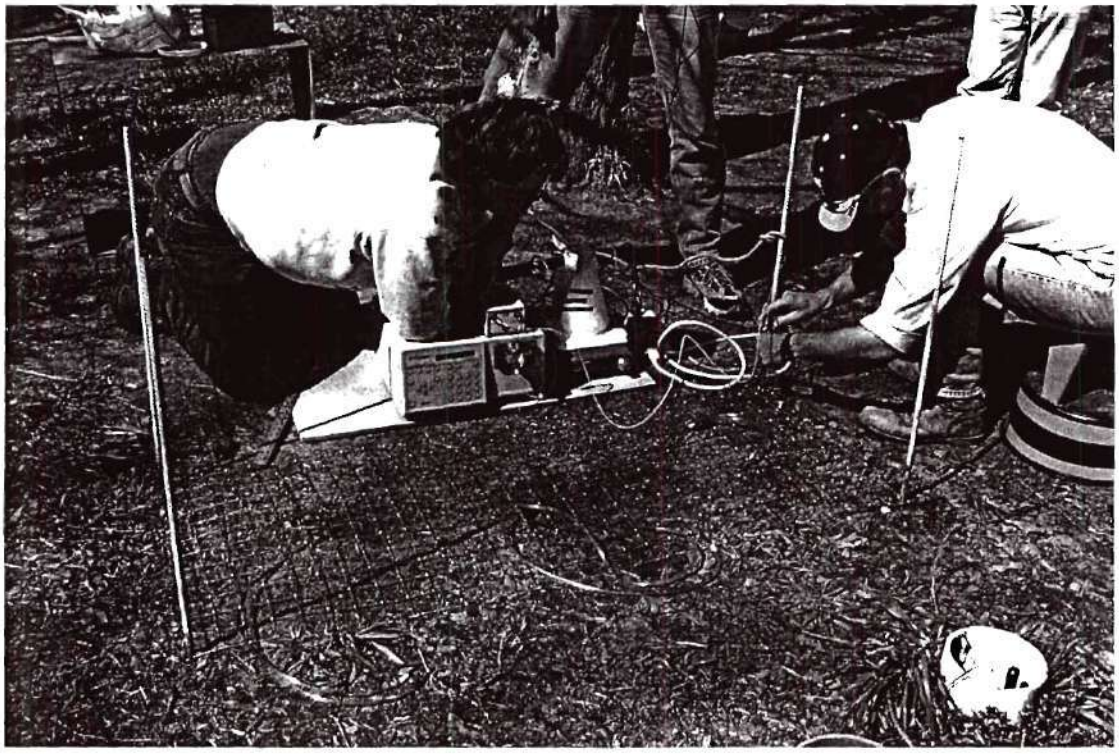

Figure 2.7. Injection of microsphere solution within mesh grid.

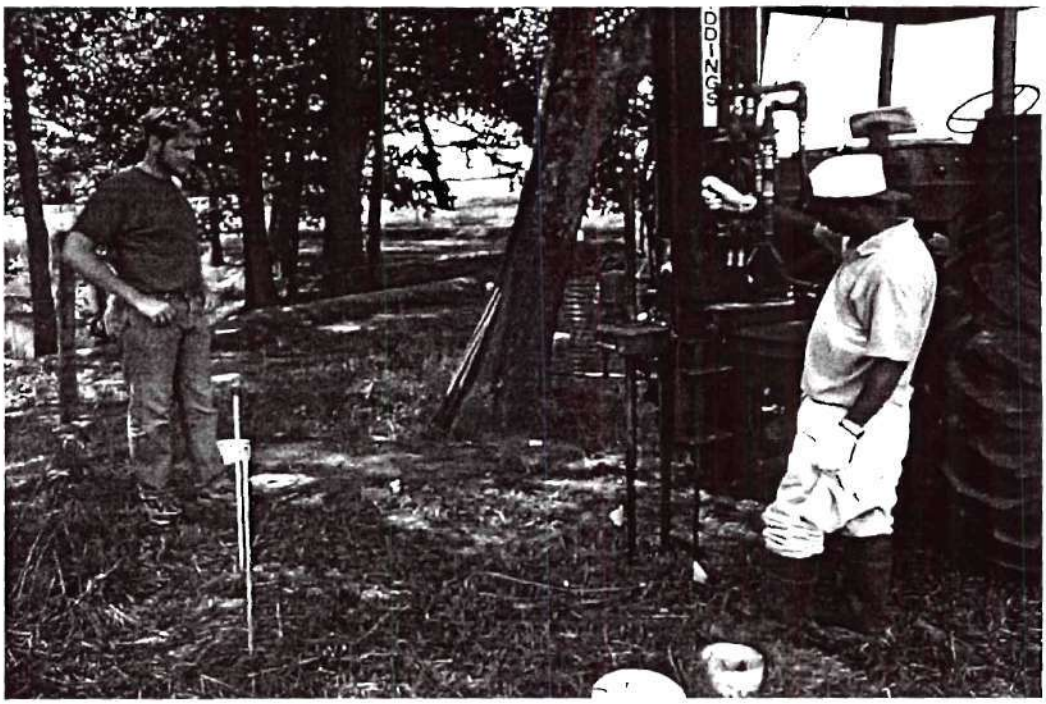

Figure 2.8. Operation of the Giddings probe to collect soil cores from the spiking area.

Figure 2.9. Removal of butyrate plastic liners containing soil from the core tube.

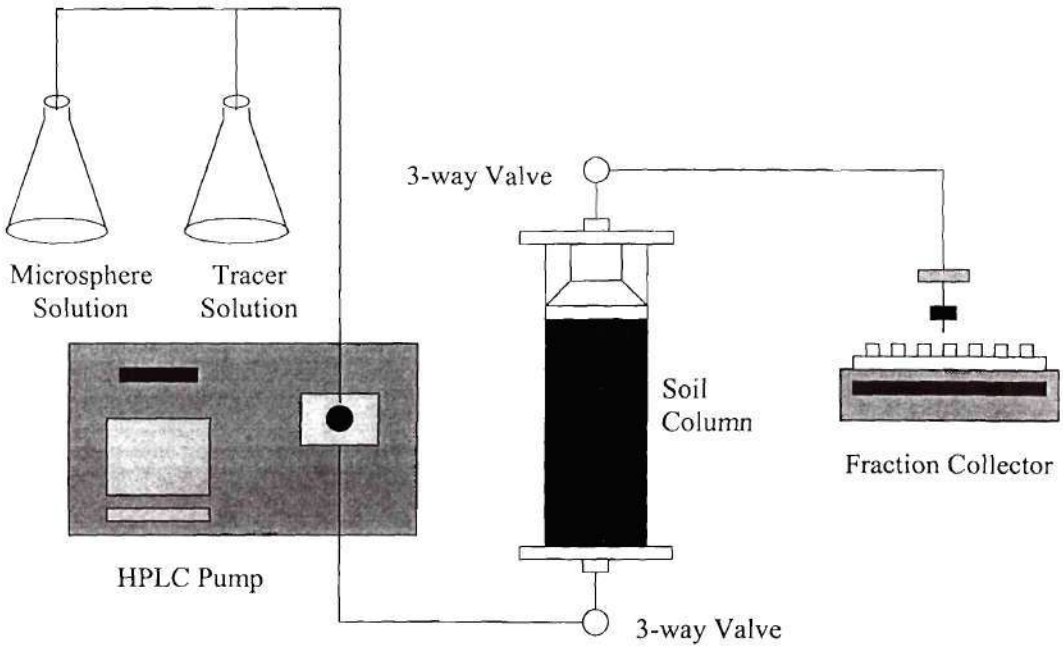

Figure 2.10 Schematic diagram of the laboratory column apparatus

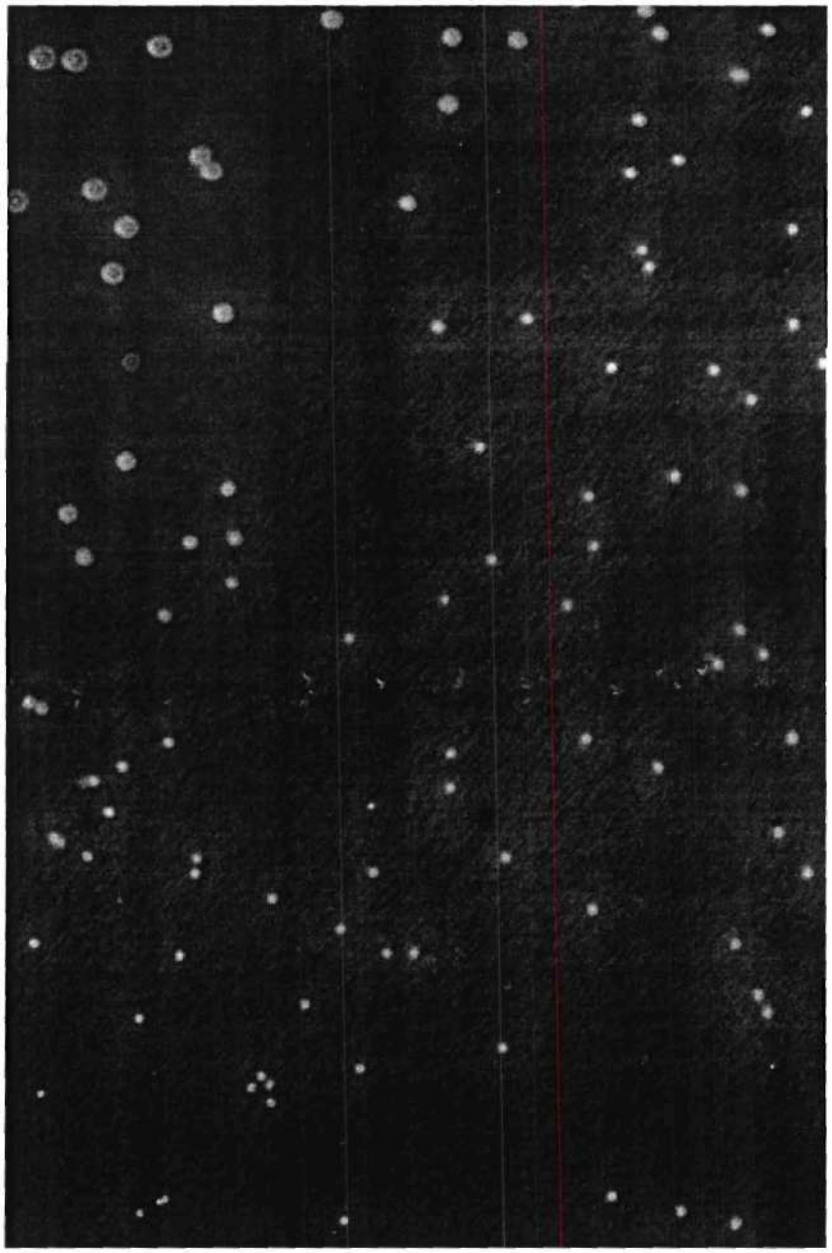

Figure 2.11. Image of polystyrene microspheres obtained with photomicrographic system using the epifluorescence microscope (magnification = 200X, wavelength > 455 nm).

Page intentionally left blank

CHAPTER 3
HYDROLOGIC AND TRANSPORT MODELING

HYDROLOGIC ANALYSIS

Description and Analysis of Water Budget Approach

The initial phase of hydrologic site characterization involved the development of a water balance equation that incorporated the main components of the hydrologic cycle:

$$(P + GW\ underflow + SRI) - (ET + SRO + IF + GW\ outflow) = \pm\Delta SWS \pm \Delta GWS \qquad (3.1)$$

where P = precipitation

GW underflow and GW outflow = groundwater flowing beneath the site

ET = evapotranspiration

SRI and SRO = surface runon and runoff, respectively (both assumed zero)

IF = interflow, or shallow subsurface water flow

ΔSWS = change in soil water storage

ΔGWS = change in ground water storage

Each term in the equation has dimensions of length, obtained by dividing the volume of water by the area of the watershed. Monitoring devices and methodologies, described previously, were specifically designed to quantify each of the main components of the hydrologic cycle. Prior to the field spiking experiments, site contouring was performed to prevent surface water inflow and outflow from the research plot, thereby minimizing the runoff terms, SRI and SRO. Monitoring well data were used to quantify groundwater underflow and outflow. Groundwater underflow was considered to be the component of groundwater that enters the subplot from the east, and flows west. Estimates of groundwater flow rate were obtained using Darcy's Law ($Q = A\ K_{sat}\ dh/dx$), where Q is the groundwater flow rate, A is the cross-sectional area taken as the product of the saturated thickness and the length of the flow domain perpendicular to the flow direction, K_{sat} is the saturated hydraulic conductivity, and dh/dx is the

hydraulic gradient. Equipotential contour lines were generated from piezometer readings, and the direction of water flow was assumed to be perpendicular to these contours. The hydraulic gradient (dh/dx) normal to the flow path was then obtained. Groundwater outflow was considered to be the component of groundwater that flows beneath the western boundary of the subplot and is not connected to the spring.

Water flow from the spring can be considered to result from interflow and shallow groundwater flow, and an attempt was made to evaluate both two terms. Change in storage (ΔSWS) was monitored based on soil water content data obtained from the TDR system and the monitoring well data. Differences in water flow from the spring before, during, and after a rainfall event, coupled with monitoring of groundwater levels and soil water content allowed for estimation of interflow (IF). Although spring water flow data were collected continuously using the automated datalogger system, TDR, tensiometer and monitoring well data were recorded manually. Therefore, direct comparison of these two data sets is based on the assumption that single-point data are representative of average daily hydrologic processes. Average soil water storage (SWS) was then calculated using the following relationship:

$$SWS(t) = \frac{\sum_{j=1}^{5}\left(\sum_{i=1}^{5}\theta_i z_i\right)}{5} \tag{3.2}$$

where i and j subscripts = depth and location, respectively

z = depth range of measurement (15, 15, 30, 30, 30 cm for i = 1 to 5)

Ground water storage (GWS) was estimated by first measuring the water level elevation relative to the flume elevation for the 11 northernmost wells. These data were then analyzed using Surfer32 (v 6.01, Golden Software, Golden, CO), which generated a water surface by kriging the spatially distributed data, and then obtaining object volumes using either Simpson's rule or the trapezoidal rule for integrating underneath a surface. The resulting value was an estimate of the water volume existing above the flume elevation. These estimates were used to track whether or not soil water percolating downward could account for increases in groundwater storage.

Baseflow and interflow components of the water budget are extremely important at the W2 site because of the strong correlation between soil water movement and interflow. It was hypothesized at the outset of the project that shallow soil water movement toward the water table might be a dominant mechanism for particle transport. Therefore, separating the interflow component from total flow, and then analyzing particle movement during times of predominant soil water movement, would provide some basis for testing this hypothesis. Numerous methods of baseflow separation and recession are available, including graphical partitioning and digital filtering. Given that the spring flow data collected to date exceed 100,000 records, digital filtering was the most efficient method. Recursive digital filtering is commonly used in signal analysis (Lyne and Hollick, 1979), and was first employed in streamflow filtering by Nathan and McMahon (1990), using the assumption that high frequency stream responses from surface runoff and interflow could be removed from low frequency baseflow responses. The interflow equation, as modified by Chapman (1991), is:

$$f_k = (3\alpha - 1)(3-\alpha)^{-1} f_{k-1} + 2(3-\alpha)^{-1}(y_k - \alpha y_{k-1}) \qquad (3.3)$$

where f_k = the interflow response at time, k

α = filter parameter that controls attenuation of the signal

y = the total springflow

As α increases toward unity, high frequency responses of baseflow are removed and the spring flow is dominated by interflow. In practice, α values less than 0.9 result in identical responses, and given the similarity in this value as used by others (e.g., Chapman, 1991; Mau and Winter, 1997), a filter factor of 0.90 was chosen. As recommended by Mau and Winter (1997), the filter was passed three times over the data set (e.g., forward, reverse, forward). Daily average flow data were used in the filtering, rather than data collected at 5-minute intervals, greatly reducing the time necessary for filtering.

PARTICLE TRANSPORT MODELING

One-dimensional Flow Model

To provide a basis for the more complex two-dimensional (2-D) flow domain and to evaluate laboratory column data, a one-dimensional (1-D) model was developed. For field application, the model incorporates known soil layering, meteorological conditions and parameter optimization. Parameter optimization provides estimates of the soil hydraulic properties using observed soil water content as an auxiliary variable, allowing the model to self-calibrate. Once the 1-D model was able to successfully simulate changes in soil water content using observed meteorological and soil water conditions, the complexity of the model was expanded to include solute transport of the bromide tracer and microsphere beads. Initially simulating the transport behavior of the tracer and microspheres in a 1-D framework allows for more precise analysis of flow and transport parameters (e.g., dispersion coefficient, retardation factors), which can then be utilized for subsequent 2-D model development and simulation.

One-dimensional modeling of water flow and solute transport was performed using the HYDRUS-1D code (Šimůnek et al., 1998) and CXTFIT (ver. 2, Toride et al., 1995). HYDRUS-1D numerically solves Richards' equation for simulating water flow in unsaturated, partially saturated and fully saturated porous media, while CXTFIT assumes steady-state flow conditions. In other respects the governing equations of the two models are similar, and hence, the development presented herein will focus on the more complex transient case simulated with HYDRUS-1D. The governing flow equation is solved using Galerkin linear finite element schemes for a wide variety of time-dependent or time-independent boundary conditions. The mixed form of Richards' equation is shown below for one-dimensional flow:

$$\frac{\partial \theta}{\partial t} = \frac{\partial}{\partial z}\left(K(\psi)\frac{\partial H}{\partial z} \right) = \frac{\partial}{\partial z}\left(K(\psi)\left(\frac{\partial \psi}{\partial z} + 1 \right) \right) - S \qquad (3.4)$$

where θ = volumetric water content (L^3/L^3)

t = time (t)

z = vertical coordinate (L) positive upward

K = the hydraulic conductivity (L/t)

ψ = soil water potential (L)

H = total head (L)

S = sink term that represents water loss through plant root uptake (L^3/L^3t)

Though several representations for retention curves are available, the following van Genuchten (1980) relationship, was chosen for modeling:

$$\Theta = \frac{\theta - \theta_r}{\theta_s - \theta_r} = \frac{1}{\left(1 + (\alpha\psi)^n\right)^m} \tag{3.5}$$

where Θ = relative volumetric water saturation

r and s subscripts = residual and saturated volumetric water contents, respectively

α = fitting parameter approximately equal to the inverse air entry value

n = pore size distribution parameter

m = (1-1/n).

The Mualem van Genuchten function (Mualem, 1976; van Genuchten, 1980) was used to represent hydraulic conductivity, $K(\theta)$:

$$K(\theta) = K_s \Theta^{1/2}\left(1 - \left(1 - \Theta^{1/m}\right)^m\right)^2 \tag{3.6}$$

where K_s = saturated hydraulic conductivity (L/t)

$0 < m < 1$ (van Genuchten, 1980).

As will be discussed in the following sections, the fitting parameters used in these closed-form representations were obtained through parameter optimization, but the initial input values were taken from data collected at the West Unit of the ARS facility (Bruce et al., 1983). Paired values of water content and water potential ($\theta(\psi)$), and saturated hydraulic conductivity, were derived from laboratory experiments on soil cores. Fitting of the retention curve was done using

the paired values as input to RETC (v1.0, van Genuchten et al., 1991), which optimizes the fitting parameters based on the method of least squares. The residual water content, θ_r, was taken as the water content at 15 bar potential, and the saturated water content, θ_s, was taken from the soil porosity assuming complete water saturation:

$$\theta_s = 1 - \frac{\rho_b}{\rho_s} \tag{3.7}$$

where ρ_b = soil bulk density (M/L^3)

ρ_s = soil particle density (M/L^3 assumed at 2.65 g/cm^3)

Bruce et al. (1983) analyzed core samples collected at the field site to determine soil bulk density. Thus, of the five possible parameters in the retention and conductivity curve that could be varied (θ_r, θ_s, α, n, and K_s), known data from field samples reduce this number to two (α and n). A reduction in the number of fitted parameters places greater emphasis on known data and reduces the potential for strongly correlated or non-unique parameter sets.

During parameter optimization, HYDRUS-1D solves the governing equations for water flow using assigned initial and boundary conditions, compares the results to observed conditions in the field, and then reinitializes the simulation using updated parameters. After each simulation, the program calculates an objective function (called SSQ in HYDRUS) that compares the simulated versus observed space-time variables:

$$\Phi(b,q) = \sum_{j=1}^{m_q} v_j \sum_{i=1}^{n_{qj}} w_{i,j} \left[q_j^*(z,t_i) - q_j(z,t_i,b) \right]^2 \tag{3.8}$$

where m_q = number of different sets of measurements

n_{qj} = number of measurements in a particular measurement set

$q_j^*(z,t_i)$ = specific measurements at time t_i for the jth measurement set at location $z(z,t_i)$

$q_j(z,t_i,b)$ = corresponding model predictions for the vector of optimized parameters b

(e.g., θ_r, θ_s, α, n, and/or K_s)

v_j and $w_{i,j}$ = weights associated with a particular measurement set or point, respectively.

The right-hand side represents deviations between the measured and calculated space-time variables (e.g., observed pressure heads and/or water contents at different locations and/or time in the flow domain, or the actual or cumulative flux versus time across a boundary of specified type) (Šimůnek et al., 1998). Measured soil water content was used as the sole auxiliary variable (e.g., j = 1). Weighting coefficients were calculated as the inverse product of the measurement variance and the number of observations for each auxiliary variable (Clausnitzer and Hopmans, 1995), which causes the objective function to become the average weighted squared deviation normalized by the measurement variances. HYDRUS-1D stops iterating when differences in $\Phi(b,q)$ between two successive iterations is less than a user-defined value (e.g., 0.001), indicating that a minimum was found. Parameter estimation uses the Marquardt (1963) nonlinear optimization routine. The measure of success in the optimization is based on maximizing the correlation coefficient, and minimizing $\Phi(b,q)$.

The sink term on the right hand side of Equation 3.4 represents water removal through plant water uptake. The model of Feddes et al. (1978) was used for the simulations. Here S is a function of ψ, as shown:

$$S(\psi) = \alpha(\psi) S_p \tag{3.9}$$

where α = water stress response function ($0 < \alpha < 1$)

ψ = soil water potential

S_p = potential water uptake rate [1/T].

The response function accounts for the reduction in water uptake as the soil water potential is reduced below an optimum value. Conditions of soil saturation lead to a reduced uptake because of anaerobiosis in the root zone, and conditions of extreme dryness lead to wilting conditions. Root zone distribution with depth is generally regarded as non-uniform, where the mass of roots near the soil surface is greater, with decreasing mass with depth.

This non-uniform distribution can be approximated using a root zone distribution function (Vogel, 1987):

$$S_p = \frac{b(z)T_p}{L_z} \tag{3.10}$$

where b(z) = normalized water uptake function (0] b(z)] 1) at depth, z

L_z = rooting depth of the plants

T_p = potential transpiration rate [L/T].

Though b(z) is not typically known for many plants Garrot and Mancino (1996), showed a linear decrease with depth for turf grass species; given the predominance of grasses at the W2 site, this approach was adopted. By substituting Equation 3.9 into Equation 3.10 and integrating over the depth domain, z, the actual transpiration rate, T_a, is:

$$T_a = \frac{1}{L_z}\int_0^z \alpha(\psi)b(z)dz \tag{3.11}$$

Subsurface layering for the 1-D case was determined by soil textural analysis from continuous soil core collected at W2 during site characterization activities. Table 3.1 shows the changes in textural components, and the associated soil texture.

Table 3.1

Textural classification for soil samples collected at W2 site

Sample #	Bottom depth (cm)	Sand (%)	Silt (%)	Clay (%)	Soil Type
W2-1	15	66	20	14	Sandy Loam
W2-2	30	76	16	8	Sandy Loam
W2-3	46	70	18	12	Sandy Loam
W2-4	61	84	10	6	Loamy Sand
W2-5	76	90	6	4	Sand
W2-6	91	78	12	10	Sandy Loam
W2-7	107	70	16	14	Sandy Loam
W2-8	122	62	28	10	Sandy Loam
W2-9	137	60	32	8	Sandy Loam
W2-10	152	56	24	20	Sandy Loam
W2-11	168	56	22	22	Sandy Clay Loam

Soil texture is approximately uniform, except for the presence of a thin lens of sand at 76-cm depth, grading upward to a sandy loam, and the presence of a sandy clay loam at a depth below our interest. The profile was subdivided into four layers at approximate depths of 45, 75, 80, and 165 cm. The model domain was subdivided into 101 nodal elements, each 1.65-cm thick.

Initial conditions of soil water content and soil water potential were estimated by simulating a constant flux of 0.05 cm/d at the upper boundary for a period of 2000 days, allowing the soil profile to approach mechanical equilibrium at a steady inflow rate. At this time, inflow should equal outflow, so that changes in soil water conditions do not change with time. Root water uptake was set to zero during these simulations to more quickly achieve equilibrium. Resulting water potential profiles taken from model output were used as input to the inverse simulation model; the retention function was then used to convert water potential to corresponding water contents.

Boundary conditions during the inverse simulation were taken directly from measured

data in the field. Potential transpiration data was taken from the latter gauging station, which is fully equipped for measurement of potential evapotranspiration (PET) using the Bowen Ratio System. Soil evaporation was set to zero. The inverse simulations covered a 180-day period, from July 1, 1999 through December 31, 2000. During this period, the TDR probe installed at Location 4 (~12 m and up-gradient of the spring) was sampled 41 times, providing 205 data points for the inverse parameter estimation (5 depths were sampled for each time period). The resolution of all meteorological and soil data was limited to a daily value.

Following the successful inverse modeling, and identification of a viable parameter set for the soil profile, forward modeling to simulate 1-D transport of bromide tracer and microspheres was completed. This modeling was performed in two steps. The first step simulates water flow from July 1, 1999 through February 28, 2000, or a total of 243 days between the onset of monitoring and the date of tracer application. The purpose of this first step was to establish the initial soil water conditions in the soil profile prior to injecting the tracers. The second step simulates water flow and chemical transport from February 28, 2000 through August 31, 2000, or a total of 186 days after application. The purpose of this second step was to estimate transport parameters of the soil material (e.g., soil dispersivity, filtration coefficient), to be used in the 2-D simulation model.

HYDRUS utilizes a convective-dispersion approach to solve the governing equations for solute transport in porous media. The model is capable of simulating physical and chemical nonequilibrium, multiple phases, and sequential first-order decay reactions. The model operates in both forward and inverse modes, but the simulator was run in forward mode only. The governing equation for one-dimensional chemical transport of solutes during transient water flow in variably saturated, rigid porous medium is:

$$\theta \frac{\partial c_k}{\partial t} + \frac{\rho_b \partial s_k}{\partial t} = \frac{\partial}{\partial z}\left(\theta D_k \frac{\partial c}{\partial z}\right) - \frac{\partial q_z c_k}{\partial z} - q_z \lambda c_k \qquad (3.12)$$

where c = aqueous (liquid) phase solute concentration (M/L^3)

s = sorbed (solid) phase solute concentration (M/M)

q = Darcy velocity (L/t)

D_k = dispersion coefficient for the liquid phase (L/t)

λ = filter coefficient (described below).

k subscript = k^{th} chemical species being modeled.

This form of the transport equation, Equation 3.12 accounts for first-order decay in the aqueous phase and sorption by solid phase. The sorption term on the left hand side of Equation 3.12 represents a reversible adsorption-desorption. Several treatments of this term have been used to describe this process for the transport of biosolids, including first-order rate-limited desorption; reversible, instantaneous linear adsorption; and saturation-limited sorption (Harvey et al., 1991; Johnson et al., 1995). To simplify matters somewhat, an instantaneous (local equilibrium assumption), linear sorption model was employed initially:

$$s_k = K_d c_k \tag{3.13}$$

where K_d = linear distribution or partition coefficient (L^3/M).

Incorporating Equation 3.13 into Equation 3.12, yields a reduced form of the one-dimensional convective-dispersion equation:

$$R_F \frac{\partial c_k}{\partial t} = \frac{\partial}{\partial z}\left(v_z \alpha_l \frac{\partial c_k}{\partial z} \right) - \frac{\partial v_z c_k}{\partial z} - v_z \lambda c_k \tag{3.14}$$

where R_F = the retardation factor ($R_F = 1 + \rho_b K_d/\theta$)

v = the pore water velocity

α_l = the longitudinal dispersivity (L) ($\alpha_l = D_k/v_z$).

Prior to or simultaneously with the microsphere transport experiments, a transport experiment was conducted using a non-reactive tracer, such as $CaBr_2$ or KI. Effluent concentration data were then fit to the solution of Equation 3.14 by varying α_l until the differences between predicted and observed concentrations are minimized (i.e., least squares

fitting procedure). An R_F of unity was assumed for the non-reactive tracer, that is, the ideal tracer was not subject to sorption processes ($K_d = 0$).

Transport and retention processes for the microspheres were treated in a manner described by Amirtharajah (1988), and shown to be useful in hydrologic studies by Harter et al. (2000). In this approach, particles attach and detach from solid matter through a series of near-term mechanisms that can be estimated from knowledge of physical properties of the pore space (porosity, median grain size, bulk density), particles (density, mean diameter, particle diffusion coefficient) and the water (density, viscosity, pore velocity). Incorporating these mechanisms into the trajectory theory approach requires estimation of the filtration coefficient (λ), which describes the relationship between colloid deposition onto uniform spheres in a clean packed filter bed:

$$\lambda = \frac{1.5(1-\theta)}{d_c}\alpha_e \eta \tag{3.15}$$

where θ = volumetric water content of the filter bed or porosity

d_c = mean grain size

α_e = empirical constant called the collision efficiency

η = single collector efficiency.

The single collector efficiency may be calculated including the effects of hydrodynamic retardation, electrical double layer interactions, and London-van der Waals forces, using the Rajagopalan and Tien (1976) equation:

$$\eta = 4A_s N^{1/3} Pe^{-2/3} + 0.00338 A_s N_G^{1.2} N_R^{-0.4} + A_s N_{Lo}^{1/8} N_R^{15/8} \tag{3.16}$$

where As = Happel's flow field factor

Pe = Peclet number ($q_i d_c/D$)

N_G = gravitational number (settling velocity/pore water velocity)

N_R = size group (particle diameter/mean particle diameter)

N_{Lo} = London—van der Waals constant.

Based on knowledge of the porous medium, the fluid, and the particle characteristics, η can be calculated and then used to derive λ. Following the transport experiments with the ideal tracer, the same column is used to conduct transport experiments with the microspheres, which is described above in the section titled *Microsphere Spiking Experiment*. The change in microsphere concentration is evaluated with time, and the observed data are fitted to the analytical solution by incorporating the fitted values of v_i and α_l, and varying λ until differences in predicted and observed outflow concentrations are minimized. The value of λ was then used in the 2-D modeling, as described below.

Two-dimensional Flow Model

A two-dimensional (2-D) model was developed at the W2 site to simulate lateral transfer of water and solutes from the ground surface to the water table, and then toward the spring. Orientation of the model is in the x-z plane. The HYDRUS-2D model (v 2.0, Šimůnek et al., 1999) was selected for the following reasons: 1) widely available and utilized by the hydrologic community, 2) includes an effective pre- and post-processor, and 3) ability to simulate multiple-phase interactions between contaminants, and solid, liquid, and gases and multiple species.

The model solves Richard's equation for water flow in unsaturated, partially saturated and fully-saturated porous media in two dimensions (either x-y or x-z planes). The governing flow equation is solved using Galerkin linear finite element schemes for a wide variety of time-dependent or time-independent boundary conditions. The mixed form of Richards' equation is shown below for two-dimensional flow:

$$\frac{\partial \theta}{\partial t} = \frac{\partial}{\partial x_i}\left(K(\psi)\left(K_{ij}^{A}\frac{\partial \psi}{\partial x_j} + K_{iz}^{A} \right)\right) - S \qquad (3.17)$$

where x_i = spatial coordinates (i=1,2)

K_{ij}^{A} = components of a dimensionless anisotropy tensor (diagonals = 1 for isotropic medium).

Representations of hydraulic properties (e.g., $\theta(\psi)$ and $K(\theta)$) are identical to those

obtained in the 1-D inversion modeling. Root water uptake functions and depths of root penetration are also kept the same, to the extent possible.

The flow model was constructed with a flow domain taken from known W2 characteristics. The site was represented as a vertical plane (x-z) oriented approximately east-west looking north, so that water entering the flow domain would flow west toward the spring. Figure 3.1 shows the model domain as a single object, annotated appropriately. Ground surface elevations were obtained from site surveys, so that the gentle slope toward the right side of the model domain does lead westward to a sharp slope break as the spring is encountered. The depth of the domain (3-m) was chosen so that saturated material would encompass approximately one-half of the total soil profile thickness, and so that the spring could be placed higher in the profile to allow for groundwater underflow. The east-west extent of the domain, 12-m total, was enough for the spiking area and the spring to be included in the model.

A single, continuous object forms the computational domain. Boundaries were then defined as no-flow, constant head, seepage face, and atmospheric. The no flow boundary was defined at the bottom of the domain where horizontal ground water flow was assumed. Constant head boundaries were used on the left and right hand sides so that a hydraulic gradient at the water table would be formed, allowing water to flow into and out of the domain. The seepage face boundary was used to simulate the spring. The remaining nodes were assigned as an atmospheric boundary to simulate water gain and loss due to precipitation and evapotranspiration, respectively.

The computer module, MESHGEN-2D, automatically generates the finite elements, given user-defined numbers of boundary nodes. MESHGEN-2D generates an unstructured triangular mesh, and then checks the mesh to improves its' smoothness, reduce elements with extreme angles, and eliminate six-sided elements. To keep the model efficient, the number of boundary nodes were limited, resulting in 953 elements for an area approximately 30 m^2.

The 2-D modeling was done in parts. The first part simulated water movement from July 1, 1999 through February 28, 2000, or up to the day of microsphere spiking. This 243-day period also provided an opportunity to quantify flow from the spring, allowing us to adjust the conceptual model of flow at the seepage face. Soil water pressure data were then used as initial conditions for the second model, which ran from February 28, 2000 – August 31, 2000.

Meteorological conditions collected at or adjacent to the site were used for the atmospheric boundary, similar to that used in the 1-D case.

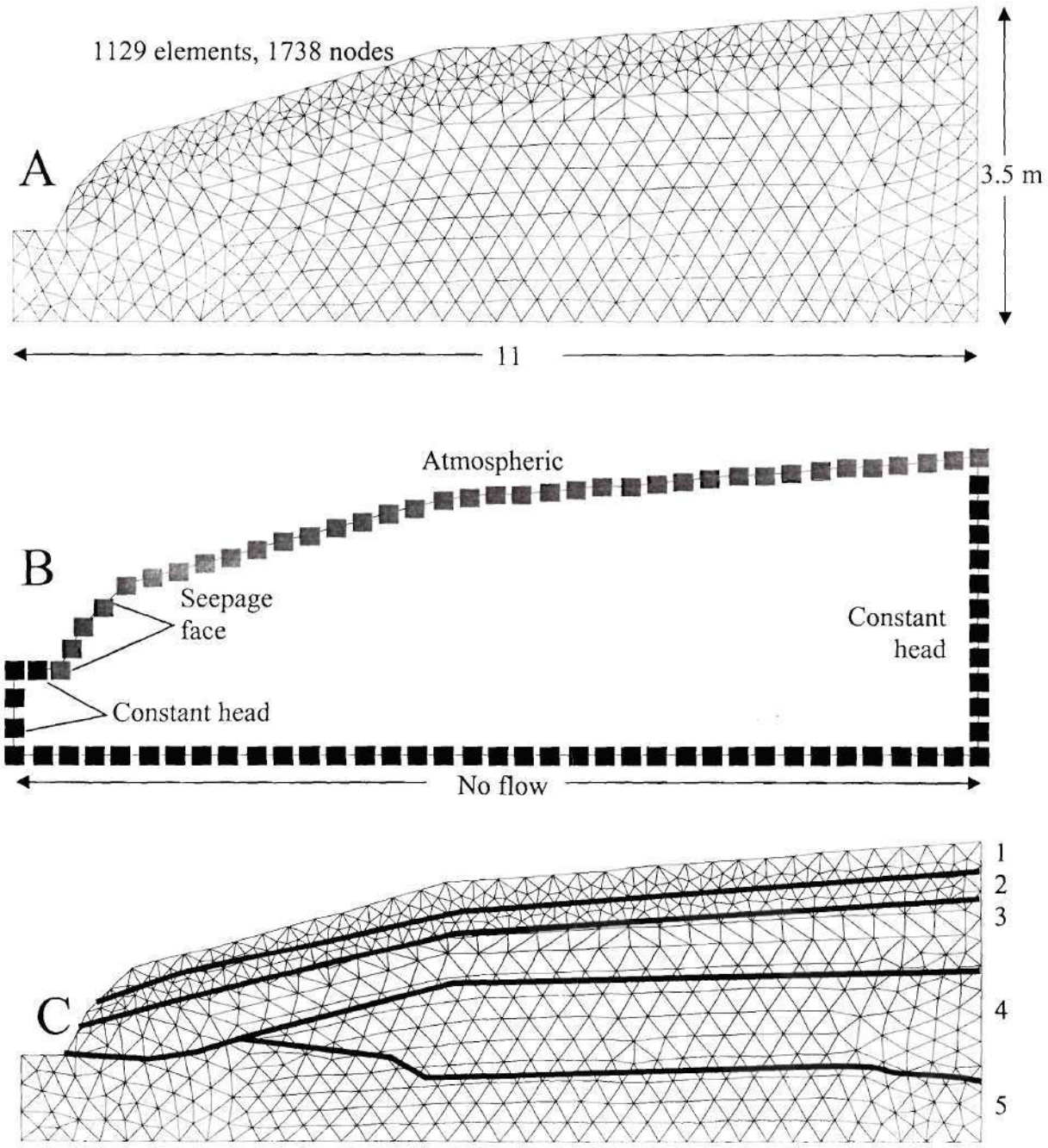

Note: Layering corresponds to soil in Table 3.2, except for Layer 5 (Layer 4 properties with

Figure 3.1 – Modeling domain for 2-D simulations. (A) – finite element geometry; (B) - boundary conditions; (C) - subsurface layering.

CHAPTER 4
RESULTS AND DISCUSSION

HYDROLOGY OF FIELD SITE

Results of Geophysical Survey

Results of inversion analysis performed on data (EM-31) obtained during the geophysical survey are shown in Figure 4.1a. The contour intervals for the solid lines represent the depth to the interface between two layers. The top layer is considered to be unsaturated soil, and the bottom layer is soil of some critical saturation value, unknown at present without data from the ground. Both plots show that the saturation depth to the interface decreases toward the wetland, most likely because ground surface elevation also decreases in that direction (note the dashed elevation contours). It is clear, however, that the change in slope is more uniform in the vertical orientation. Average differences between the horizontal and vertical orientation is very slight (RMSE = 0.072 m), and there is a general trend of decreasing depth to the interface.

Figure 4.1b shows an inverse image (black is negative polarity) of unprocessed ground-penetrating radar (GPR) data compiled from traces collected south to north along Line 6 (furthest from the wetland) at 1-m spacing, using a 50-MHz antenna in bistatic mode. The figure is seen oriented facing west toward the wetland. Preliminary analyses yield an estimated radar velocity of 75 to 85 m/ns in the shallow part of the section, and the measured two way travel time to the presumed water table reflection yields a maximum depth of approximately 1.4 m at the left side of the plot, 3 to 3.4 m at the lowest point, and 2 to 2.25 m at the right side (Annotations are provided in Figure 4.1b). Poorly imaged material above the water table may be weakly developed soils that have slumped downslope. The strong reflector below the water table is probably the top of the saprolite, and the deep northward dipping reflectors will migrate to discrete lens-like features during processing.

Preliminary analysis of the Schlumberger vertical electrical sounding (VES) survey data, using linear filtering forward calculations, yields a best-fit model characterized by an approximately 40m-thick layer with an apparent resistivity of 480 Ω-m overlying a half-space of infinite apparent resistivity. Fine-scale oscillations at small electrode spacing were obtained that

represent real and well-constrained resistivity variations in the vertical structure of the shallow subsurface, and can probably be attributed to subtle changes in soil stratigraphy and water content.

The results of the geophysical survey indicate that the depth to the water table, or to material with some critical saturation value, has been identified using the two methods. The EM-31 and GPR studies indicate that the depth can be expected to vary between 2-3 m in the area upgradient of the wetland. The elevation contours shown in Figure 4.1a combined with the critical depths to saturation and the location of the wetland area indicate that ground water flow is westerly. This information was confirmed after the monitoring wells were installed.

Soil Properties at Field Site W2

The textural classification of soil samples collected from Borehole MW2 (Table 2.3 in Chapter 2) shows a dominantly sandy loam texture, with some distinct grading into and out of a sandy material at 60-75 cm depth. Though textural analyses were not performed for other core samples collected at the site, visual inspection indicated a lack of significant spatial variability of soil texture for the subplot used for transport experiments. Thus, textural analysis was limited to samples collected from the MW2 borehole.

Soil textural data allows one to relate changes in particle size distribution to changes in soil hydraulic properties. Given the level of effort that would be required to conduct large numbers of core analyses for determining retention and conductivity functions, however, hydraulic properties were estimated using the pedo-transfer function method of Schaap and Bouten (1996) and Schaap et al. (1998). Schaap et al. (1998) employed a neural network approach to estimate the van Genuchten (1980) parameters given either soil texture, textural components, bulk density, and/or known points on the soil water retention curve. This approach provides for an increasing degree of accuracy as new data are included in the analysis. Schapp et al. (1998) incorporated this method into the computer program Rosetta, which is embedded in the HYDRUS-2 D model (Šimůnek et al. 1999). Inputting the known textural data (Table 2.3) into Rosetta provides an estimate of the van Genuchten parameters for each MW2 core increment (Table 4.1) and generalized for the W2 study area as a function of depth/soil horizon

(Table 4.2). The resulting soil water retention (pressure-saturation) and unsaturated hydraulic conductivity functions are shown in Figures 4.2a-4.2k.

Table 4.1

Estimated van Genuchten parameters using the textural data listed in Table 2.3 and the neural network approach of Schaap et al. (1998)

Sample #	Bottom Depth (cm)	α (cm^{-1})	N	θ_r (cm^3/cm^3)	θ_s (cm^3/cm^3)	K_{sat} ($cm\ d^{-1}$)
W2-1	15	0.030	1.388	0.0492	0.3838	32.35
W2-2	30	0.039	1.528	0.0417	0.3841	65.56
W2-3	46	0.034	1.416	0.0463	0.3829	41.05
W2-4	61	0.037	1.900	0.0454	0.3814	139.06
W2-5	76	0.035	2.555	0.0492	0.3791	334.99
W2-6	91	0.036	1.556	0.0470	0.3802	67.53
W2-7	107	0.032	1.403	0.0500	0.3814	36.29
W2-8	122	0.027	1.403	0.0413	0.3872	37.62
W2-9	137	0.025	1.412	0.0373	0.3899	42.73
W2-10	152	0.023	1.371	0.0600	0.3911	16.76
W2-11	168	0.024	1.356	0.0630	0.3915	14.88

Table 4.2

Fitted values of van Genuchten parameters for soil hydraulic properties at W2

Bottom Depth (cm)	α (cm^{-1})	N	θ_r (cm^3/cm^3)	θ_s (cm^3/cm^3)	K_{sat} ($cm\ d^{-1}$)
43	0.052	1.38	0.041	0.366	603
76	0.054	1.5	0.083	0.378	225
81	0.079	2.93	0.2	0.3	873
165	0.034	1.52	0.092	0.34	823

Analysis of Site Water Budget

Previous research conducted at the W2 site spring by Fisher et al. (2000) showed significant fecal coliform spikes after rainfall events with rapid declines following the spikes. These findings suggest that fecal coliforms were being leached downward through the soil profile from the ground surface, and then migrating toward the spring via groundwater interflow. The significance of interflow as a transport mechanism for pathogens needs to be studied and better understood, especially if spring water contains pathogens only during times of rapid flushing of the soil. The goal of the water budget analysis was to understand the link between the flow in the spring and soil water conditions.

Water budget components are represented in units of volume (m^3) whenever possible, allowing each component to be added or subtracted as needed. Since ground water flow in the northern portion of the subplot did not appear to drain into the spring, water volumes corresponding to this area were not included in the water budget. Therefore, the water budget analysis was limited to the southern-most area of the subplot, defined by the monitoring wells as shown in Figure 4.3. The dimensions of this area are 9.33 m north-south by 31.86 m east-west, yielding a total area of 297.13 m^2.

Precipitation

The field site, as well as a large portion of Georgia, experienced a sustained drought starting in May 1998. Total rainfall for year 2000 recorded by various gages near the site was between 800 and 930-mm. As a result, year 2000 was one of the driest years since 1937 (64 years), when records were started to be kept at the ARS location. The long-term yearly average rainfall based on the ARS data is 1264-mm. Prior to 2000, the record for the driest month was held by 1954 when total precipitation was only 855-mm. Other dry years were: 1988 (876-mm), 1965 (910-mm) 1987 (914-mm) and 1955 (915-mm). Precipitation in 1999 ranked the year as the 18th driest. Monthly precipitation was also below the long-term average from February 2000 through August 2000. During this eight-month period, a total of 47.9cm (18.8 inches) of rainfall was recorded, which is about 50% less than the long-term average. The total rainfall water volume was 142.27 m^3 in box area shown in Figure 4.3. Rainfall during the first 2.5 months

represented about 50% of total during the monitoring period, illustrating the very dry conditions experienced at the site during the latter portion of the transport experiment. Rainfall during the remaining 5.5-month period was the result of a few storms of relatively high intensity and short duration, conditions that did not result in replenishment of the soil water deficit.

Precipitation patterns in the watershed (W2) during calendar year 2000 are presented in Figures 4.4 and 4.5. Cumulative precipitation was only 200 mm during this reporting period, May 12, 2000 to August 31, 2000, with only 24 measurable precipitation events. Two events exceeded 25 mm, three events were between 10 and 13 mm, and nine events were between 5 and 10 mm. The remaining rainfall events were less than 5 mm. Monthly precipitation has been below the long-term (60 years) average since February (Figure 4.5). The overall water deficit was about 220 mm for the period May through August 2000.

Water losses due to cumulative evapotranspiration (ET) are shown in Figure 4.6 relative to cumulative precipitation for calendar year 2000. A total of 97.43 cm (38.36 in) of ET was recorded, equivalent to a volume of 289.49 m^3. When compared to the precipitation measured at the site, it is apparent that loss of water through ET was substantial, more than twice the amount of precipitation.

Soil water

Soil water content values recorded at the site since July 1999 are shown in Figure 4.7. The graph illustrates that ground water recharge occurred during Winter 1999. Soil water content was highest in January 2000, and then declined steadily until mid-May. Soil water content was lowest during the last reporting period. Near-surface soil profiles (0-30 cm depth) were driest, with steady increases in water content with depth. A small increase in soil water content was apparent following rainfall events toward the end of June and July 2000, including soil depths of 90-120 cm. However, no significant increase in spring discharge rates were observed following these events, indicating that most of the precipitation replenished the soil water storage, and did not significantly recharge ground water. Only the deep tensiometers, where soil water content remained at or above 20%, provided reasonable readings. Soil water potentials of material surrounding the shallow and mid-depth tensiometers were no longer in tensiometer range, causing the tensiometers to bubble and release water. Servicing the

tensiometers for each reading would eventually moisten the soil surrounding the porous cup, biasing the readings. The tensiometers were restored to service when sufficient rainfall occured.

Soil water storage (SWS) data for year 2000 is shown in Figure 4.8. These data illustrate the strong effect of ET and low precipitation on the available soil water, especially from Day 100 and later. The values plotted on the graph represent the product of SWS(t) obtained from Equation 3.2 and the area of the subplot. Dividing through by subplot area yields an average SWS between 40 and 20 cm. The steady decline in SWS corresponded to the decline of total spring flow and GW underflow, as the entire site underwent a drying period.

Ground water

Ground water elevations continued to decline throughout the reporting period. Figure 4.9 shows the average elevation change from the 11 piezometers, normalized to the elevations recorded nine days before the microsphere injection on February 28, 2000. Except for two brief periods of recharge (March 15, 2000 and June 24, 2000), ground water elevations have been falling, with an average decline of 300 mm recorded during the reporting period. Contours of ground water (piezometric head) elevations for four selected time periods since well installation are shown in Figure 4.10. In these plots, the most westerly point (parallel to x-axis and toward the left) is the flume (spring outlet). Contours are represented at 5 cm intervals. The piezometric surface indicates a consistent, westerly flow toward the spring and wetland, regardless of the time period or severity of the drought. The small scale ground water trough in the center of the field site (Graph 4.10B) during recharge periods appears now to be more of a ridge (Graph 4.10D), causing slightly divergent flow patterns near the spring. The graphs indicate convergence of flow toward the spring during high water table conditions. Under dry conditions, convergence appears to be somewhat reduced, and the ground water surface is relatively flat near the spring.

As discussed in Chapter 2, groundwater underflow enters the subplot at the eastern plot boundary and flows west, toward the spring. The magnitude of GW underflow is highly dependent on the saturated hydraulic conductivity (K_s) of the soil material found below the water table. The estimated value of K_s, obtained from the numerical inversion modeling in the 1-D case (i.e., 8.23 m/d), was used for these calculations. Although the K_s value is rather high, it is in

fact representative of sandy material. As an initial estimate, and without the benefit of laboratory core data, this value should be suitable for subsequent modeling efforts. Daily and cumulative GW underflow data obtained for calendar year 2000 are shown in Figure 4.11. The daily underflow data show a trend toward decreasing input to the hydrologic system as either the hydraulic gradient or groundwater levels (or both) decreased during the summer months. A total of 188.78 m^3 of water entered the site along the southern portion of the monitored subplot during the period of the study. Precipitation and GW underflow represent the only two measured components that added water to the subplot area, totally 331.05 m^3. The values do not represent deeper groundwater, which could potentially flow upward and discharge into the spring.

Cumulative ground water baseflow and interflow during calendar year 2000 are shown in Figure 4.12. The total spring flow (not shown) is therefore considered to be the sum of baseflow and interflow. During the late spring, and throughout the summer, both flow components were significantly lower than the winter months of 1999-2000. The interflow rate was essentially zero during most of latter part of the study period because of drought conditions. The cumulative value of interflow and base flow was 654.80 and 1759.63 m^3, respectively, or about 27% and 73% of total spring flow. Ground water storage (GWS) is plotted on Figure 4.13 and shows a similar pattern of loss during the summer period.

Spring flow

The lack of normal precipitation patterns was seen very clearly in spring flow. Spring levels have not been observed at these levels, or as consistently low, as during this study period. Flow rates were virtually a trickle for most of the reporting period. The period started with spring flow between 1 and 2 L/min (consequence of dry period in the previous reporting period). Throughout June, 2000 and until the first week in July, 2000, spring flow ranged between 0.5 and 1.0 L/min. Since that time, flow has remained below 0.5 L/min. Recalling that long-term base flow was about 5 L/min with spikes of up to 38 L/min encountered after heavy precipitation events, the very low base flow rates are extremely unusual.

Further complicating the spring flow monitoring was an apparent diurnal response of the transducer that appears strongly correlated to ambient air temperature. The fluctuations were accentuated during periods of low flow. The response varied between a low at 6 PM to a high at

9 AM. This represents a variation of up to 1.5 mm of head from the mean, which represents a flow variation of 0.23 L/min, or about 50% of low flow conditions. Transducer specifications indicate that temperature variations of ±1.05 mm are within specification, so the field results are very close to factory specifications. To resolve this issue, transducer output will be calibrated as functions of pressure and temperature. The flow data were then developed based on the resulting regression equation.

Figure 4.14 shows the results of the high frequency filtering for spring flow in Year 2000, resulting in separate estimates of baseflow and interflow over time using Equation 3.3. As a reference, DOY 59 corresponds to the microsphere spiking event (February 28, 2000). The graph shows the relatively rapid response of the interflow component (bottom trace) versus that of the low frequency baseflow (top trace). The very rapid rise and fall of the interflow component (kinks in bottom trace) shows the responsiveness of the system to precipitation. For example, the rapid rise in interflow on DOY 79 occurred after a 3.5-cm precipitation event, and the subsequent decline in interflow shows the relatively rapid internal drainage of the soil toward the water table. The increase in spring discharge rates due to the interflow component represents a relatively rapid transfer of soil water to the groundwater component.

Water Budget Analysis

With knowledge of the water budget components, Equation 3.1 can be modified slightly to account for the lack of surface runon/runoff, and the assumption that deep ground water does not play a significant role in the shallow system:

$$P - (ET + IF) = \pm \Delta SWS \pm \Delta GWS \tag{4.1}$$

If water budget measurements are conducted soon after precipitation occurs, water added to the subplot should be reflected by increased values of soil water storage (SWS) and ground water storage (GWS). To evaluate the relationship between precipitation and water storage components, a linear regression approach was applied to the observed increases in SWS and GWS following rainfall events versus the amount of precipitation as shown in Figure 4.15 (slope = 1.19; $r^2 = 0.86$; SE = 15.8 m^3). The near unit slope indicates a close 1:1 relationship between rainfall and the sum of GWS and SWS. Removing the GWS component and assuming that

precipitation will be completely absorbed by SWS, yielded a slope of 0.52 (not shown), a much poorer relationship. This analysis demonstrates that water moved quickly through the soil profile and into the shallow ground water system.

The site water budget focused on the shallow hydrologic system, and the source of the high frequency component of the spring. However, it became apparent that the total spring flow (BF + IF) could not be accounted for by the GW underflow alone. In fact, the total volume of GW underflow was only about 8% of the total flow. Therefore, it was hypothesized that significant quantities of deeper ground water were discharged at the spring, which was expressed as base flow:

$$GW\ underflow + deep\ GW = BF \tag{4.2}$$

Though this component could not be measured directly due to a lack of nested piezometers, it is well understood that groundwater flow will have a vertical component when flowing toward a discharge point, such as a spring, river or lake (Freeze and Cherry, 1979). Therefore, the interflow component was assumed to be representative of downward percolation of soil water, whereas base flow was considered to represent deeper groundwater. Solving Equation (4.2) for deep GW and plotting the time series (Figure 4.16) shows that much of the base flow occurring during the early part of 2000 (DOYS 0-130) was actually deep groundwater, but that the spring no longer acted as a discharge point during the late Spring and early Summer. For this eight-month period, 89% of all baseflow can be classified as deep GW. Therefore, the concentration of microspheres and tracer injected into the soil, or added directly to the piezometers, would be significantly diluted, reducing the ability of the monitoring system to detect their presence in spring outflow.

TRANSPORT EXPERIMENTS

Bromide Spiking Experiments

Accuracy of Bromide Specific Ion Electrode

As discussed in Chapter 2 in the section titled, *Method of Detection*, results using the bromide specific ion electrode (SIE) for the first bromide tracer experiment were not validated because of problems associated with the SIE. Calibration of SIE become suspect immediately after the first bromide tracer experiment as the bromide mass recovery according to the probe was approximately 75 times greater than what was originally injected. To confirm bromide mass recovery, 14 water samples collected with the Sigma sampler were analyzed using the SIE (in the laboratory) and independently analyzed by ion chromatography at the University of Georgia. All samples yielded bromide concentration below detection limits using both analytical methods. Further laboratory testing and consultation with the manufacturer (Innovative Sensors Inc., Anaheim, CA), showed that the original calibration curve was essentially correct. After studying the probe configuration used in the field (i.e., horizontal orientation), it was hypothesized that air bubbles might have attached themselves to the probe membrane, causing the voltage response to decrease (decreasing voltage levels would indicate increasing bromide concentration). The SIE field installation was modified so that the probe membrane would be at the bottom of the conveyance pipe, reducing the chance for air bubbles attachment. The sensor was again used to detect bromide breakthrough after a second injection on February 10, 2000 at one of the two 5.08-cm monitoring wells. However, the probe became rather unstable and showed a distinct diurnal trend in bromide concentration, with values below detection limit at low temperatures and higher concentrations at elevated temperatures. As a result the SIE measured concentration could not be used to assess bromide mass recovery.

For subsequent bromide breakthrough and mass recovery determinations, discrete samples were collected over time using the Sigma sampler and analyzed for bromide at Georgia Tech using ion chromatography. The research team understood at the time of purchase that the SIE probe might not perform well under ambient environmental conditions, but felt that this risk was acceptable given the potential for the probe to reduce personnel costs, and to capture the bromide breakthrough period accurately.

Due to the problems encountered with the bromide specific ion electrode, results of the first two bromide tracer experiments could not be used to assess bromide transport to the spring. The third bromide tracer test, conducted in conjunction with the microsphere bead release, was initiated on February 28, 2000. Approximately 4.5 g of bromide (as NaBr) were injected just below the soil surface of the spiking area. Over the next five months (March 1, 2000 to August 1, 2000) 164 water samples were collected and analyzed for bromide using ion chromatography. Water samples were obtained from monitoring wells 1 and 2 (84 samples), the FTC (15 samples), and the Sigma sampler (65 samples) at regular intervals. Water samples obtained from the zero-tension lysimeters (ZTLs) were not analyzed for bromide due to the small volume of water collected, the rinsing procedure used to recovery microspheres, and the fact that no ZTL samples were collected from May to August 2000 due to the dry conditions.

Bromide concentration data for Monitoring Well 1 (MW1) and the spring water are shown in Figures 4.17 and 4.18, respectively. Monitoring Well 1 was located just down gradient from the location of the microsphere and NaBr spiking area. For MW1, a small spike in bromide concentration occurred on 4/25/00, while a second and larger spike occurred on the 6/20/00 and 6/23/00 sampling dates (see Figure 4.17). The second bromide spike corresponds to a relatively large rainfall event (3.5 cm) that occurred after a period of prolonged dry conditions (see Figure 4.4). Elevated bromide concentrations were observed in the spring water on 7/5/00 and 7/7/00, approximately 14 days after those observed in the MW1 (see Figure 4.18). If one assumes that these bromide spikes observed in MW1 and spring are related (i.e., represent the same pulse of bromide moving through the domain) the interstitial (pore-water) groundwater velocity would be approximately 0.65 m/day (2.1 ft/day). Using a hydraulic gradient of 0.055 m/m, obtained from the piezometric surface observed on 6/12/00 (Figure 4.10D), and assuming a porosity of 0.33 m^3/m^3, the resulting saturated hydraulic conductivity (K_s) calculated from Darcy's Law would be approximately 38.6 m/day. This value is consistent with the range of hydraulic conductivities reported for silty sands (Freeze and Cherry, 1979), and is similar to the value obtained for ground water underflow (8.23 m/day) estimated by numerical inversion. The discussion above is not meant to be an absolute treatment of the bromide data, but rather serves to illustrate that the coincidental bromide spikes observed in MW1 and the spring water are likely to be related, and

that the estimated travel time of the bromide pulse is consistent with groundwater flow within the domain. Additional treatment of these data is presented in the *Numerical Analysis* section of this chapter.

Microsphere Spiking Experiments

Transport of Microspheres in Soil Water

A total of 1,168 water samples were collected and analyzed for microsphere beads from the various devices, which are summarized in Table 4.3.

Table 4.3

Microsphere beads appearance in water samples

Collecting Method[a]	Location	# Samples Collected	# Samples with Microspheres	Percent Positive
ZTL	30-cm	10(5/5)[b]	7(5/2)[b]	100/40
ZTL	60-cm	10(5/5)[b]	4(2/2)[b]	40/40
ZTL	90-cm	12(5/7)[b]	8(5/3)[b]	100/42.9
MW1	7-m to spring	56	9	16.1
MW2	12-m to spring	46	7	15.2
FTC	At spring	35	8	22.9
Sigma	At spring	999	23	2.3

[a] ZTL (zero-tension lysimeter); FTC (Flow through centrifuge); Sigma® (sampler)

[b] In parenthesis are numbers for ZTLs inside/outside spiking area

Samples collected at the spring with the Sigma samples were 999. Thirty-two samples were collected from ZTLs, of which 15 came from inside and 17 outside the spiking area. The percentage of ZTL samples that contained microspheres at some point in time varied from 40% to 100%. All 5 samples from the 30-cm ZTL inside the spiking area had some microspheres,

while 40% of those from 30-cm ZTL outside the spiking area were positive for microspheres for at least one sampling date. The five samples each from the 60-cm ZTLs inside and outside the spiking area were 40% positive for microspheres. Of the 12 samples from the 90-cm ZTLs, 5 were from inside and 7 from outside the spiking area, and were 100 and 42.9% positive, respectively, for microspheres. The number of microspheres counted in the ZTL samples ranged from 0 to 232,642. The high count was observed on March 20, 2000, in the 30-cmm ZTL within the spiking area. A much lower count (1,547) was obtained on March 21, 2000 from the 90-cm ZTL within the spiking area. These initial findings indicated that the microspheres migrated downward through the unsaturated zone beneath the spiking area, primarily as a result of the 30-mm rainfall on March 20, 2000. This rainfall event was the first of that magnitude after the February 28, 2000 injection of microspheres into the surface soil. Samples obtained from the ZTLS were generally very small (a few milliliters). After the samples were collected, the ZTLs were further flushed with deionized water to ensure recovery of all microspheres. No samples were collected from the ZTLs between May 2000 to August 2000 due to the dry conditions.

Funding ran out in August for the student worker responsible for manual monitoring and collection of samples. ARS, using their own resources, collected samples from the ZTLS on 11/21/2000 and 02/07/2001. The November 2000 samples contained 1151, 865, 568 microspheres from the 30-cm inside and outside the spiking area, and 90-cm inside spiking area ZTLs, respectively. The other November samples contained from 0 to 30 microspheres. All of the February samples from the ZTLs inside the spiking area contained relatively high numbers of microspheres; 5358, 280, 729, from the 30-cm, 60-cm, and 90-cm ZTLs, respectively. The sample obtained from the 30-cm ZTL outside the spiking area contained 492 microspheres. The precipitation recorded in November 2000 and December 2000 was just above the long-term monthly average. These data indicate that a portion of microspheres still remaining near the surface soil migrated through the soil profile under the favorable soil water conditions following the November and December 2000 rainfall events.

A total of 102 water samples were collected (see Table 4.3) from the two monitoring wells: 56 from the one near the spring (MW1) and 46 from the second one (MW2). Respectively 9 and 7 of these samples had microspheres. The maximum number of microsphere observed in MW1 and MW2 were 5 (10 beads/L) and 3 (6 beads/L), respectively. A total of 35 flow-through centrifuge (FTC) samples were analyzed for microspheres between March 29, 2000 and August

1, 2000. Of these, 8 samples contained microspheres. The largest number of microspheres observed was 5 (0.17 beads/L) from the sample obtained on March 29, 2000. The largest number of samples analyzed for microspheres were obtained from the Sigma sampler. ARS continued to collect and process samples after August 2000 for microspheres enumeration at Georgia Tech. A total of 999 samples were analyzed between 3/20/00 and 11/13/2000. Bead counts ranged from 0 to 12 (60 beads/L) per sample, with 23 positive samples. In summary, these data clearly indicate that a small number of beads migrated through the unsaturated zone to the shallow water table, perhaps via preferential flow paths, and subsequently appeared in the spring water. It should also be noted that substantial retention of beads by the soil matrix was anticipated based on the results of column studies reported in the literature and performed in the laboratory at Georgia Tech.

Retention of Microsphere Beads

Destructive soil sampling was conducted on August 10, 2000 to assess microsphere transport, both vertically and laterally, within the soil profile. Four soil cores were collected inside the spiking area, and two additional cores were collected immediately down gradient (west) from the spiking area. Soil samples were collected using a Giddings soil coring probe, and contained inside butyrate plastic liners (2.2 cm i.d. x 122 cm length). The cores were sectioned into increments ranging from 2-cm to 10-cm in length, with the smallest increment applied to the upper 12-cm of cores obtained from within the spiking area. Microsphere beads were extracted from soil core samples following the procedure described in Chapter 2, although repeated washes with the sucrose solution were required for samples containing large numbers of beads.

The total number of beads recovered from each of the spiking area cores ranged from 1.82×10^6 to 12.0×10^6 beads. Approximately 20 billion (2.025×10^{10}) microsphere beads were applied just below the surface of the spiking area (152 cm x 76 cm), yielding an average delivery concentration of 1.75×10^6 beads/cm^2. Based on the inside diameter of the butyrate core liner (2.2 cm), and assuming a completely uniform application and vertical (downward) migration, each core extracted from the spiking area would contain a maximum of approximately 6.65×10^6 beads. Although bead recovery varied considerably with position, the average number of beads

recovered from the soil cores (7.2×10^6) was consistent with the application rate. The distribution of microsphere beads (# beads/g soil) with depth is shown in Figure 4.19 for the spiking area cores. These data clearly illustrate that the majority of beads were retained within the upper 10 cm of the soil profile, although it must also be recognized that beads were observed in all core increments. The observed trends in bead distribution with depth at the field scale was remarkably similar to the results obtained for the laboratory column studies, which are discussed below.

For the soil cores collected outside the spiking area very few beads were observed. Soil cores 4 and 5, collected approximately 1 m west of the spiking area (toward the spring), contained 24 and 15 beads, respectively. All of the beads in core 5 were located in the upper 2 cm increment, while the beads in core 4 were found in the upper 10 cm of the boring, with 13 beads in the upper 2-cm increment. The sixth core, collected between piezometer number 5 and number 6 and approximately 4 m from the spiking area, contained no beads. These findings suggest that lateral migration of the beads was minimal, and most likely resulted from surface erosion and lateral transport, or cross-contamination during application and subsequent sampling.

Laboratory Column Experiments

Non-reactive Tracer Studies

A series of one-dimensional (1-D) soil column experiments was conducted to investigate transport and retention processes influencing the fate of *Cryptosporidium parvum* oocysts in porous media, using fluorescent microsphere beads as a surrogate. The column experiments were specifically designed to evaluate the effects of pore-water velocity and soil properties on microsphere retention and transport, and to evaluate mathematical models to describe these processes. The properties and flow conditions of each soil column are summarized in Table 4.4.

Page missing from thesis

Prior to introducing microspheres, a non-reactive, conservative tracer study was performed for each soil column. In these experiments, a pulse (~1.5 pore volumes) of 0.01 M KI solution was flushed through the soil column at a constant flow rate, followed by 2.0 pore volumes of background electrolyte solution (0.01 M KCl). Representative tracer breakthrough curves (BTCs) for each solid phase, plotted as relative concentration (C/C_o) versus dimensionless pore volumes, are shown in Figure 4.20. The tracer BTCs obtained for 20-30 mesh and F-70 Ottawa sands were symmetrical in shape, with solute breakthrough at 1.0 pore volume corresponding to a relative concentration of approximately 0.5. Both of these observations are indicative of ideal transport of a non-reactive solute. Therefore, a simplified form of the 1-D advective-dispersive reactive (ADR) solute transport equation, which assumes local equilibrium, linear sorption, and homogeneous conditions, was used to describe these data. In dimensionless form, this 1-D ADR transport equation may be written as:

$$R_F \frac{\partial C^*}{\partial pv} = \frac{1}{Pe} \frac{\partial^2 C^*}{\partial X^2} - \frac{\partial C^*}{\partial X} \tag{4.3}$$

and

$$R_F = 1 + \frac{\rho_b K_D}{\theta}; C^* = \frac{C}{C_0}; pv = \frac{vt}{L}; Pe = \frac{vL}{D_H}; X = \frac{x}{L} \tag{4.4}$$

where, R_F = the retardation factor

ρ_b = soil bulk density (g/cm^3)

K_D = the linear distribution coefficient (mL/g)

θ = volumetric water content (cm^3/cm^3)

C* = the relative solute concentration (mg/L)

C = measured solute concentration (mg/L)

C_0 = influent solute concentration (mg/L)

pv = dimensionless pore volumes

v = pore-water (interstitial or seepage) velocity (cm/hr)

t = time (hr)

L = the column length (cm)

Pe = the Peclet number

D_H = the hydrodynamic dispersion coefficient (cm^2/hr)

X = dimensionless distance

x = distance along the column (cm).

The CXTFIT program (ver 2.0, Toride et al., 1995) employs a least-squares procedure to fit the experimental BTC data to the 1-D ADR equation. This approach was used to obtain values of R_F and Pe for the 20-30 mesh and F-70 Ottawa sand non-reactive tracer experiments. The fitted parameters are summarized in Table 4.5, while the solid lines shown in Figure 4.20 represent the simulated BTCs.

Table 4.5

Column parameters for non-reactive tracer experiments

Column Parameter	Column OS1	Column OS2	Column OS3	Column OS4	Column OS5	Column OS6	Column F71	Column F72	Column CL1	Column CL2	Column CL3
Flow Rate (mL/min)	1.0	1.0	2.5	2.5	5.0	5.0	5.0	5.0	5.0	5.0	7.5
Influent KI Conc. (mg/L)	1660	1630	1680	1670	1650	1660	1650	1630	1700	1620	1700
Pulse Width (mL)	161.3	160.9	149.3	145.0	161.2	153.4	149.9	150.0	160.9	195.9	210.4
Pe	212.7	227.5	213.0	211.6	204.9	224.3	167.3	137.5	76.1	91.8	38.5
D_H (cm^2/hr)	0.67	0.63	1.62	1.68	3.47	3.17	4.25	5.17	7.61	6.31	14.04
Dispersivity (cm)	0.070	0.067	0.070	0.071	0.072	0.067	0.090	0.109	0.197	0.163	0.260
R_F	1.02	1.00	0.99	0.98	1.00	1.00	1.02	0.99	1.00	1.00	1.00
ω									0.17	0.24	0.26
α_m (hr^{-1})									0.19	0.27	0.65
β									0.66	0.79	0.80
θ_m (cm^3/cm^3)									0.28	0.34	0.37

The values of R_F ranged from 0.98 to 1.02, which is expected for a non-reactive tracer. The Peclet numbers for 20-30 mesh Ottawa sand ranged from 205 to 228, which corresponds to dispersivities of 0.067 to 0.072 cm. The Peclet numbers obtained for F-70 Ottawa sand were slightly lower, yielding dispersivity values of 0.09 and 0.11 cm. The latter result was anticipated given the smaller median grain size and wider grain size distribution of F-70 Ottawa sand.

In contrast to the Ottawa sands, early breakthrough of the non-reactive tracer and tailing were observed for the columns packed with Cecil soil. This behavior is indicative of physical nonequilibrium (i.e., diffusion-controlled), which typically results from the presence of immobile water. Early appearance of tracer in the column effluent occurs because not all of the pore water is directly influenced by advective flow, while tailing along the distal portion of the BTC results from rate-limited mass transfer of the solute from regions of immobile water back into the mobile (flowing) water. Consequently, the non-reactive tracer BTC data obtained for Cecil soil were described using a two-region (mobile-immobile water) nonequilibrium form of the 1-D ADR transport equation (Toride et al., 1995). In this form, the following two dimensionless terms are incorporated into Equation 4.3:

$$\omega = \frac{\alpha_m L}{q} \tag{4.5}$$

$$\beta = \frac{\theta_m + f\rho_b K_D}{\theta + \rho_b K_D} = \phi_m \frac{R_m}{R_T} \tag{4.6}$$

where α_m = the solute mass transfer coefficient between mobile and immobile water (1/hr)

θ_m = volumetric content of mobile water (cm^3/cm^3)

f = the fraction of solid phase in contact with the mobile water

Φ_m = the ratio of mobile water to immobile water

R_m = the retardation factor for the mobile water

R_T = the total (equilibrium) retardation factor.

For the case of a non-reactive tracer, the retardation factor is 1.0 regardless of location, and therefore $\beta = \Phi_m$. The values of ω obtained for the three Cecil soil column experiments ranged from 0.17 to 0.26, which corresponds to a mass transfer coefficient (α_m) of 0.19 to 0.65

1/hr. The value of β or in this case the fraction of mobile water (Φ_m), ranged 0.66 to 0.80. Although the extent of physical nonequilibrium was relatively minor based on the observed values of β and ω, such behavior was not initially expected because the Cecil soil was air-dried and sieved to pass a 20-mesh screen prior to packing. These pretreatments would tend to reduce the size and number of soil aggregates, which could potentially contain regions of immobile water. However, the Cecil soil non-reactive tracer experiments were conducted at relatively high flow rates (5.0 and 8.1 mL/min), corresponding to pore-water velocities of 37 and 54 cm/hr. Given that the columns were only 10 and 15 cm in length, such high water velocities would accentuate mass transfer limitations between regions of mobile and immobile water.

Microsphere Bead Transport and Retention

Following the tracer experiment, a single pulse of microsphere beads was introduced into each soil column. The concentration of microsphere beads in the influent solution ranged from approximately 2,400 to 3,400 microspheres/mL. The pulse width varied from approximately 400 to 600 mL (4 to 5 pore volumes), which was followed by approximately 775 to 1400 mL (6 to 14 pore volumes) of background solution. The column effluent solution was collected continuously in 20-mL vials, which was then filtered and counted for microspheres using an epifluorescence microscope. Upon completion of each microsphere transport experiment, the columns were sectioned into 1.0- to 1.5-cm increments and the microsphere beads were extracted following the procedure described in Chapter 2. The overall recovery of microsphere beads from the solid phase and effluent solution ranged from approximately 53% to 100%. The lowest recovery rates were obtained for columns packed with Cecil soil, although these values are consistent with data reported for *C. parvum* oocyst recovery from fine-textured sands (Harter et al., 2000). Microsphere experimental conditions and recovery rates are presented in Table 4.6.

Table 4.6

Column parameters for microsphere bead experiments

Column Parameter	Column OS1	Column OS2	Column OS3	Column OS4	Column OS5	Column OS6	Column F71	Column F72	Column CL1	Column CL2	Column CL3
Flow Rate (mL/min)	1.0	1.0	2.5	2.5	5.0	5.0	5.0	5.0	5.0	5.0	7.5
Influent Bead Conc. (#/L)	3381	3381	2751	2429	2885	2885	2740	2693	2546	2833	2588
Pulse Width (mL)	451	456	424	447	513	504	423	422	515	544	557
Beads Eluted (%)	0.099	0.22	5.1	3.35	23.6	14.1	0.04	0.02	0.010	0.002	0.009
Beads Retained (%)	100.6	94.2	97.0	102.9	76.5	82.8	97.4	96.1	79.4	53.2	65.2
Bead Recovery (%)	100.7	94.4	102.1	106.3	100.1	96.9	97.4	96.1	79.5	53.2	65.2
Retardation Factor (R_F)	0.82	0.75	0.84	0.83	0.84	1.07					
Filtration Coefficient (λ) (cm^{-1})	0.47	0.41	0.20	0.23	0.14	0.12					
Collision Efficiency (α)	0.80	0.69	0.98	1.13	1.50	1.29					
Collector Efficiency (η)	0.086	0.086	0.030	0.030	0.014	0.014					

The transport and retention of microsphere beads in 20-30 mesh Ottawa sand was evaluated as a function of flow rate. As the applied flow rate was increased from 1.0 mL/min to 5.0 mL/min, the maximum relative concentration (C/C_0) of beads appearing in the column effluent increased from a value of approximately 0.002 to 0.1, respectively. Microsphere bead recovery data shown in Table 3.C3 for 20-30 mesh Ottawa sand also demonstrate that as the flow rate was increased from 1.0 mL/min to 5.0 mL/min, the fraction of beads eluted from the column increased from approximately 0.1% to 23.6%.

The effluent microsphere BTC data for 20-30 mesh Ottawa sand were fit to a modified form of the 1-D ADR transport equation, which incorporated a filtration term:

$$\frac{\partial C_w}{\partial t} + \frac{\rho_b \partial C_s}{\theta_w \partial t} = D_H \frac{\partial^2 C_w}{\partial x^2} - v_x \frac{\partial C_w}{\partial x} - v_x \lambda C_w \qquad (4.7)$$

where w and s = subscripts corresponding to the aqueous (water) phase and the solid phase concentration, respectively

λ = the colloid filtration coefficient (1/cm).

The expanded form of the colloid filtration coefficient term is defined in Chapter 3 (Equations 3.15 and 3.16). The BTC data shown in Figure 4.21 were fit to Equation 4.7 using the CXTFIT program (ver. 2.0 Toride et al, 1995), for which the first-order decay term, μ, was replaced with $v_x\lambda$ to yield dimensions of time^{-1}. The fitted parameters obtained in this manner (i.e., retardation factor and filtration coefficient) are given in Table 4.6. In all cases, except Column OS6, the fitted retardation factors were less than 1.0, indicating that the microsphere beads traveled more quickly through the columns than the non-reactive tracer. The faster travel time of microsphere beads is consistent with data reported by Johnson et al. (1995), who attributed this behavior to: a) not all pores are accessible to the colloid-size particles and b) colloid-size particles are excluded from the margins of the pore volume. As expected from the effluent concentration data, the colloid filtration coefficient (λ) decreased from 0.47 1/cm to 0.12 1/cm as the flow rate was increased from 1.0 mL/min to 5.0 mL/min.

Based on the median grain size of the solid phase and the collector efficiency (given in Table 4.6), the collision efficiency, α_c, for each column was calculated using Equation 3.15.

The collision efficiency term was strongly dependent on flow rate, and exceeded the theoretical maximum value of 1.0 at flow rates of 2.5 mL/min and 5.0 mL/min. A collision efficiency of greater than 1.0 was also reported by Harter et al. (2000) for *C. parvum* oocysts in a medium sand (d_c = 0.05 cm) at a pore-water velocity of 62 cm/hr. In theory, the collision efficiency term is a correction factor applied to the single collector efficiency (Equation 3.16) in order to account for repulsive forces at the solid surface, which would act to reduce colloid attachment. However, the influence of ionic strength on collision efficiency has been shown to be negligible at ionic strengths above 0.001 M (Jewett et al. 1995), and thus was not considered to be an important factor in the column experiments reported herein (I = 0.024 M). Differences between idealized filtration theory (Equation 3.16) and conditions of the actual porous medium, such as surface roughness or surface charge heterogeneity, could lead to enhanced particle straining. However, the strong dependence of collision efficiency on pore-water velocity suggests that the collector efficiency did not entirely represent velocity-dependent filtration processes for the system investigated in these studies.

The distribution of microsphere beads within the 20-30 mesh Ottawa sand columns was also strongly dependent on flow rate (Figure 4.22). At the highest flow rate (5.0 mL/min), beads were distributed throughout the column, while at the slowest flow rate (1.0 mL/min) almost all the beads were retained within the first 8 cm of the column. The distribution of microsphere beads retained within 20-30 mesh Ottawa sand was described using filtration theory. Assuming steady-state conditions ($\partial C_w/\partial t = 0; \partial C_s/\partial t = 0$), and minimal hydrodynamic dispersion, Equation 4.7 may be rewritten as:

$$\frac{\partial C_w}{\partial x} = -\lambda C_w \tag{4.8}$$

Integrating Equation 4.8 with respect to distance (x) yields the following expression:

$$\frac{C}{C_0} = e^{(-\lambda x)} = e^{\left(-\frac{3(1-\theta_w)}{2d_c}\alpha\eta x\right)} \tag{4.9}$$

Comparisons between the actual and predicted relative concentration of microsphere beads within the 20-30 mesh Ottawa sand columns are shown in Figure 4.23. The colloid filtration

coefficients (λ) used to obtain these predictions were derived independently from the effluent BTC fitting procedures described above. In effect, these graphs illustrate the number of beads remaining in solution over the length of the column. Therefore, at higher flow rates the C/C_o values are larger near the column inlet and decrease gradually with column length. The rather close agreement between the measured and predicted values indicates that the filtration theory yields reasonable estimates of both microsphere transport and retention in 20-30 mesh Ottawa sand, provided that the filtration coefficient is allowed to vary with velocity.

A comparison of microsphere bead BTCs for columns packed with 20-30 mesh Ottawa sand, F-70 Ottawa sand and Cecil soil, at a flow rate of 5.0 mL/min, are shown in Figure 4.24. The number of beads eluted from both F-70 Ottawa sand and Cecil soil over the course of each column experiment was minimal. As a result meaningful comparisons between measured effluent data and model predictions of bead transport were not possible. Even at a flow rate of 5.0 mL/min, the fraction of beads eluted from the F-70 and Cecil soil columns was less than 0.04% (Table 4.6). In addition, the distribution of microsphere beads within F-70 Ottawa sand or Cecil soil columns was limited to approximately 2 cm from the column inlet (Figure 4.25). These findings suggest that vertical migration of microsphere beads through fine-textured soils is likely to be minimal; limited to a very small number of particles traveling through preferential flow paths which were not present in the repacked soil columns.

HYDROLOGIC/TRANSPORT NUMERICAL ANALYSIS

One-dimensional modeling of flow and transport

Model calibration

Model calibration was performed in three stages; inverse modeling to obtain soil hydraulic parameters, forward modeling for 243 days to establish initial soil water conditions prior to solute transport experiment, forward modeling for the remaining 187 days after introduction of solute. Using soil water content data collected from five depths at Location 4 (immediately adjacent to the spiking area) as the sole auxiliary variable, HYDRUS-1D was used to simulate the transient soil water conditions to a degree of accuracy ($r^2 = 0.859$, $\Phi(b,q) =$

0.1418, mass balance error = 0.19 %) consistent with the input data. Figure 4.26 shows time series of soil water contents from July 1, 1999 to December 31, 1999, periodically measured with the TDR and simulated using HYDRUS-1D. The fitted (lines) capture the general behavior of soil water gain due to precipitation and water loss due to percolation and root uptake, using the van Genuchten parameters listed in Table 4.2. This 186-day period was selected because it encompassed the very dry conditions experienced during the summer of 1999, and the wetter periods recorded during the late Fall and early Winter. Large variations in water content provide a more robust data set for inversion modeling, compared to one where changes in water content are minimal.

Due to limitations of the inverse module of HYDRUS-1D, only 15 parameters can be designated as fitted in any one simulation. A four-layer model, with five variables (e.g., θ_r, θ_s, α, n, and/or K_s) yields 20 variables to be potentially fitted. Therefore, values of α, n, and K_s were fit first using initial values taken from Table 4.1, while holding θ_r and θ_s constant. This was done because the general shape of a retention curve is governed by α and n. The K_s variable in the conductivity function is coupled to n ($m = 1 - 1/n$), but the correlation between these two would not degrade the final paired values, only increase the time for convergence (Durner et al., 1999). By fitting these 12 variables first, and maintaining water mass balance, good estimates of the general shape of the curves can be obtained. Once established, values of θ_r, θ_s and n were fit simultaneously, while both n and K_s were kept constant. The strongest correlation among variables was limited to θ_r and θ_s because the model maintains water mass balance; thus, the difference in available moisture (e.g., $\theta_s - \theta_r$) will be approximately constant regardless of the magnitude.

It is apparent that the shallower soils responded more quickly and at a larger amplitude than the deeper soils. For example, a total of 7.14 cm of precipitation was recorded during a series of rainfall events that occurred between Days 54 and 56. Increases in water content were recorded with the TDR in successively deeper soils from Day 54 through 57, and an almost identical pattern was simulated with HYDRUS-1D.

To evaluate this trend more objectively, the time series of water content residuals ($\theta_{observed} - \theta_{predicted}$) are presented for each of the five depths listed on the plots (Figure 4.27). These plots are presented to determine if a systematic bias existed in the residuals, which would indicate a poorly chosen set of van Genuchten parameters for one or more of the soil layers.

Mean and slope values should be close to zero, indicating no systematic bias or trend, and normally distributed errors. Calculations showed that average residuals for the 7.5, 22.5, 45, 75, and 115 cm depths were 0.008, -0.010, 0.005, -0.009, and -0.003 cm^3 cm^{-3}, respectively, and the largest absolute value of the slope was 5.0 x 10^{-4}. Both of these measures are close to zero. However, though the trend is close to zero in each case, the value is greater than zero in 4 of 5 cases, indicating some serial correlation. To study the strength of this correlation, the residuals were analyzed using a Pearson Test for Serial Independence (McCuen, 1993), and found that residuals in Layers 1, 3 and 5 do contain some serial correlation at all significance levels below 5%, but that Layer 1 failed the null hypothesis by a very narrow margin. Nonetheless, with the slope values very close to zero, we believe that the practical significance of correlation in the residuals is very low and not indicative of a systematic problem with the model or the van Genuchten parameter sets.

Comparing manually-collected data with daily resolution (at best) with HYDRUS-1D, where time increments were approximately 90 minutes is not simple or entirely valid. Moreover, it is important to note that average water content measurements, taken of either 15-cm or 30-cm thick sequences, are compared to point measurements obtained with the model. Although data are compared from mid-points in the TDR probe, dynamic behavior of water movement near the surface occurs at resolutions much smaller than 15 cm. Nonetheless, given the limitations of the observed data, the geometry of the soil layers, and the estimated parameter sets, adequately represent field conditions.

Water movement and particle transport during extreme events

The drought conditions under which the microsphere transport experiment was conducted likely reduced the penetration depth into the soil, and the potential for preferential movement of microspheres through large soil pores and to the water table. Nonetheless, it has been observed that *E. coli* concentration is flow-rate dependant (Fisher et al., 2000), and it was shown herein that spring flow rate was positively correlated to increases in soil water and groundwater storage. These observations imply that high antecedent water content promotes the movement of pathogens toward the spring.

To test this hypothesis in a more rigorous manner, a series of model simulations were undertaken for two different soil profiles, and for a series of increasing antecedent water storage values. The goal of these model simulations was to evaluate the significance of internal drainage of water toward the water table, and potential movement of pathogens, given different initial and boundary conditions. From a field management standpoint, it would be beneficial to consider these conditions when deciding on grazing schedules, and their potential impact on subsurface transport of microorganisms.

HYDRUS-1D was run in a forward mode for these calculations, using precipitation that varied from 0, 1, 2.5, 5.0, 10.0, and 15.0 cm. Soil layering was taken as either a) the profile characteristics (layer thicknesses, hydraulic properties) at W2 or b) a three-layer profile dominated by sandier soil. Initial and boundary conditions were as follows:

$$\psi(z,t) = \psi_i(z) \qquad t = t_o \qquad (4.10)$$

$$K(\psi)\left(\frac{\partial \psi}{\partial z} + 1\right)_{z=0} = P_i \qquad 1 \le t < 2 \qquad (4.11)$$

$$K(\psi)\left(\frac{\partial \psi}{\partial z} + 1\right)_{z=0} = 0 \qquad 2 < t \le 10 \qquad (4.12)$$

$$q_{z=0} = K(\psi) \qquad (4.13)$$

where $\psi_i(z)$ = initial soil water potential

P_i = precipitation that varies from 0 to 15 cm/d

z = depth in the profile (0 is top of profile and -150 cm is bottom of profile)

Equation 4.13 represents a free-drainage condition with a unit hydraulic gradient. Water mass balance was taken at the bottom of the profile and accounts for flow passing the bottom plane.

The initial soil water potential ($\psi_i(z)$) was obtained by conducting a separate model simulation using a constant flux upper boundary for six different flux rates varying between 5 x

10^{-4} and 0.25 cm/d. A steady-state soil profile in water potential is established when deep drainage equals precipitation. The SWS was obtained by integrating the steady-state water contents with depth, similar to the function inside the parentheses on Equation 2.2, which was then read into the transient model described by Equations 4.10 through 4.13. The simulation period was held to eight days after cessation of precipitation. This rather short period was employed because field observations have shown that increases in spring flow rates can occur within hours of precipitation when high antecedent water contents existed, and thus it was the intention to evaluate short-term drainage.

Solute transport was also incorporated into this analysis. The purpose of adding a solute was to evaluate whether or not the potential for rapid downward migration was dependent on the antecedent water content conditions in the soil profile. Solute transport was simulated by placing a unit concentration of an ideal tracer (e.g., bromide) at 5.0 cm below ground surface, and simulating transport during and after precipitation. The placement depth for the solute was approximately the same as the microsphere and bromide injection at the field site. Migration of the "plume" was evaluated by recording the depths of maximum concentration, and the down gradient edge of the solute front (e.g., relative concentration (C/Co) = 0.01). Darcian flow was assumed throughout the soil profile (e.g., no preferential flow pathways), along with homogeneity and isotropy within each layer (e.g., no physical heterogeneities that would promote diffusion into immobile water regions). The former assumption will decrease penetration depth, while the latter assumption will increase penetration depth. Nevertheless, the simplifyied flow system will provide valuable information regarding ideal transport under these conditions.

Figure 4.28 shows iso-drainage contours of water flow to the water table as a function of antecedent water storage (SWS_i) for the soil characteristics at W2. These results show the initial SWS conditions for which deep drainage is essentially zero for most precipitation events (e.g., $SWS_i < \sim 29$ cm), and those conditions when even small events will produce some drainage ($SWS_i > \sim 32$ cm). The top portion of the plot provides the equivalent average water content for the profile. An important parameter is soil water holding capacity, which is marked by the vertical line at $SWS_i = 31.7$ cm ($\theta_v = 0.211$ cm^3 cm^{-3}). At this level, the soil profile is saturated, so that any new water falling upon the soil surface causes an equivalent displacement at the bottom of the profile. These conditions were encountered during this study in the late Winter

and early Spring when evapotranspiration was lowest, and when the spring flow rate was highest. For example, Figure 4.8 shows elevated soil water storage until about Day 100, when the values begin decreasing steadily, and Figure 4.6 shows a significant decrease in spring flow rate (specifically interflow) at the same time. These results indicate the potential for "calibrating" the soil profile so that conditions that would promote deep drainage are understood, and management steps can be taken if needed.

The migration of the ideal solute during these precipitation events, given the same initial and boundary conditions is shown in Figure 4.29. Clearly, the movement of the solute peak was independent of the SWS_i, and was influenced only by precipitation. These results indicate that solutes subject to Darcian flow and ideal transport likely will not result in rapid downward transport. Rather, processes not addressed by HYDRUS-1D, specifically preferential flow or other types of soil bypass flow, could result in more rapid downward transport. Indeed, many of the occurrences of *C. parvum* contamination of groundwater were directly tied to transport along preferential flow pathways.

Iso-drainage contours for a three-layer, two-material soil profile (sandy loam, sand, sandy loam in 50-cm thick layers) are shown in Figure 4.30. Maximum precipitation for this soil was 10 cm, given the significantly lower water holding capacity of the profile versus the W2 case, and the higher recorded drainage. It is apparent that internal drainage will occur under wetted conditions even without precipitation, and that internal drainage will be initiated under lower rainfall conditions than in the W2 profile. The sandier soil led to a lower water holding capacity of approximately 26.4 cm, or equivalent to a $\theta_v = 0.159$ cm^3 cm^{-3}, which is at the limit of the x-axis. These two profiles respond differently with respect to water holding capacity and conditions that would lead to downward drainage.

Field Methodologies Used for Microsphere Collection

Two field sampling techniques were used in this study that warrant special discussion. Both provided a means of collecting water samples that improved the potential identification of microspheres in the water samples during the field transport study.

Zero-tension lysimeters

The zero-tension lysimeters (ZTLs) were installed in the soil directly below the spiking area for microspheres and bromide. The ZTLs were chosen for this study because they are designed to allow the passage of colloid-sized particles through a mesh with 150 μm openings. Conventional soil pore water samplers are typically made of porous ceramic or stainless steel with openings of between 0.5 and 20 μm. Openings of this size would: (1) filter out microspheres at the soil/sampler interface and (2) exceed the bubbling pressure unless the porous material was saturated. Both cases would render the sampler ineffective for the purpose of collecting microspheres. Bulk water samplers, a class of samplers that includes the ZTLs, tend to collect water traveling through larger pores and not through smaller pores. For this study, smaller pore classes were not expected to transmit significant numbers of microspheres; so, this disadvantage was greatly outweighed by the ability to sample microspheres in pore water.

The basic design of the zero-tension lysimeters was modified slightly by the research team from that originally suggested by Thompson and Scharf (1994). In this new design, the floor of the sampler was fabricated at an angle of 30°, rather than close to 0° in the original design, ensuring that all water collected by the sampler can be withdrawn. Thus, the 1/8 inch tubing that penetrates the outside of the sampler does not need to be sealed, because the upper chamber is now completely isolated from the lower chamber. The design allows additional security from shearing loose the sampling tubing during installation.

The results of the transport studies indicated the limitation and success of the ZTLs. The limitation of the sampler is that very moist conditions are needed before the sampler will collect water. Even with the new sampler design, the unusually dry conditions prevented the samplers from being more effective. The success of the samplers is shown that almost 90% (7 of 8) of samples collected with the ZTLs were found to contain microspheres. Conventional samplers would have yielded zero microspheres. The weather patterns dominating the southern U.S.A. during the Summer 2000 were unfortunate from the standpoint of the field study. Normal rainfall patterns would have promoted better collection of soil water, and hence the potential collection of particles.

Flow-through Centrifuge

As described in Chapters 2, the flow-through centrifuge (FTC) was used for "sampling" large volumes of spring water, without the associated problems of collecting and storing large samples. The centrifuge effectively removed colloid-sized particles (e.g., microspheres) in laboratory conditions. Efficiencies of approximately 99.9%, 83.3%, and 78.8%, were obtained for microsphere collection in the bowl during centrifugation, from original concentrations of 1.0 x 10^5, 1.0 x 10^3, and 1.0 x 10^2 #/L, respectively. The results show that percent recovery was positively correlated to particle concentration, and that even lower concentration mixtures should yield good recovery.

In the field environment, the FTC provided a means of continuously sampling spring water at > 2 L/min for 60 minutes. Assuming that microsphere attachment and detachment processes would randomize the occurrence of microsphere at the spring, the ability to process continuous water samples improved the likelihood of recovery not generally possible elsewhere. To our knowledge, the FTC has been used primarily for collecting colloid and larger-sized sediments in stream environments to evaluate sediment loading (Hayes et al., 1989). The FTC has not been evaluated under the conditions tested in this research study. We believe that the FTC was a valuable tool used in this study, and it could be useful in similar studies where parasite identification and collection are important.

Field Conditions That Would Promote The Transport Of *C. Parvum* Through Soil

Clearly, the experiments conducted at the ARS site during the Summer of 2000 were affected significantly by lower rainfall. As indicated in the results, the rainfall amounts were the lowest in almost 50 years. Given that particles are transported downward into the soil primarily through advective transport using water as the transport medium, it is likely that penetration depth into the soil would be deeper in the presence of higher precipitation, and vice versa. The study results described above show the presence of microspheres as deep at 100 cm in a soil core collected directly below the spiking area. However, even with the unusually low rainfall amounts (30.37 cm from 28 Feb – 30 Aug, representing only 50% of normal precipitation), microsphere transport occurred to a depth that exceeded the depth of collection. It would be

appropriate to surmise that deeper penetration would have occurred under normal, ambient conditions. Using the known positive correlation of *E. coli* with spring flow (Fisher et al., 2000), ground water transport toward the spring would have improved the number of detections in water collected with the flow-through centrifuge and/or sequential sampler.

The HYDRUS-1D transport modeling was conducted to test the hypothesis that conditions of elevated antecedent water storage, coupled with precipitation events, could lead to rapid downward drainage of existing soil water and thus a deeper penetration of tracer (or *C. parvum*) into the soil profile. The results of the modeling clearly showed that each soil profile has a characteristic water holding capacity, above which any appreciable precipitation caused an equal depth of drainage. For soil water conditions below this water holding capacity, precipitation reduced the antecedent water deficit, until that deficit was reduced to zero. After which, drainage occurred.

With respect to the tracer migration, a significant increase in the penetration depth of an ideal tracer as a function of antecedent water content was not seen. Instead, the penetration depth was found to be independent of soil wetness before the onset of precipitation, indicating that the pre-existing water moves ahead of the wetting front, and that mixing in the region of the wetting front probably accounted for most of the differences. It is important to note, however, that these results assume the presence of dissolved constituents rather than constituents in suspension, and that porous media flow dominates (e.g., matrix flow with no preferential flow pathways). Modeling preferential flow pathways requires site characterization and modeling activities that were not within the scope of this study.

Though the field conditions did not allow for a thorough study of preferential flow and transport, it would be safe to expect that near-saturated conditions in a soil with larger macropores would promote the potential for extremely rapid downward transport of solutions and suspensions. Numerous other studies have shown the potential for rapid, non-Darcian transport of ideal tracers under conditions of elevated water storage and precipitation. Indeed, given the results of column transport studies of *C. parvum* in coarse sediments (Harter et al., 2000), where velocity enhancement was quantified as a function of flux rate and grain size (higher flux rates and larger grain sizes led to higher enhancement), there is every reason to expect that these same factors would affect field transport of *C. parvum* as well.

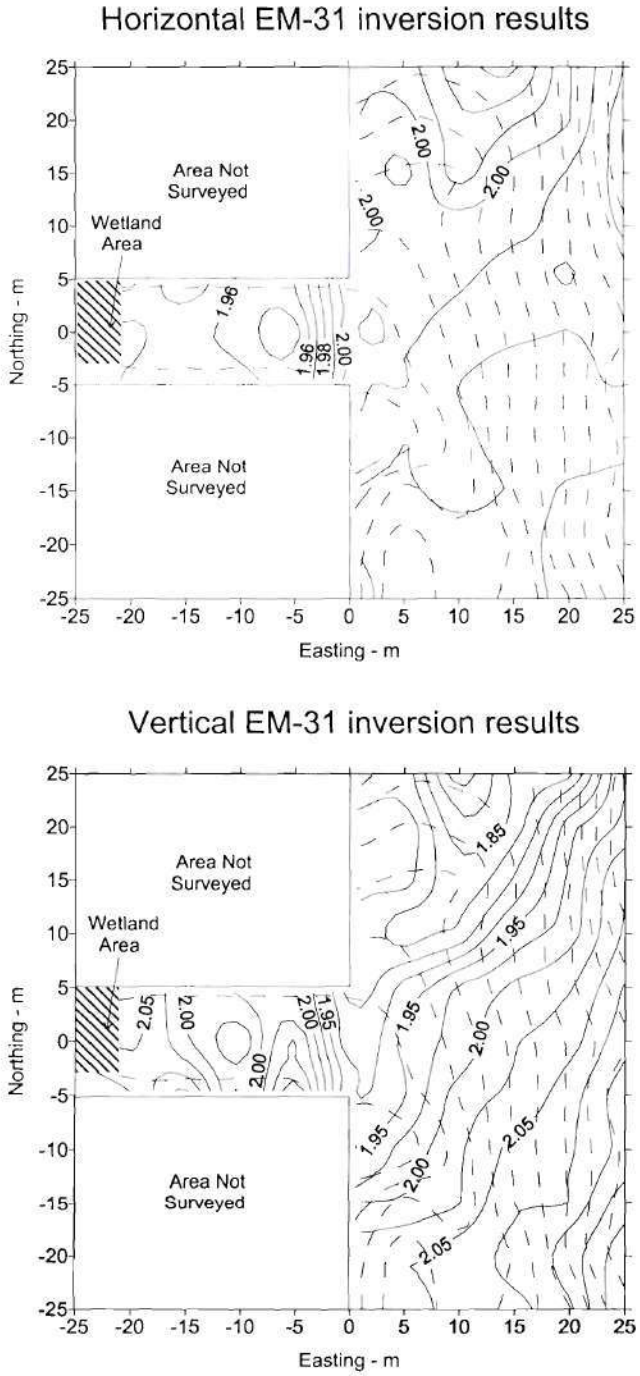

Figure 4.1a Results of numerical inversion analyses of EM-31 data. Solid lines represent depth to critical saturation and dashed lines represent elevation contours. Data assumes that "unsaturated" layer ECa = 1 mS/m and "saturated" layer ECa = 64 mS/m.

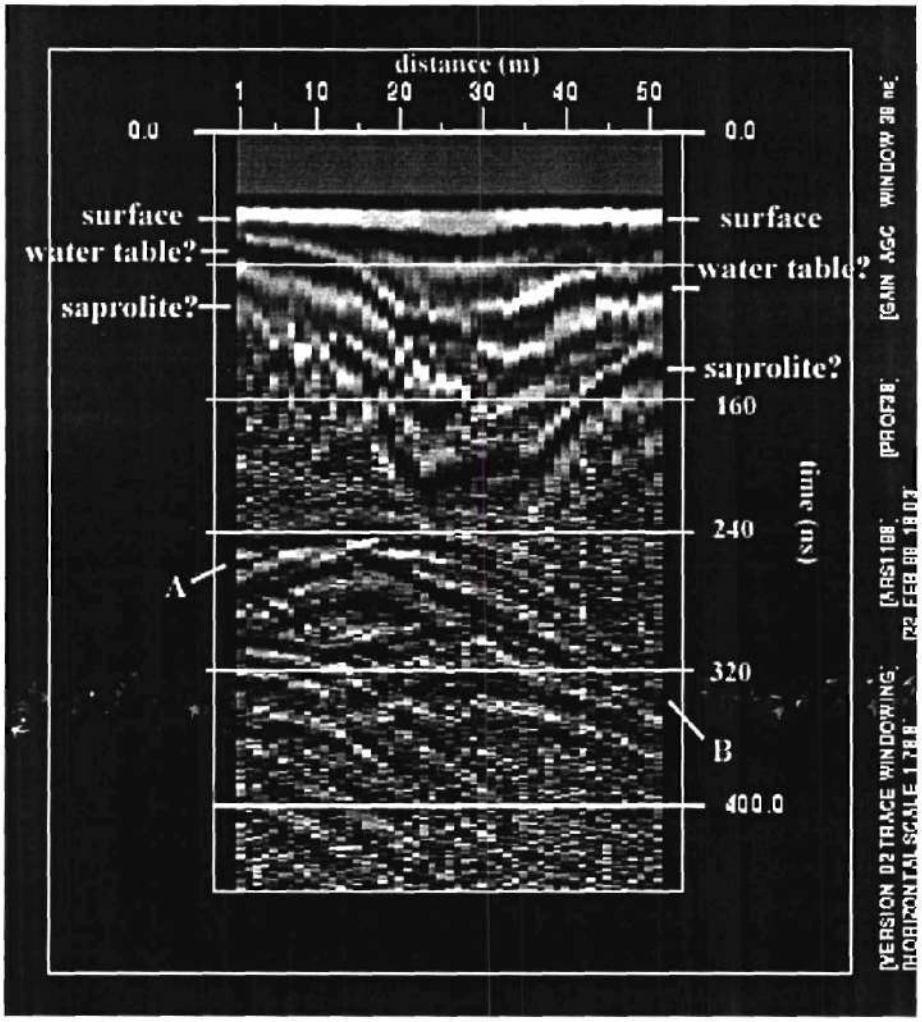

Figure 4.1b Results of GPR survey along the eastern-most portion of the study area. The vertical axis denotes two-way travel time (TWTT) in ns, but we assume that depth to the reflector at 240 ns ≈8 m. Reflectors corresponding to the ground surface, the water table (or the depth to critical saturation), and the saprolite are shown. The hyperbolic reflectors marked A-B will migrate to discrete lens-like features below the saprolite layer.

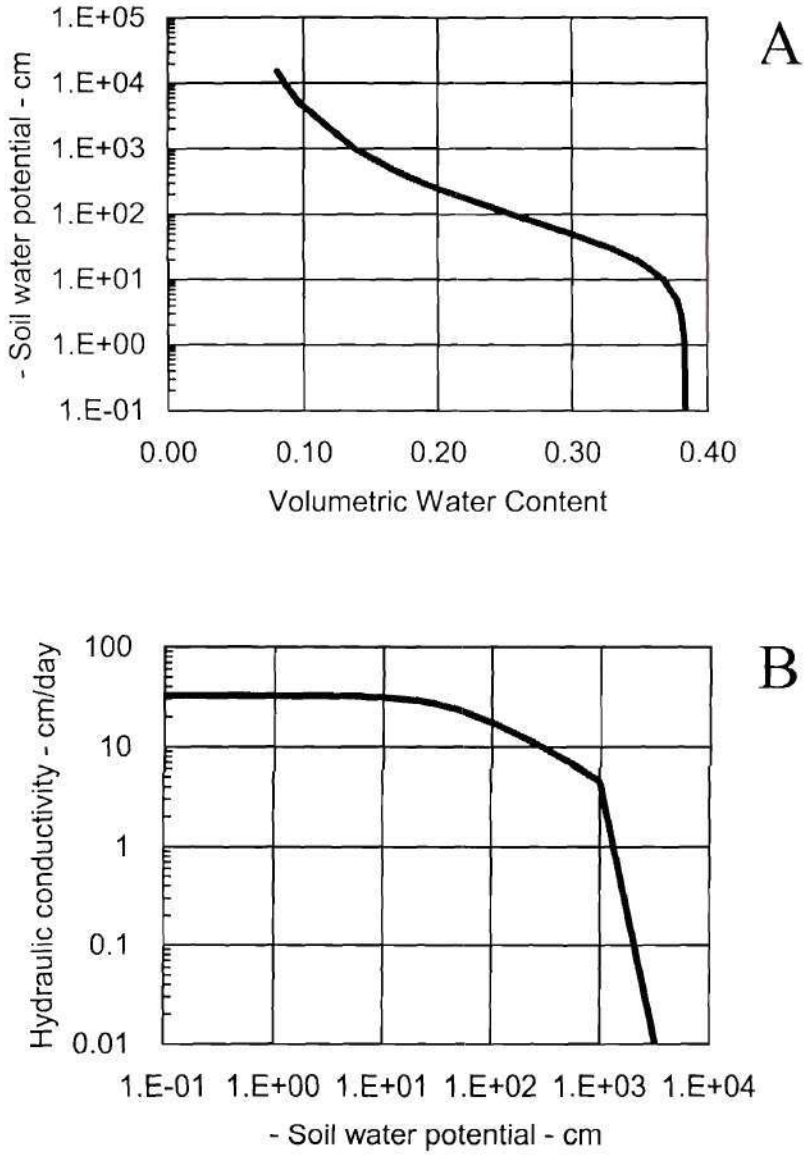

Figure 4.2a Fitted soil water retention (A) and hydraulic conductivity (B) curves for W2 soil collected between 0-15 cm depth.

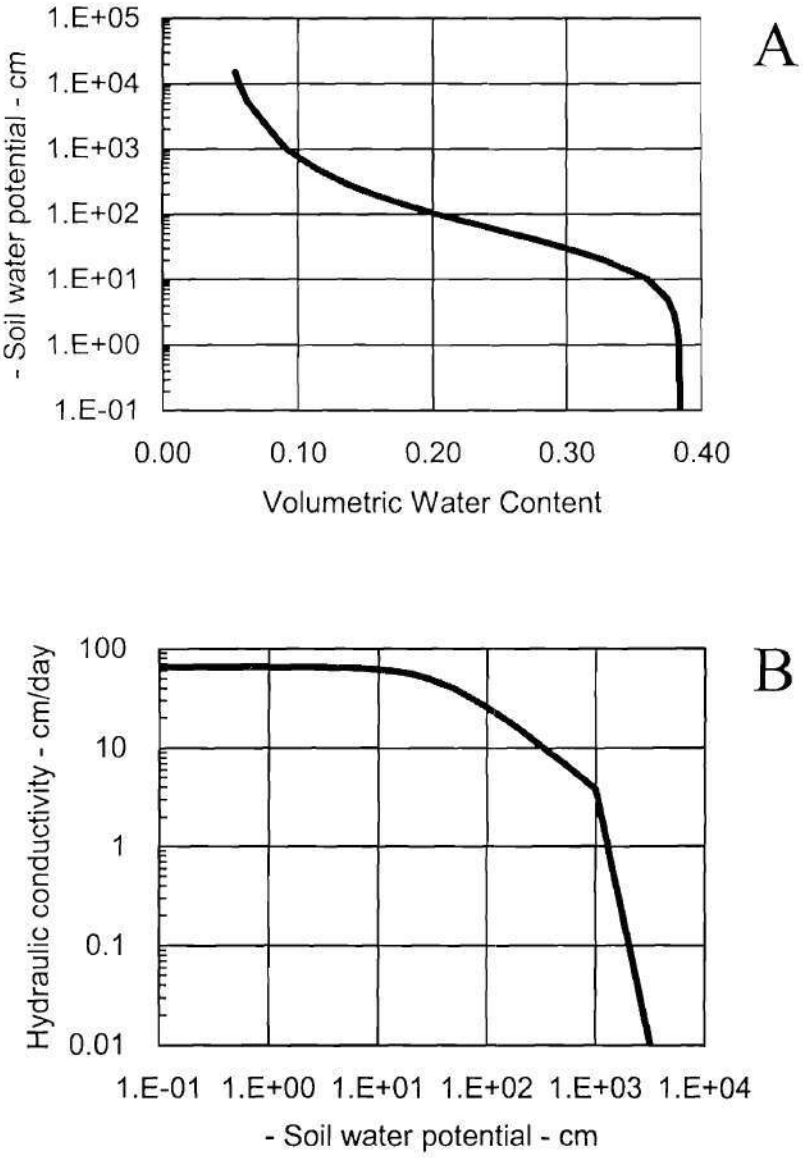

Figure 4.2b Fitted soil water retention (A) and hydraulic conductivity (B) curves for W2 soil collected between 15-30 cm depth.

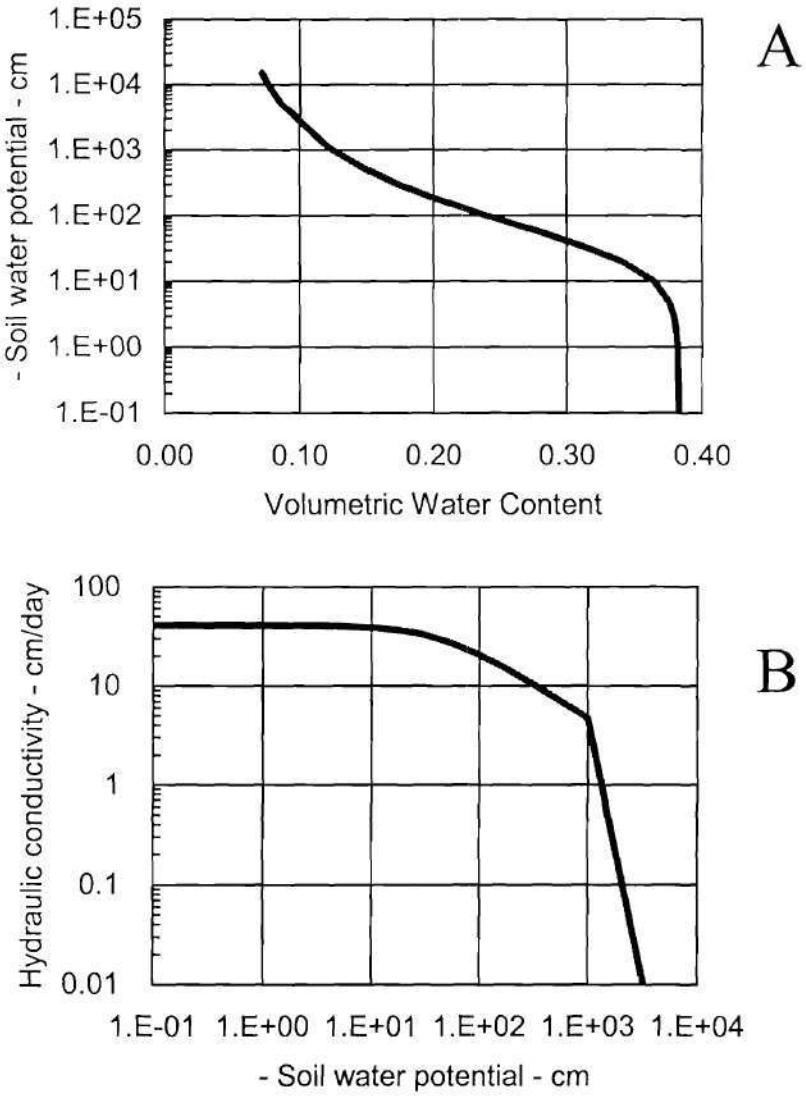

Figure 4.2c Fitted soil water retention (A) and hydraulic conductivity (B) curves for W2 soil collected between 30-46 cm depth.

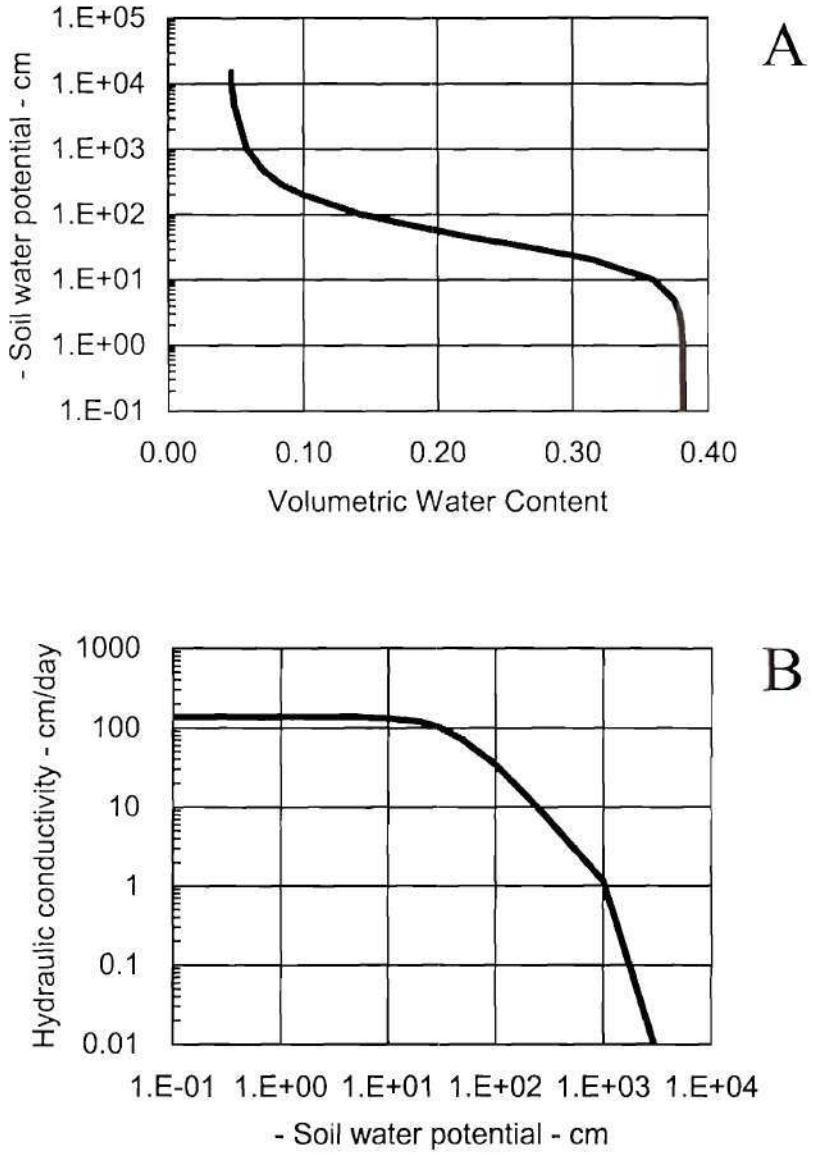

Figure 4.2d Fitted soil water retention (A) and hydraulic conductivity (B) curves for W2 soil collected between 46-61 cm depth.

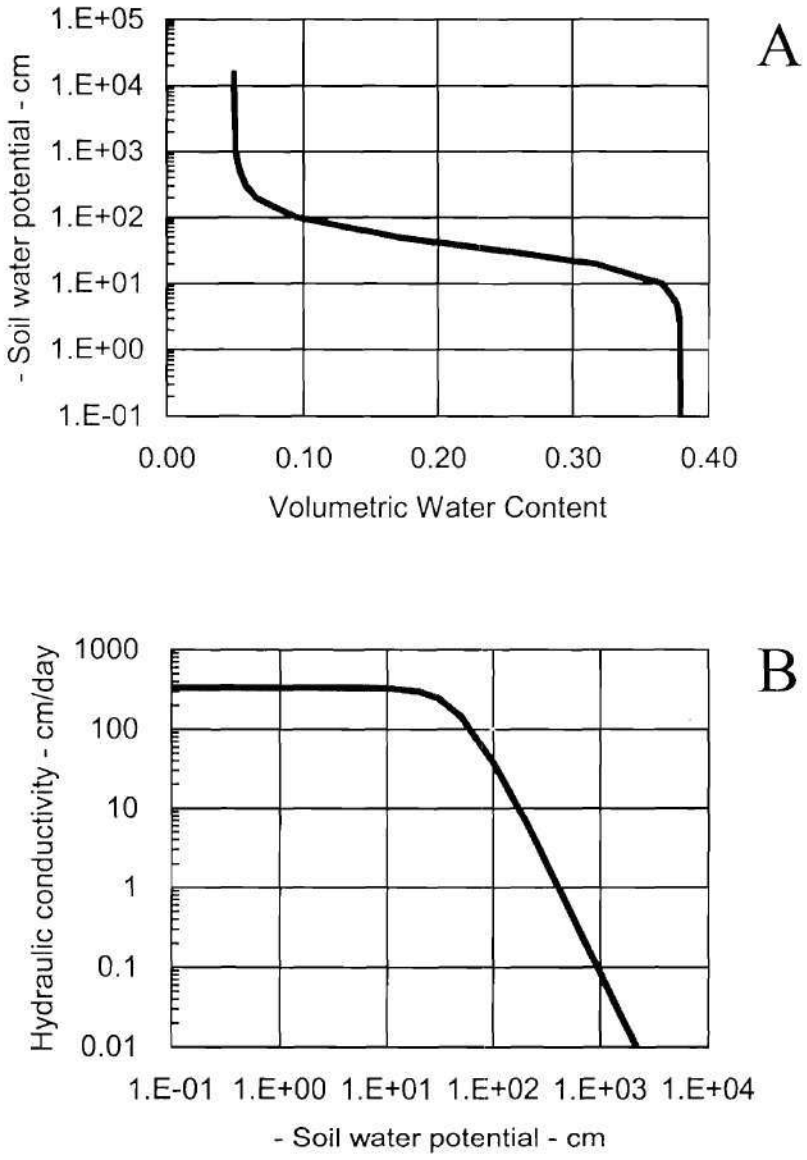

Figure 4.2e Fitted soil water retention (A) and hydraulic conductivity (B) curves for W2 soil collected between 61-76 cm depth.

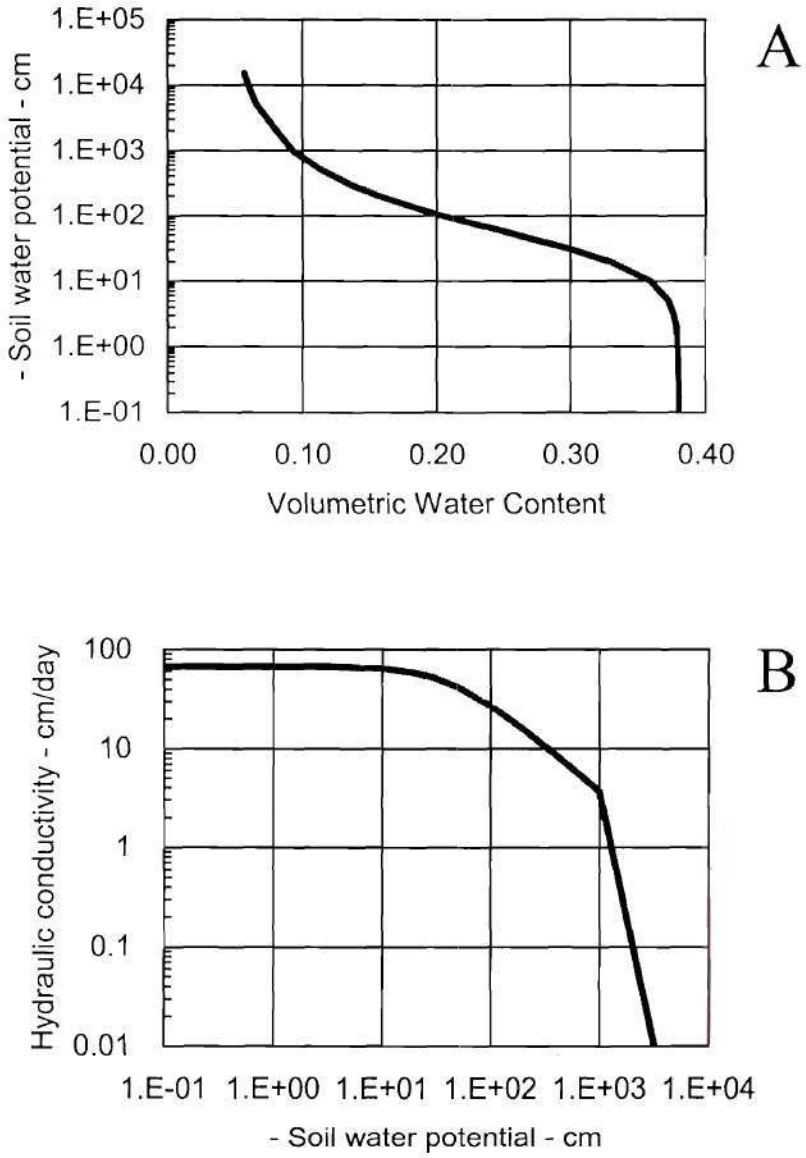

Figure 4.2f Fitted soil water retention (A) and hydraulic conductivity (B) curves for W2 soil collected between 76-91 cm depth.

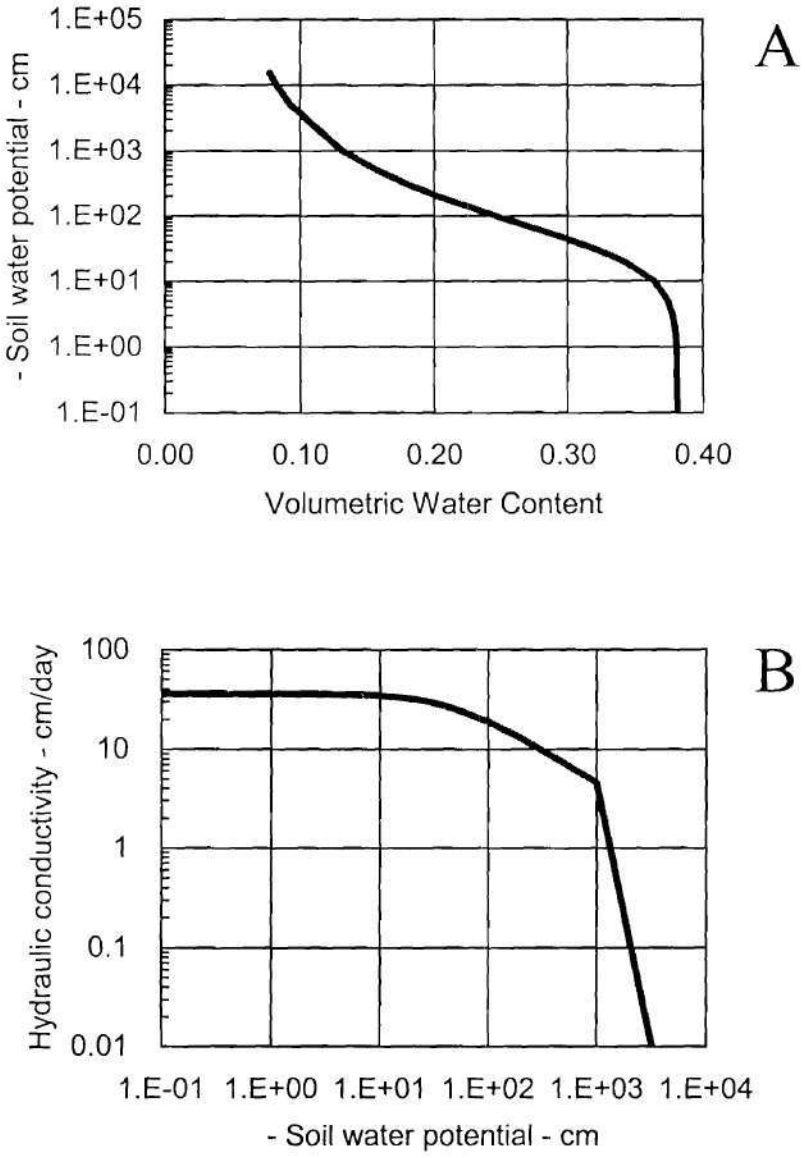

Figure 4.2g Fitted soil water retention (A) and hydraulic conductivity (B) curves for W2 soil collected between 91-107 cm depth.

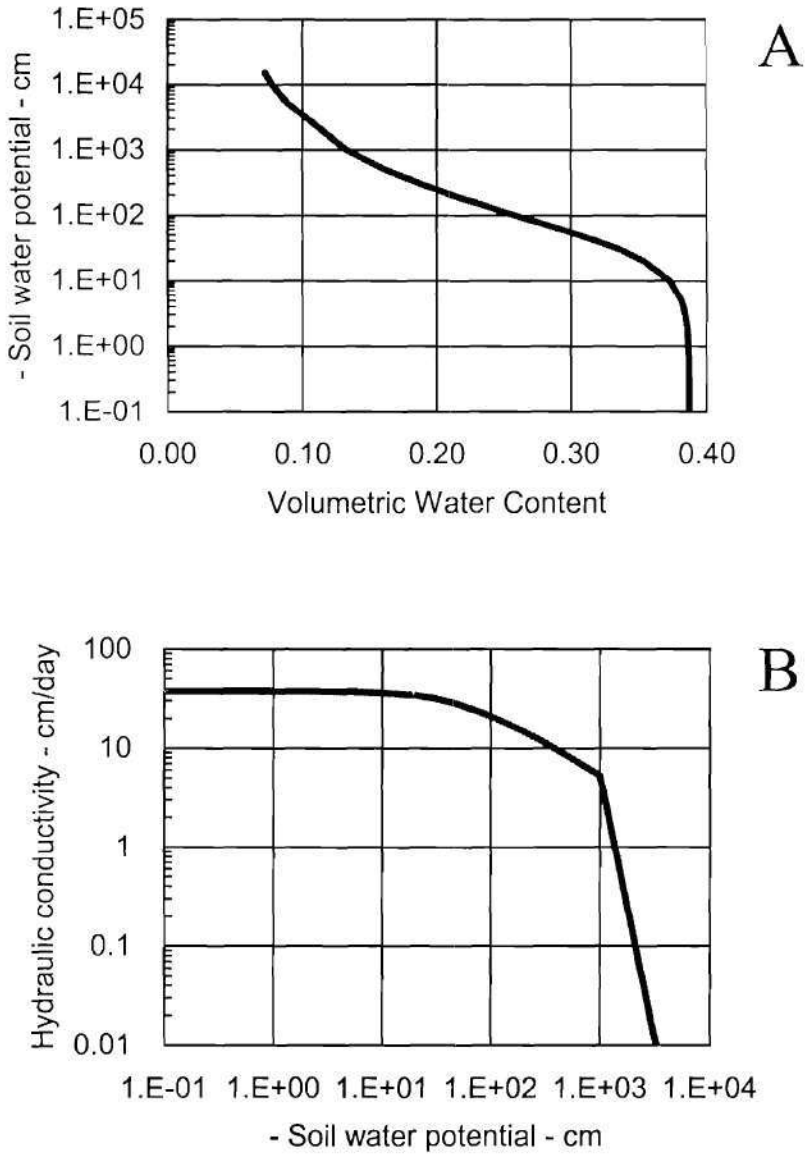

Figure 4.2h Fitted soil water retention (A) and hydraulic conductivity (B) curves for W2 soil collected between 107-122 cm depth.

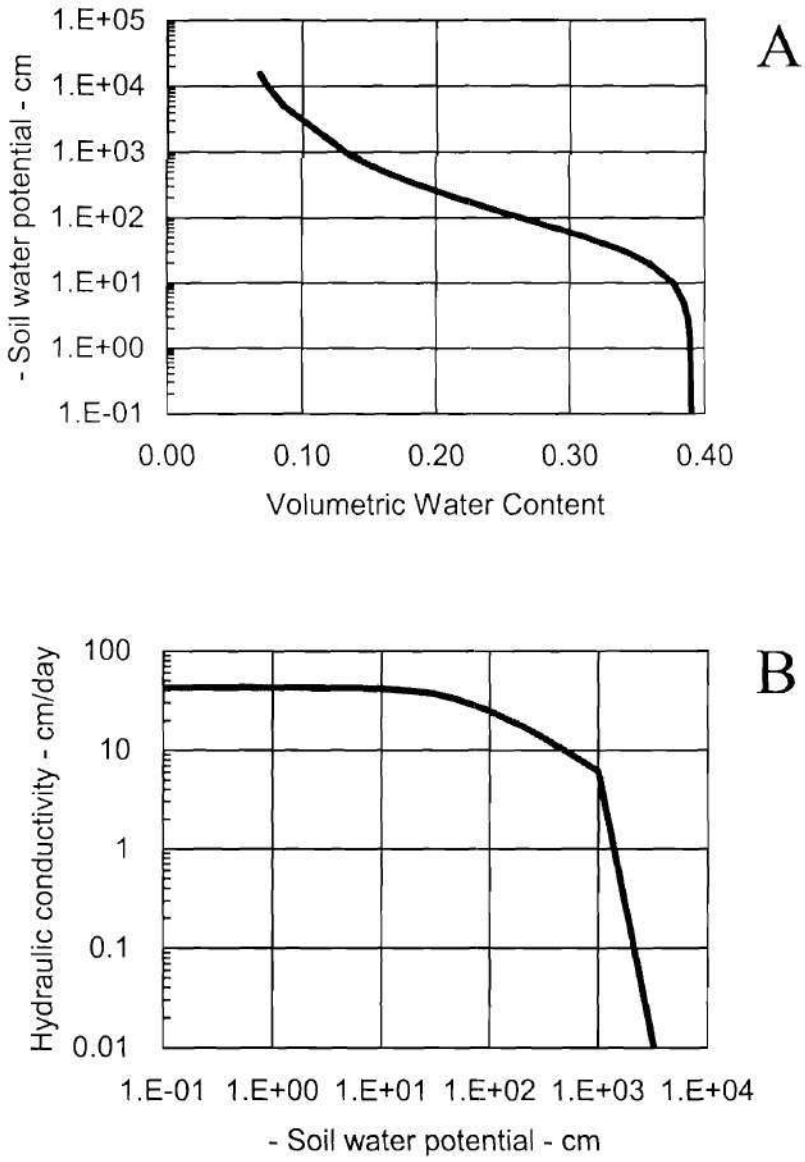

Figure 4.2i Fitted soil water retention (A) and hydraulic conductivity (B) curves for W2 soil collected between 122-137 cm depth.

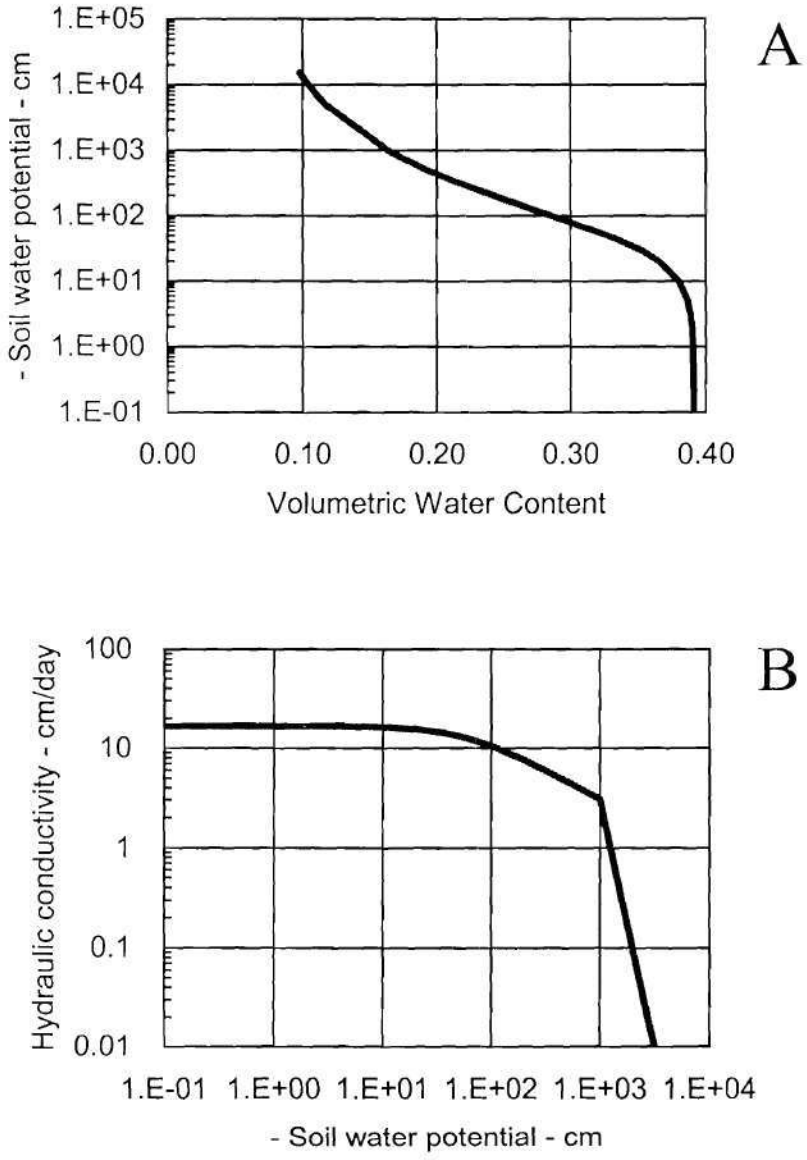

Figure 4.2j Fitted soil water retention (A) and hydraulic conductivity (B) curves for W2 soil collected between 137-152 cm depth.

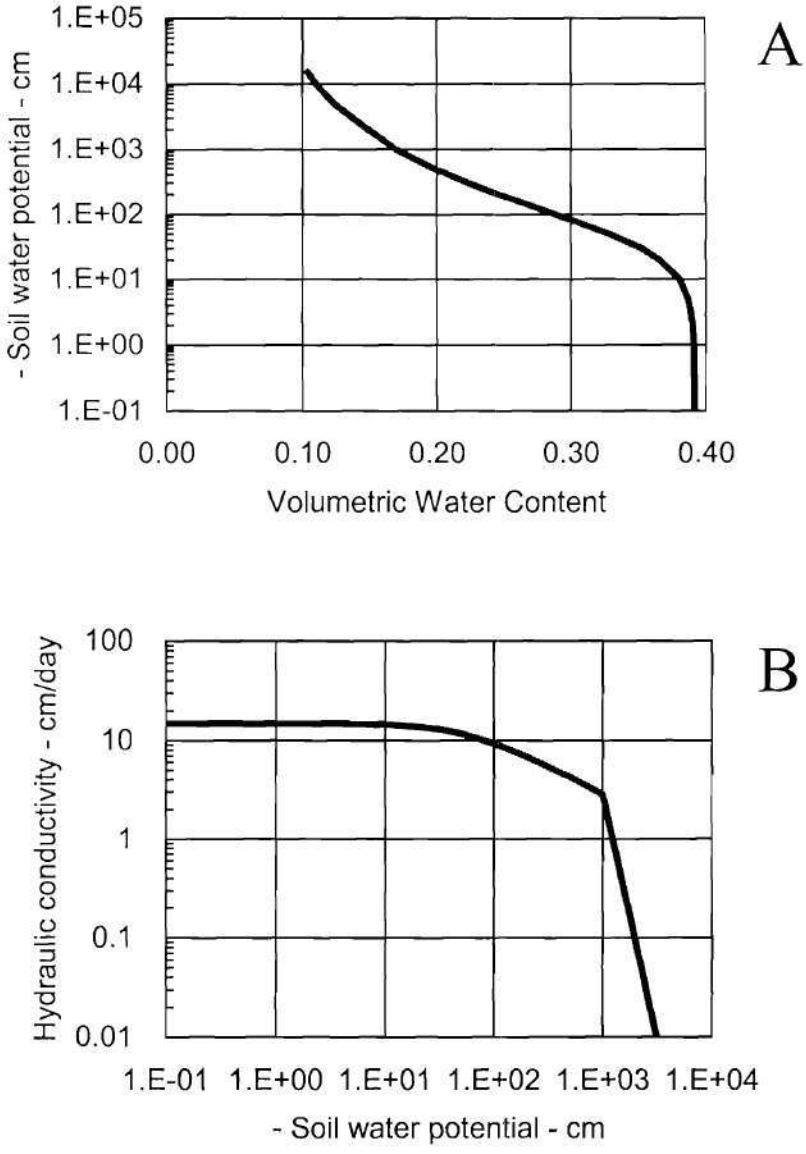

Figure 4.2k Fitted soil water retention (A) and hydraulic conductivity (B) curves for W2 soil collected between 152-168 cm depth.

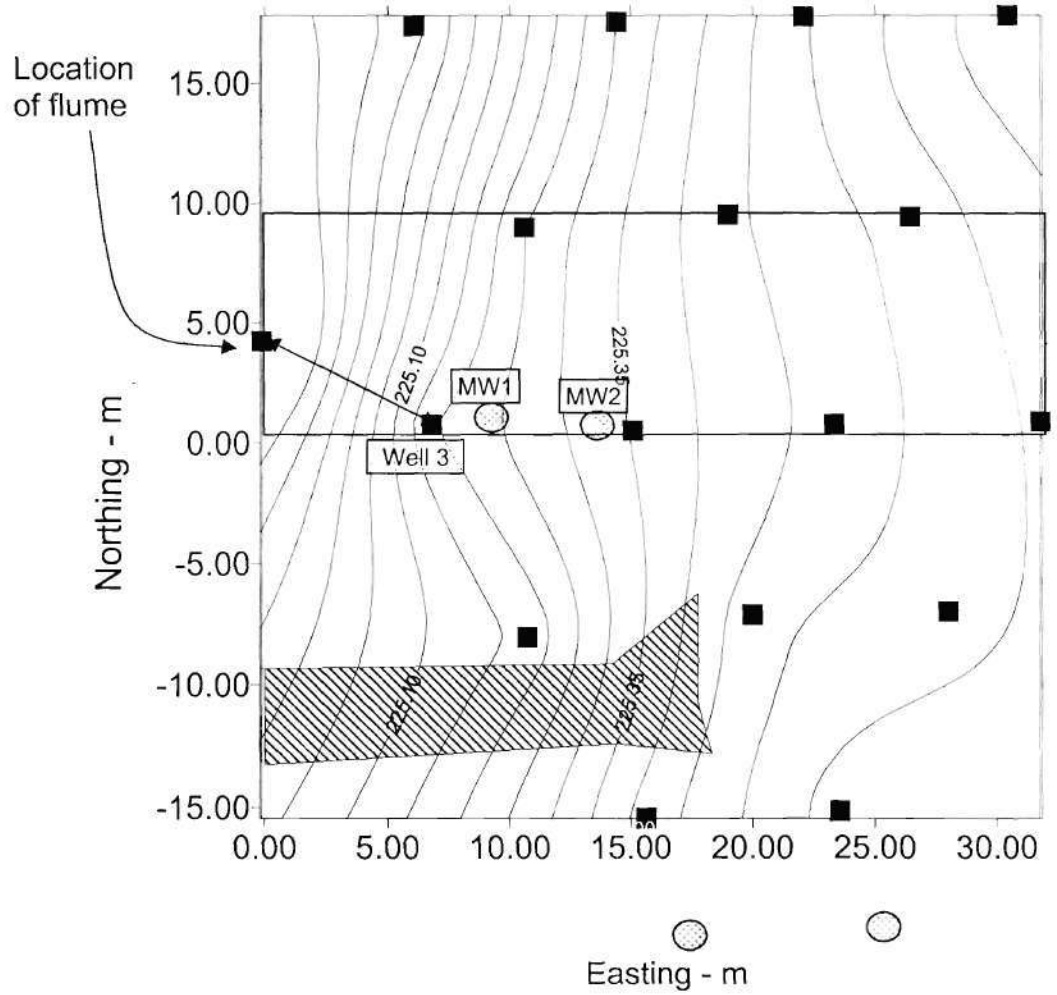

Figure 4.3 Water table elevations measured on December 30, 1999, using all Sixteen 2.54-cm wells (solid squares and shaded circles). Hatched area at bottom of figure indicates the trough of 2nd spring. Hydraulic gradient measured from Flume to well 3, shown as arrow on graph. Box in center of graph indicates area used for water balance calculations.

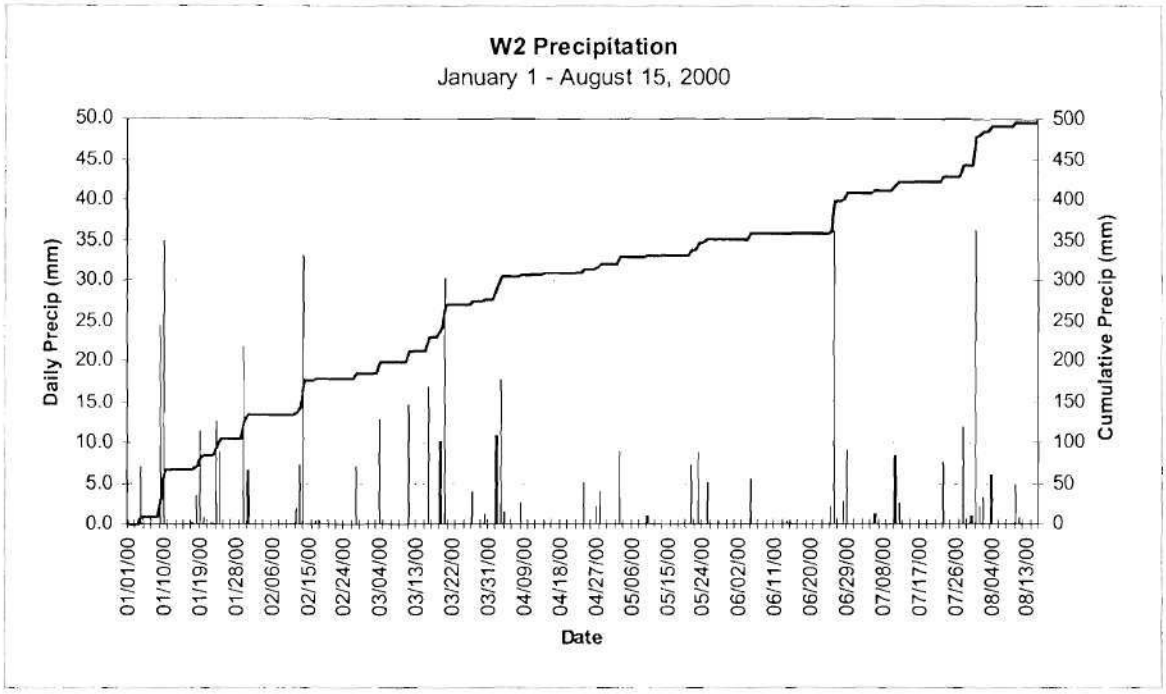

Figure 4.4. Daily and cumulative precipitation recorded by the tipping bucket rain gauge at the experiment site for 2000.

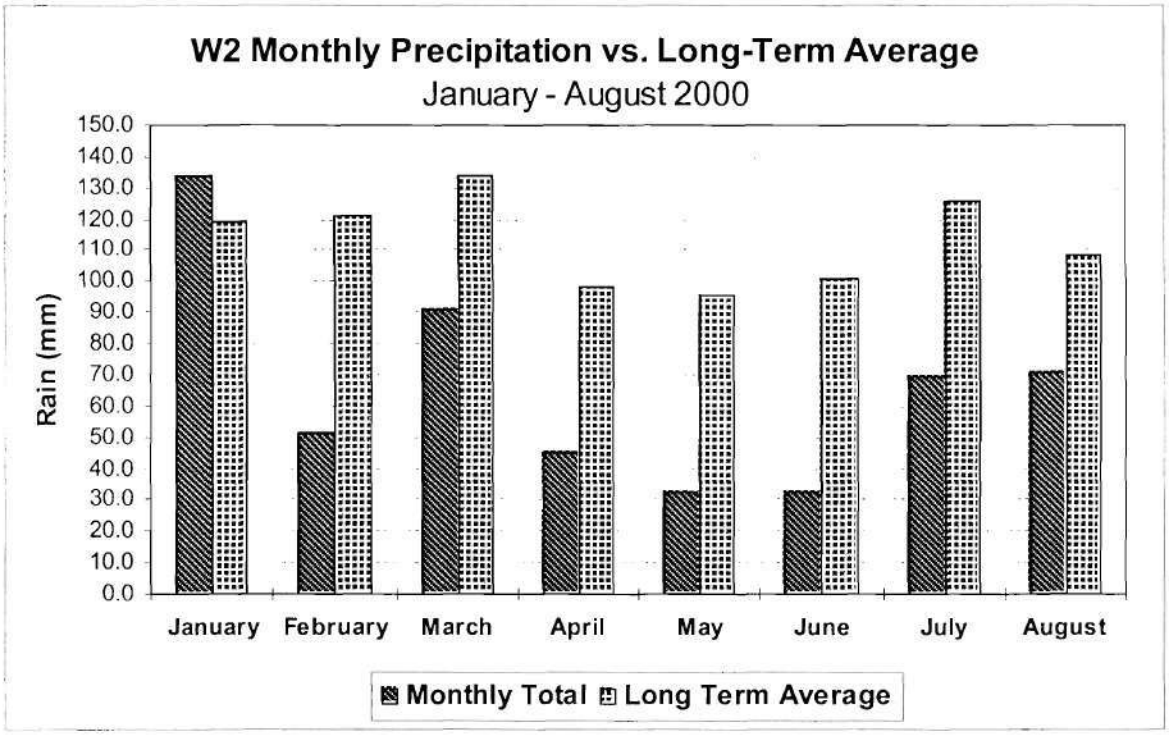

Figure 4.5. Year 2000 monthly precipitation recorded by tipping bucket rain gauge compared to the monthly long term averages for the J. Phil Campbell, Sr. Natural Resource Research Center.

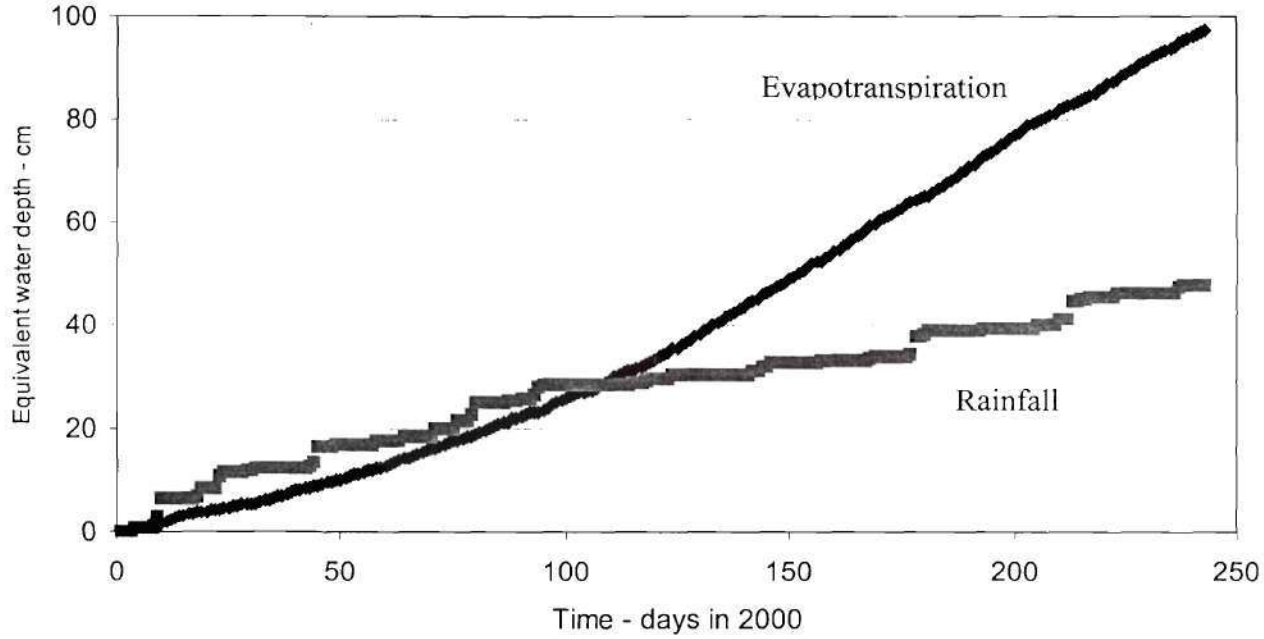

Figure 4. 6 Cumulative precipitation and evapotranspiration at W2 site.

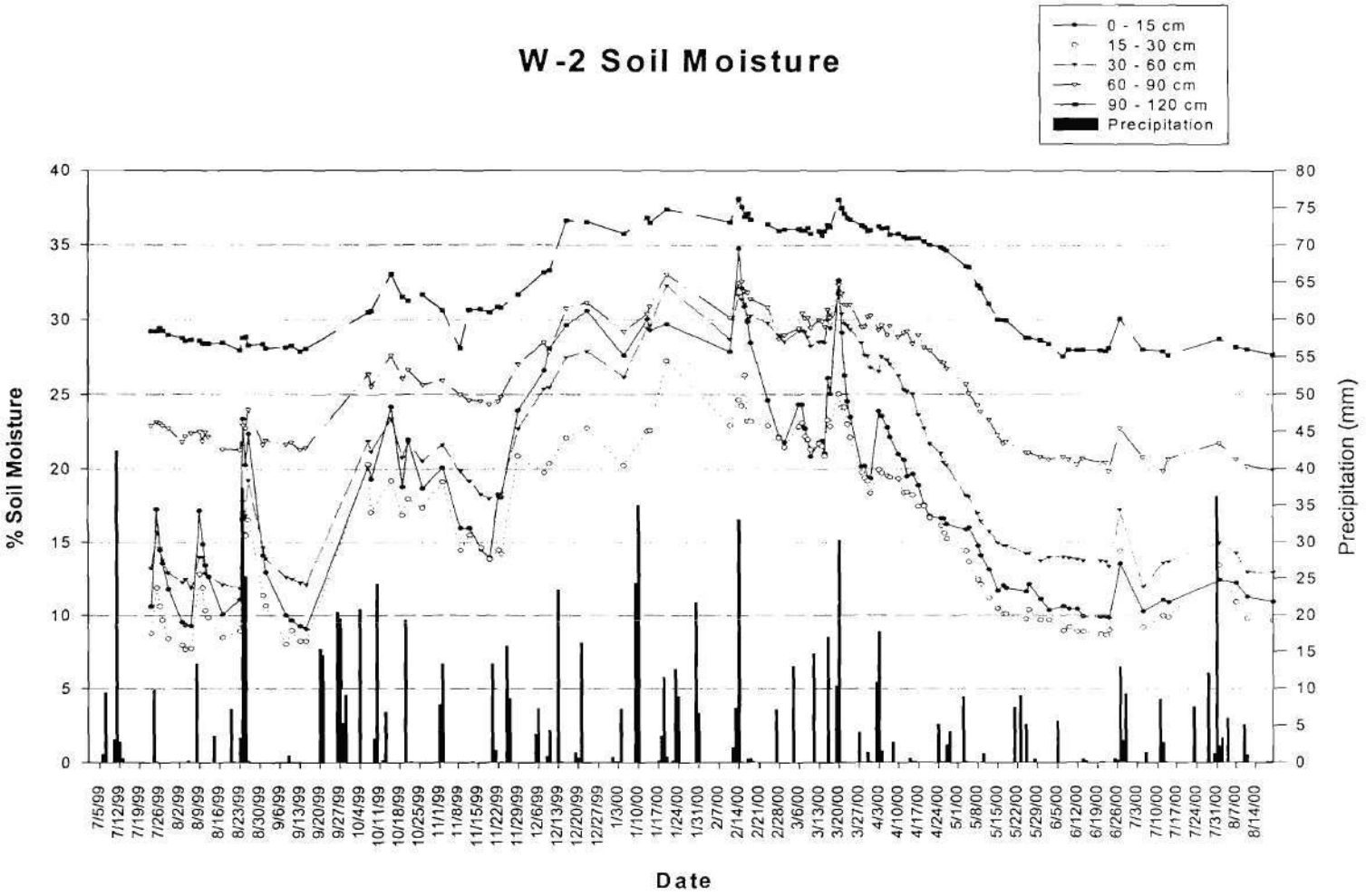

Figure 4.7. Average soil moisture for installed TDR probes and daily precipitation.

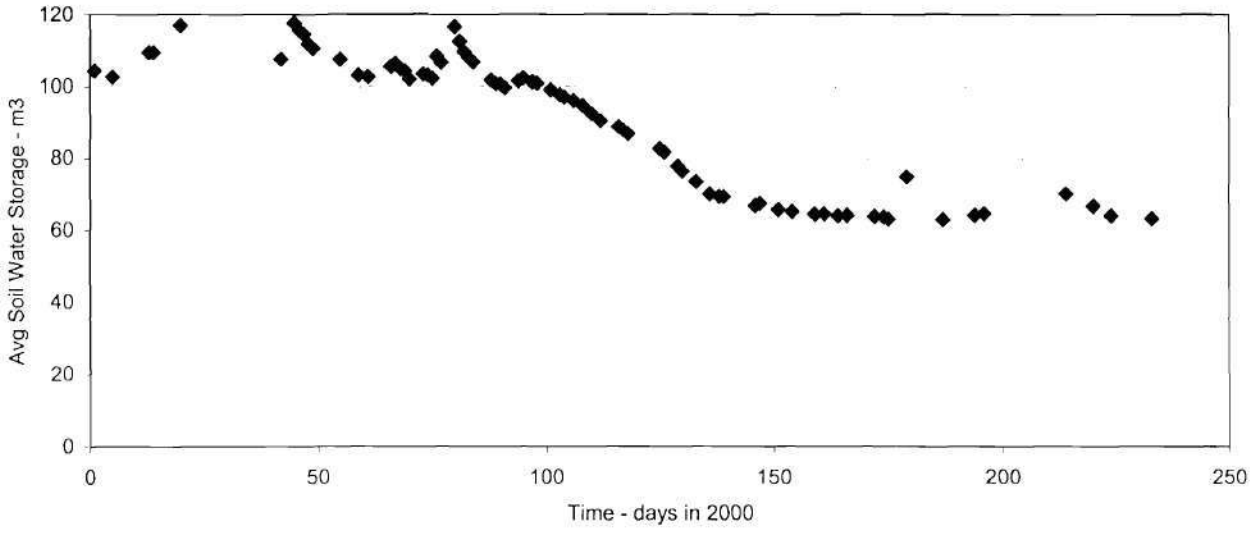

Figure 4.8 Average soil water storage for 5 TDR probes installed at W2 site.

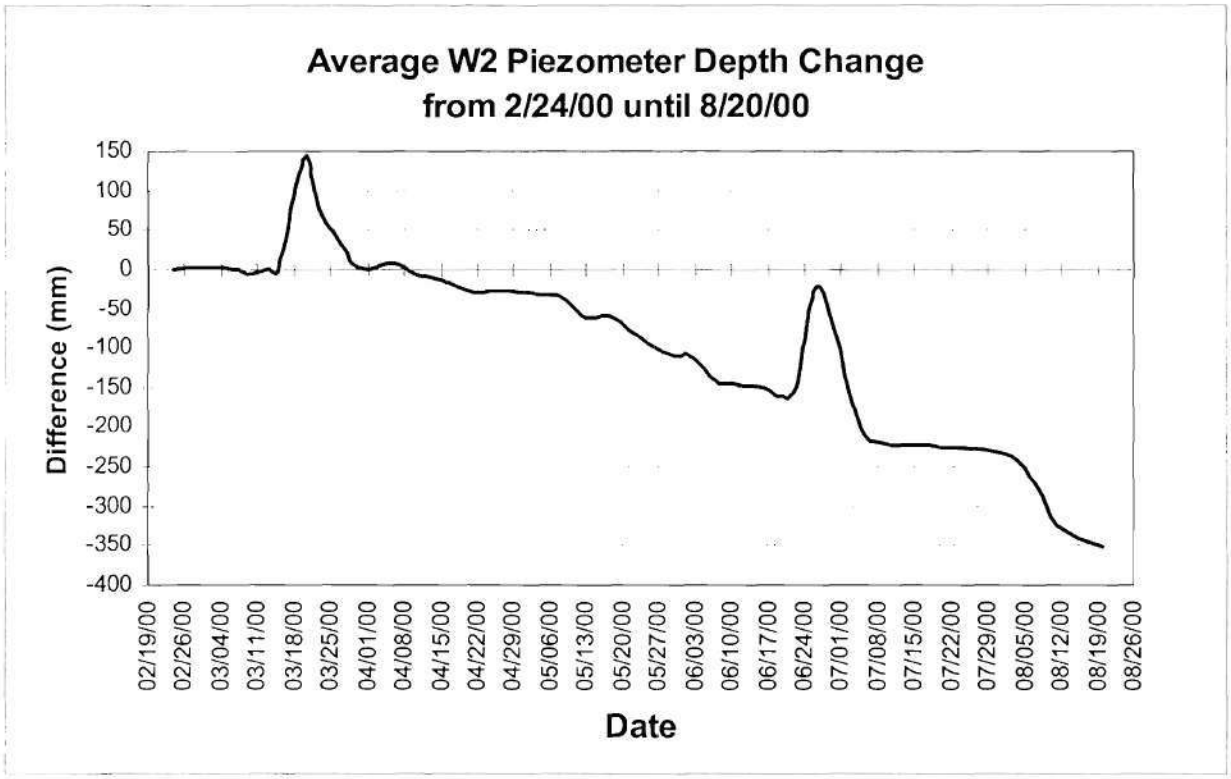

Figure 4.9. Change in average groundwater depth from soil surface on 2/24/00 (4 days before spiking) until 8/20/00 for the 16 installed piezometers.

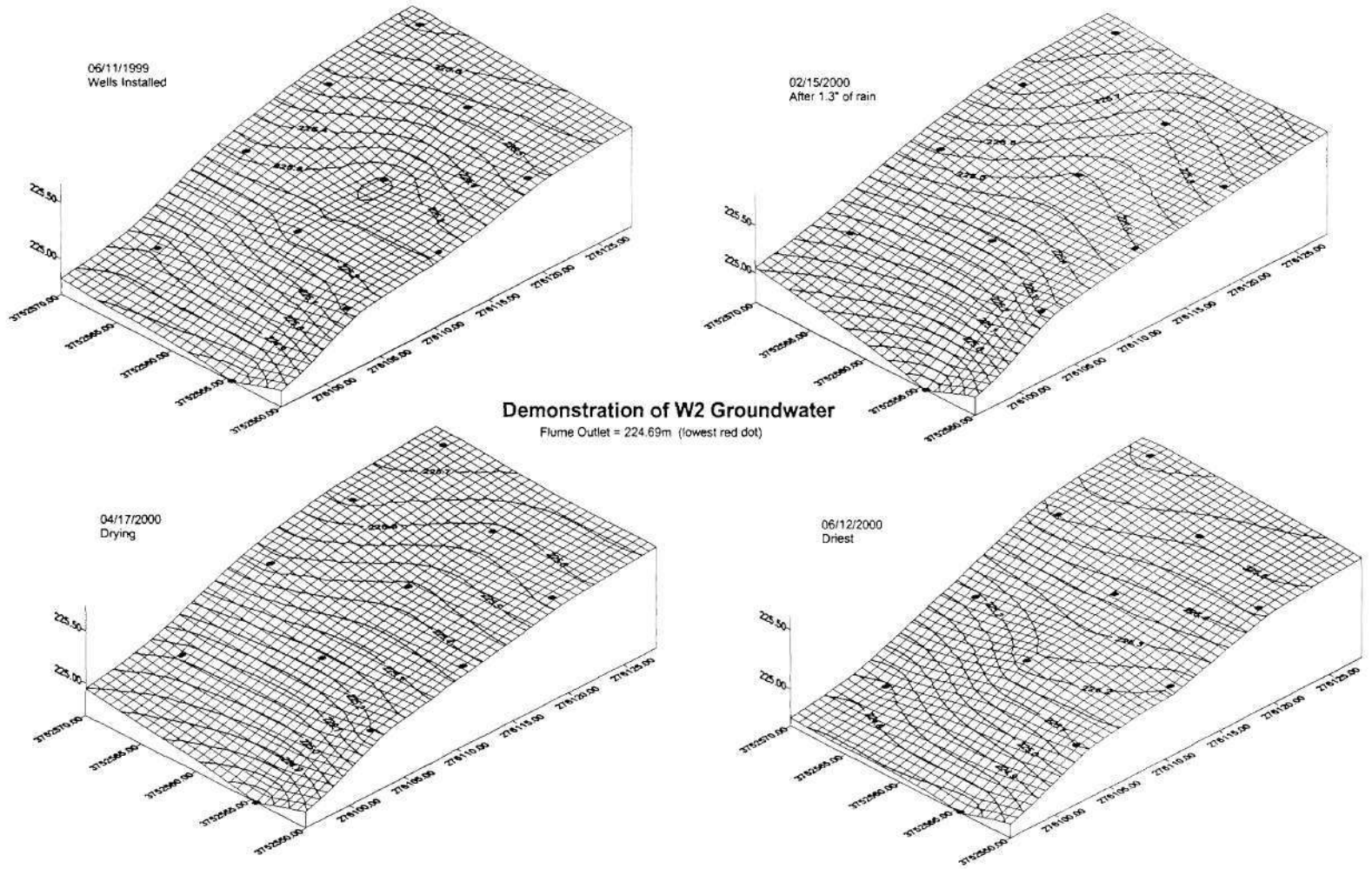

Figure 4.10. Contour maps of the groundwater as defined by the piezometers 1-11 and the flume outlet at various dates. Maps generated using Surfer and the Krigging technique to create the associated grid file. Dots indicate piezometer locations.

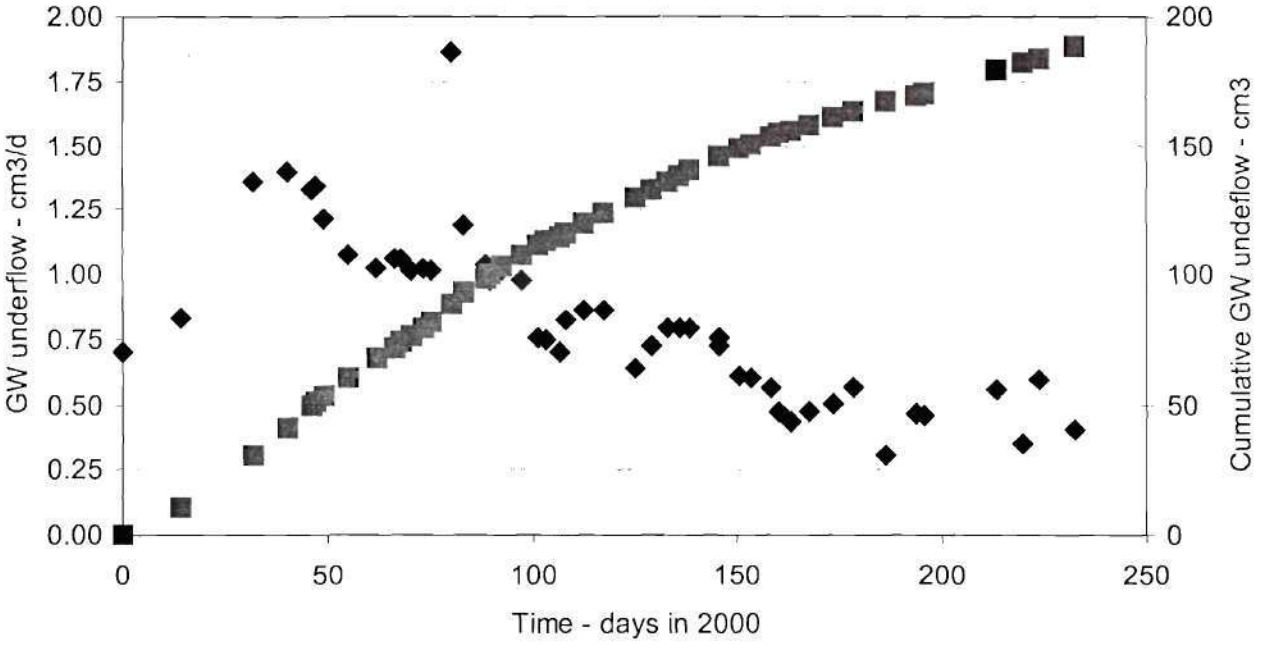

Figure 4.11 Daily (diamonds) and cumulative (squares) GW underflow estimated for the southern half of the monitored subplot.

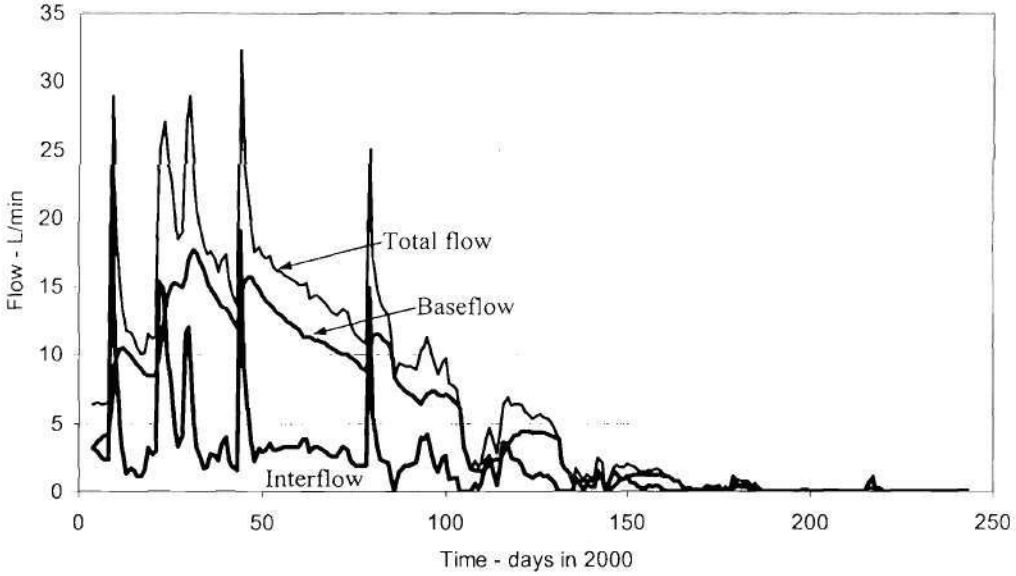

Figure 4.12 Results of baseflow separation of W2 spring for time beginning in January 1, 2000 and ending August 31, 2000.

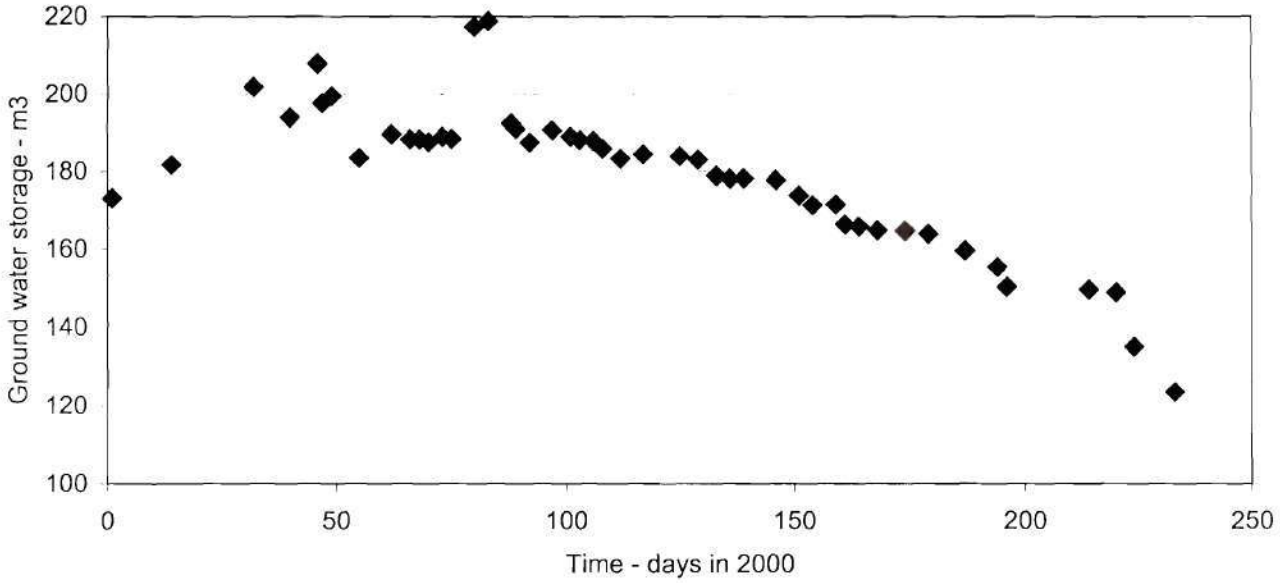

Figure 4.13 Ground water storage at W2 site

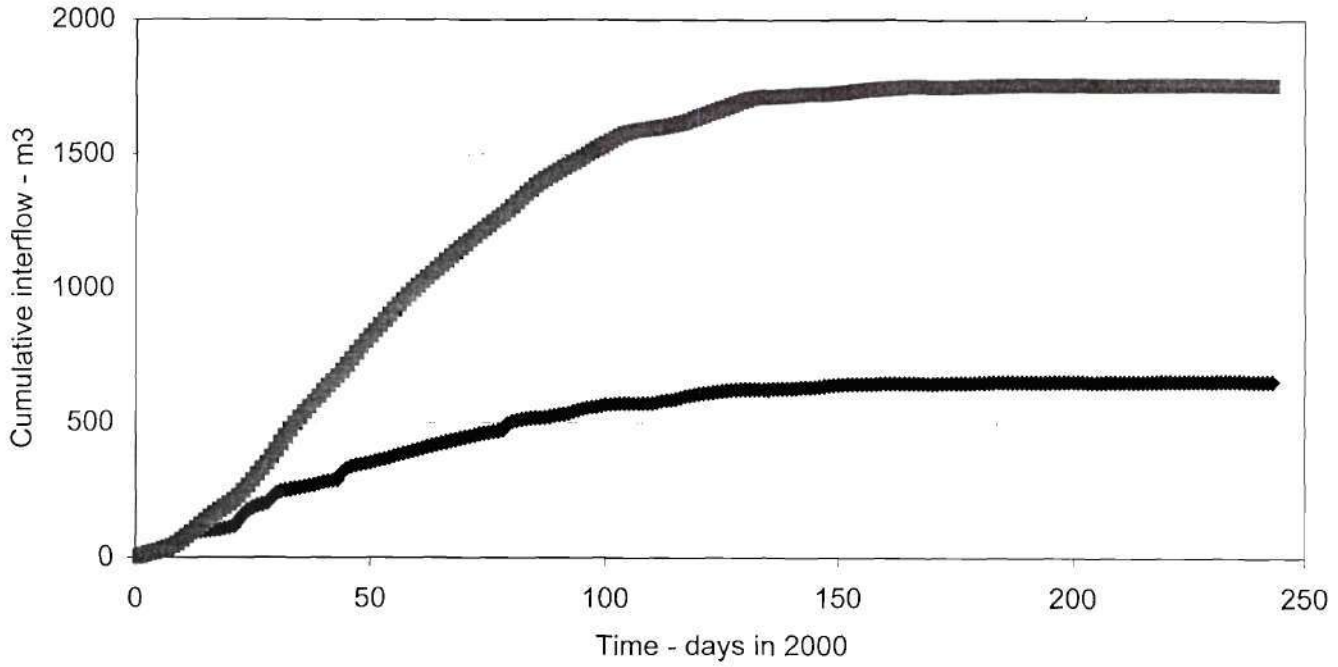

Figure 4.14 Cumulative baseflow (top series) and interflow (bottom series), separated from spring flow using Equation 3.3.

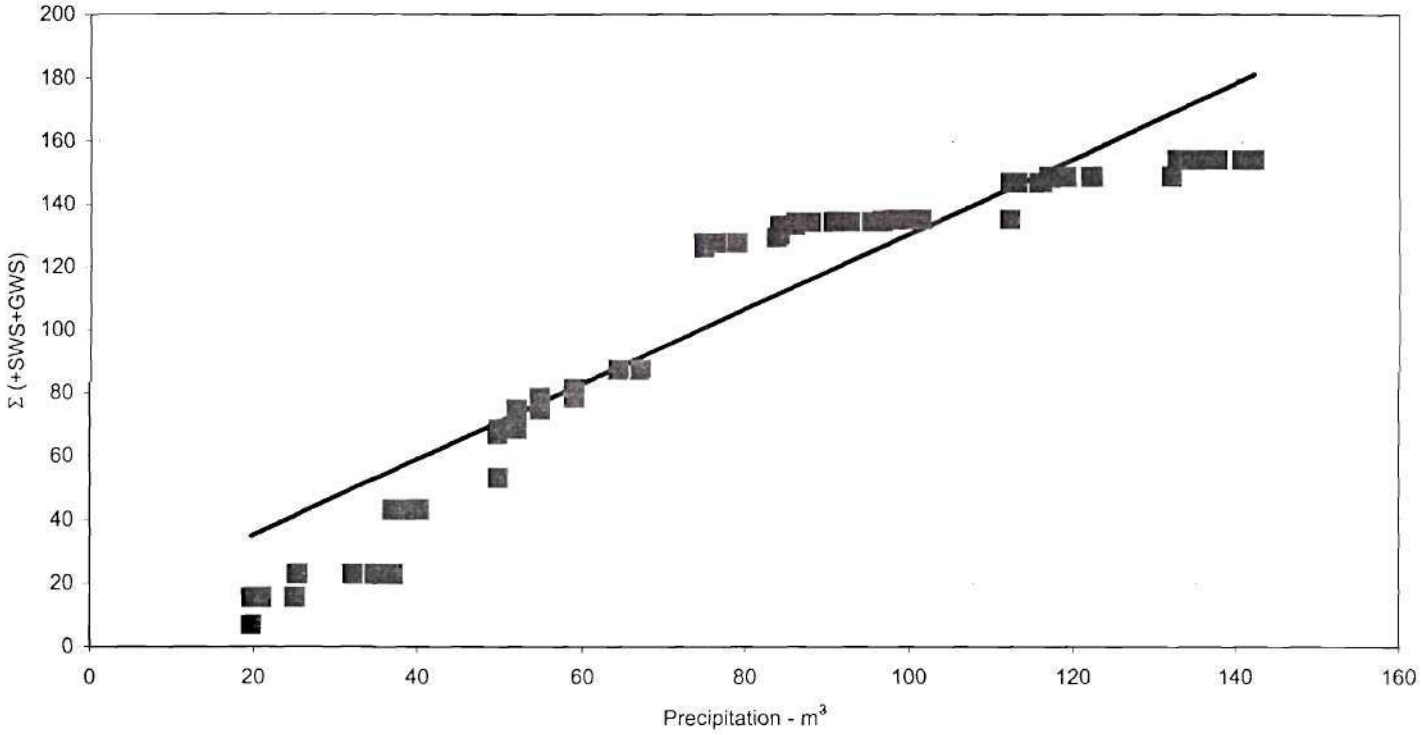

Figure 4.15 Relationship between precipitation and increased SWS and GWS. Symbols equal observed data; Line is the regression line (y = 11.18 + 1.19 (x)).

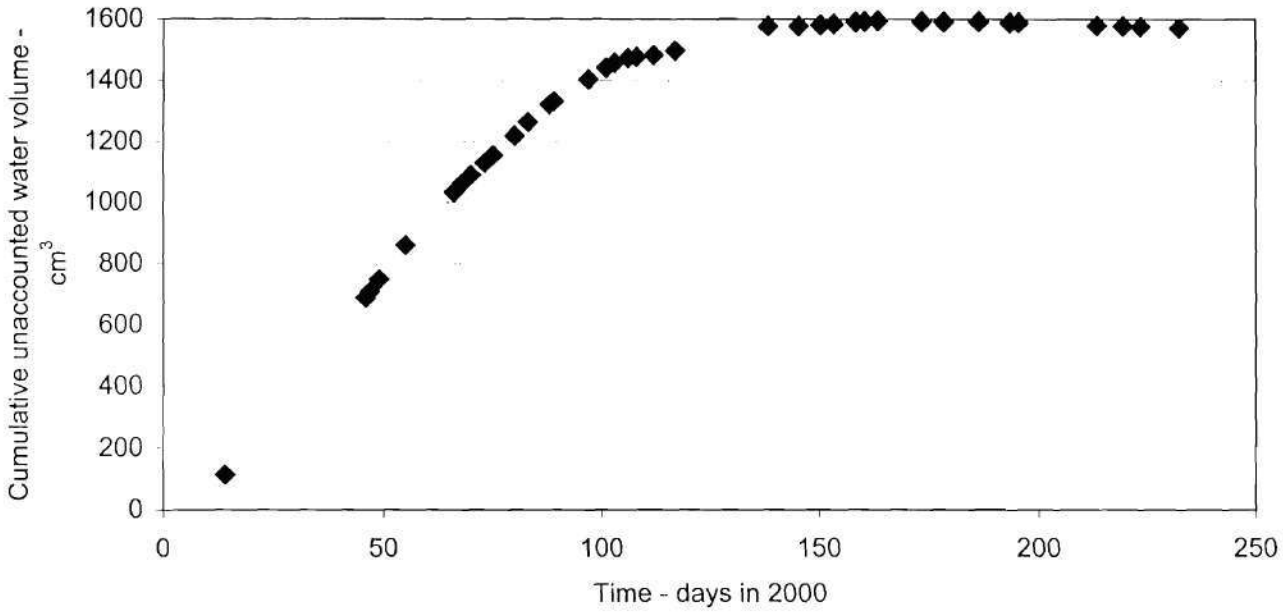

Figure 4.16 Cumulative water volume leaving the W2 subplot, but not accounted for in other water budget components. Values calculated as (baseflow – GW underflow).

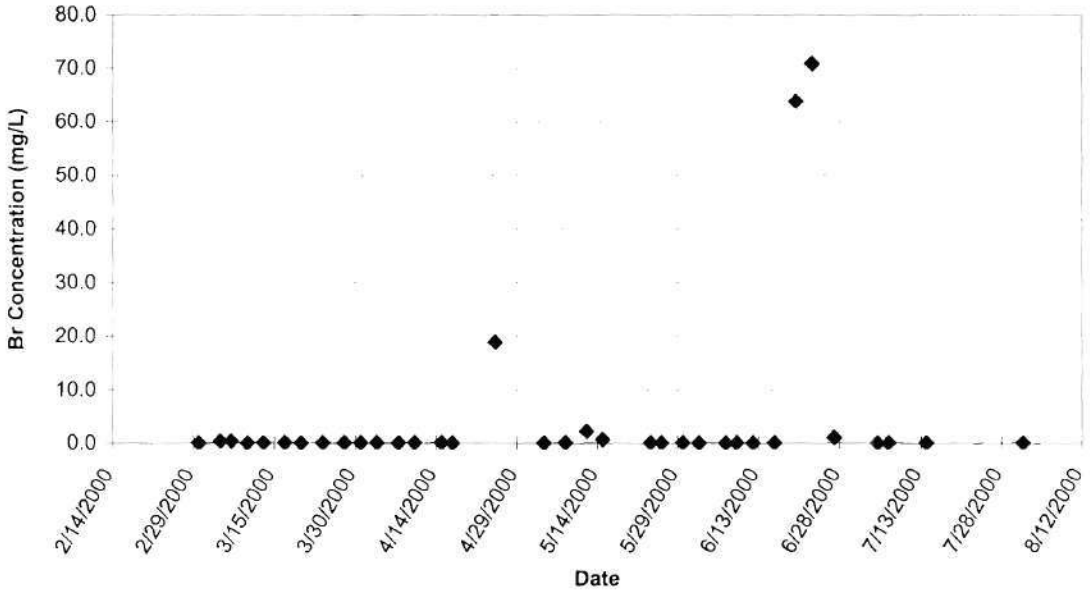

Figure 4.17. Bromide concentration of water collected from Monitoring Well 1.

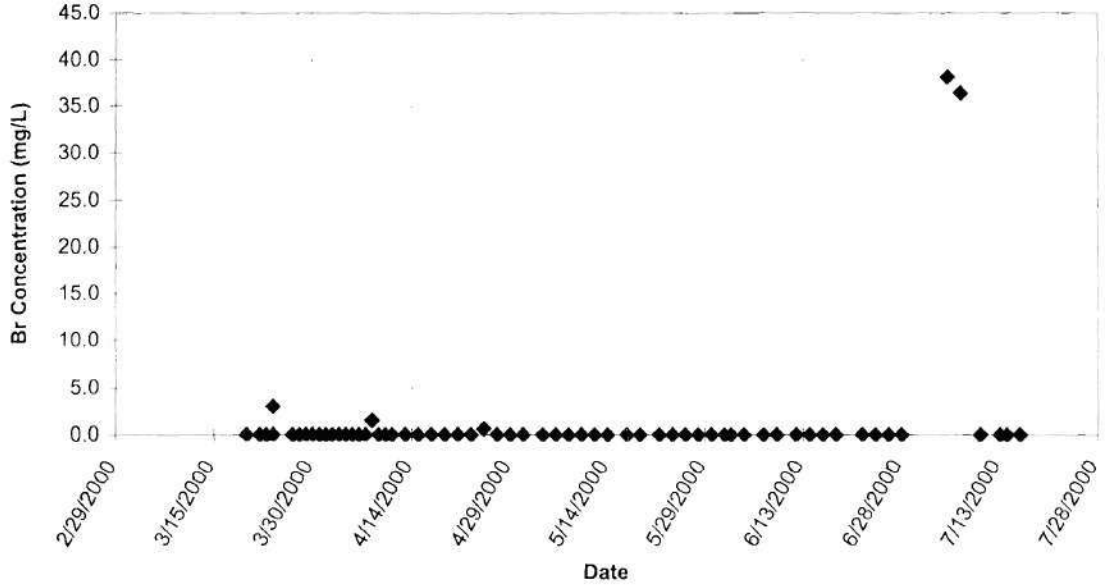

Figure 4.18. Bromide concentration of water samples collected at the spring (Sigma sampler).

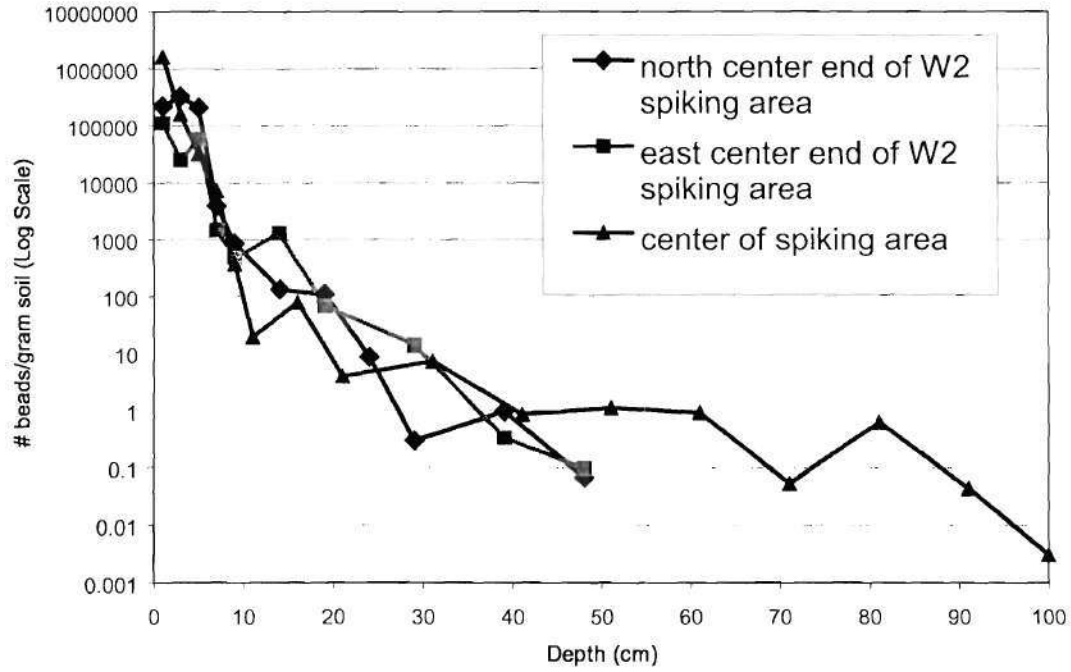

Figure 4.19. Distribution of microsphere beads retained in soil cores collected from the spiking area.

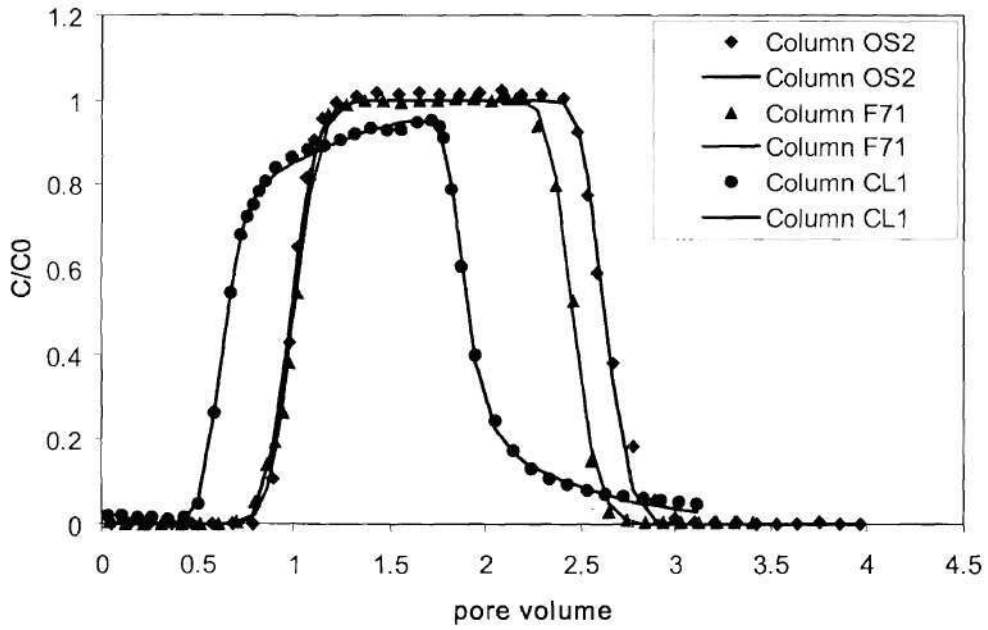

Figure 4.20. Representative non-reactive tracer breakthrough curves for 20-30 mesh Ottawa sand, F-70 Ottawa sand and Cecil soil.

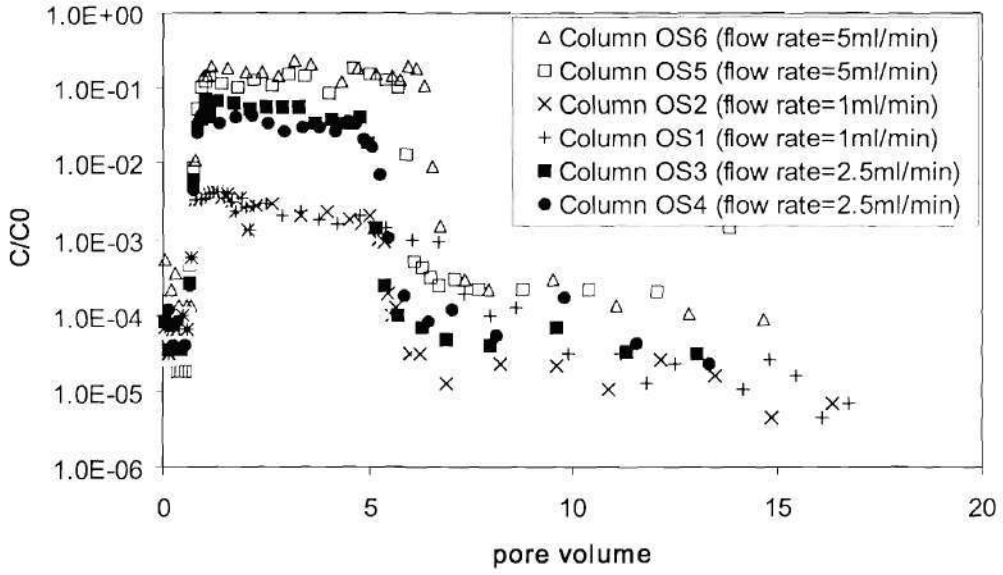

Figure 4.21. Comparison of microsphere breakthrough curves for 20-30 mesh Ottawa sand at flow rates of 1.0, 2.5, and 5.0 mL/min.

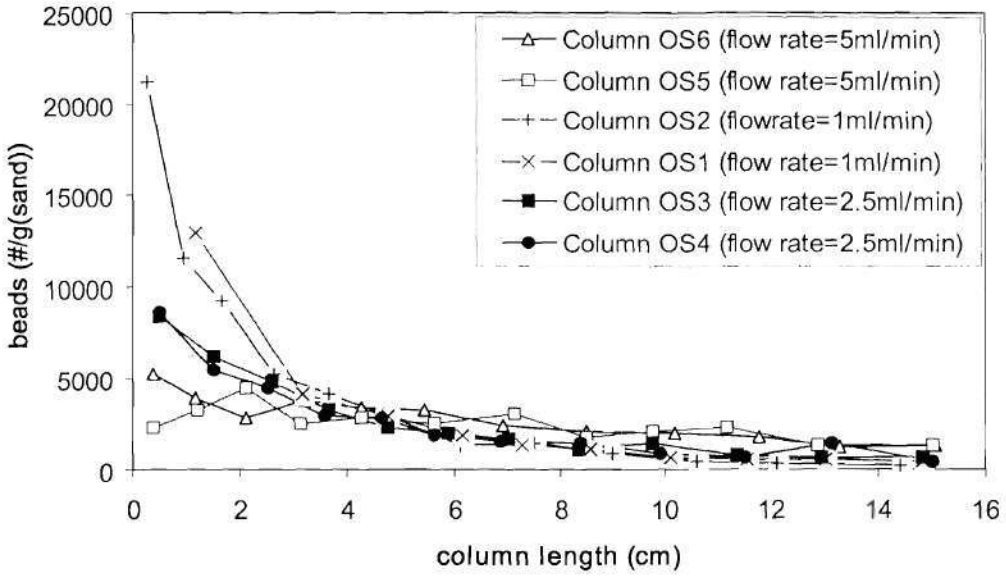

Figure 4.22. Comparison of microsphere bead retention distributions in 20-30 mesh Ottawa sand at flow rates of 1.0, 2.5 and 5.0 mL/min.

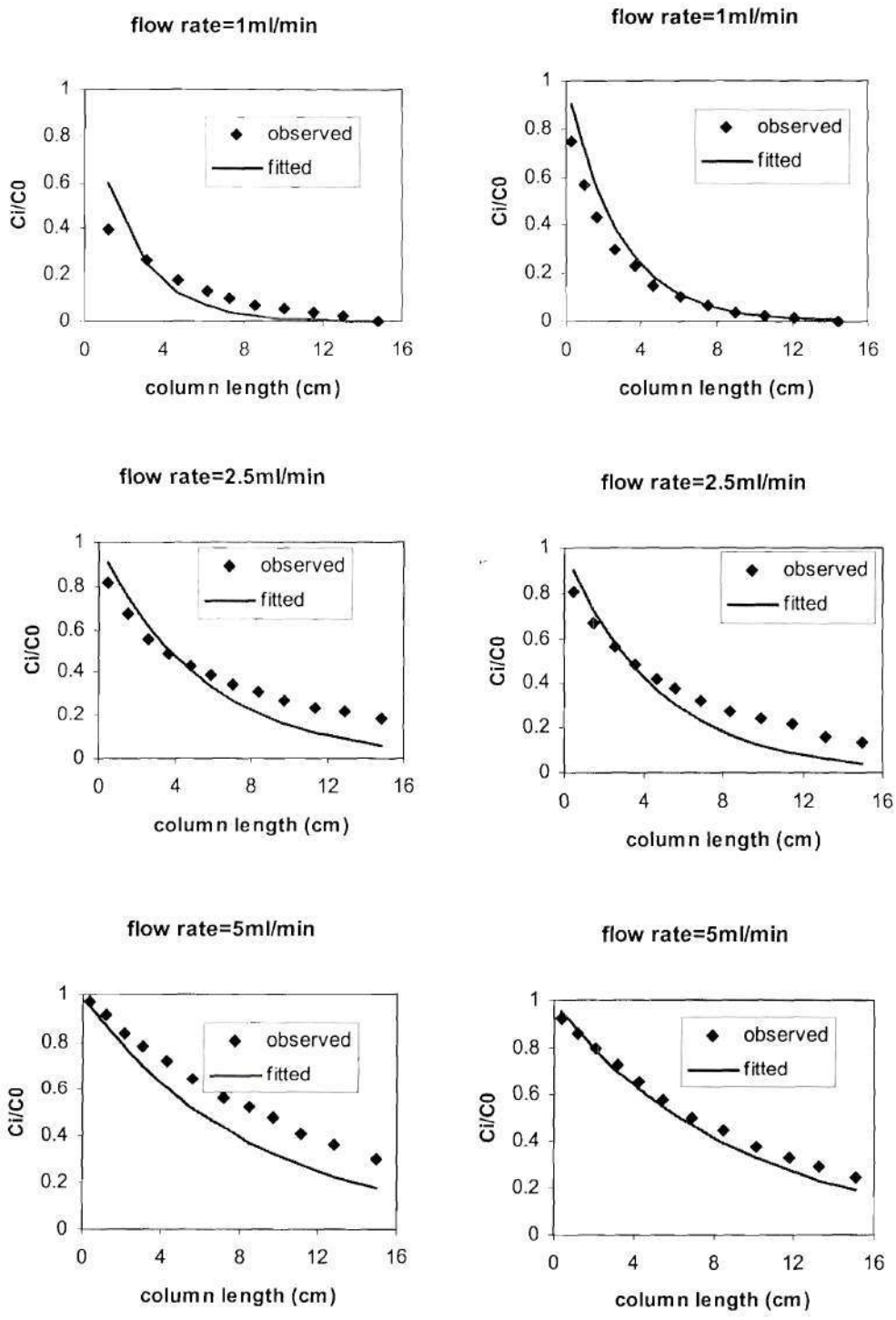

Figure 4.23. Measured and predicted distribution of beads retained within 20-30 mesh Ottawa sand soil columns at flow rates 1.0, 2.5 and 5.0 mL/min.

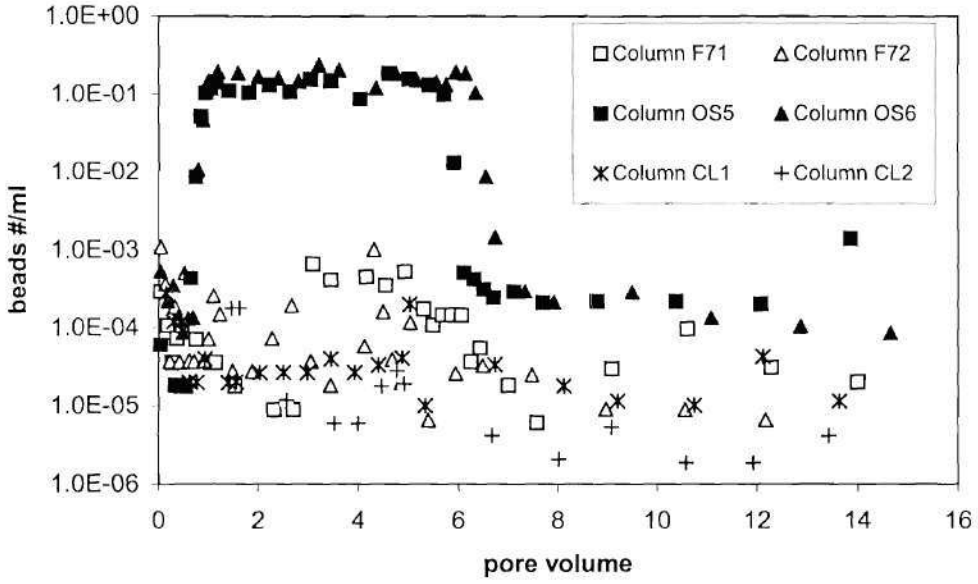

Figure 4.24. Comparison of microsphere bead breakthrough curves for 20-30 mesh Ottawa sand, F-70 Ottawa sand and Cecil soil at a flow rate of 5.0 mL/min.

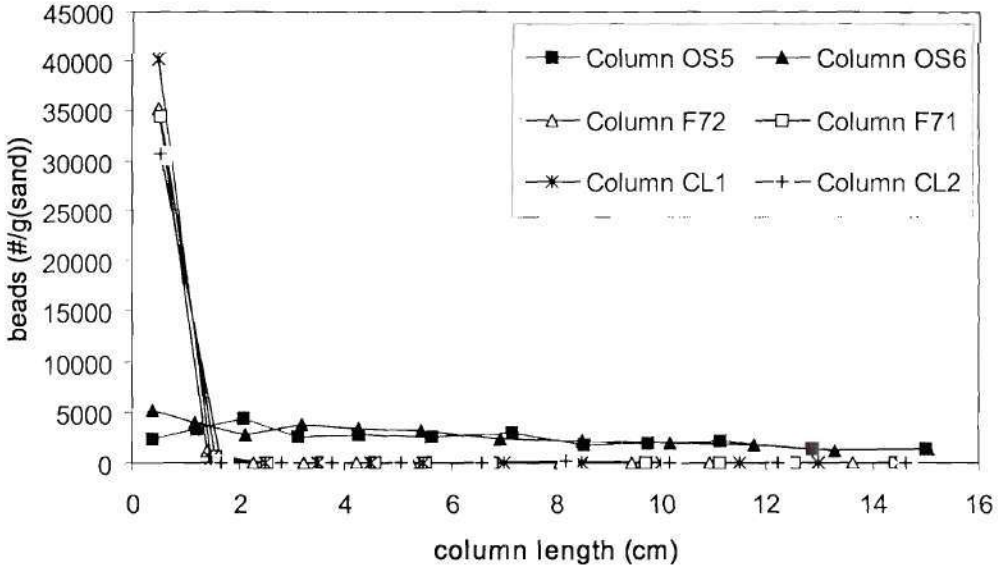

Figure 4.25. Comparison of microsphere bead retention distributions in 20-30, F-70, and Cecil soil columns at a flow rate of 5.0 mL/min.

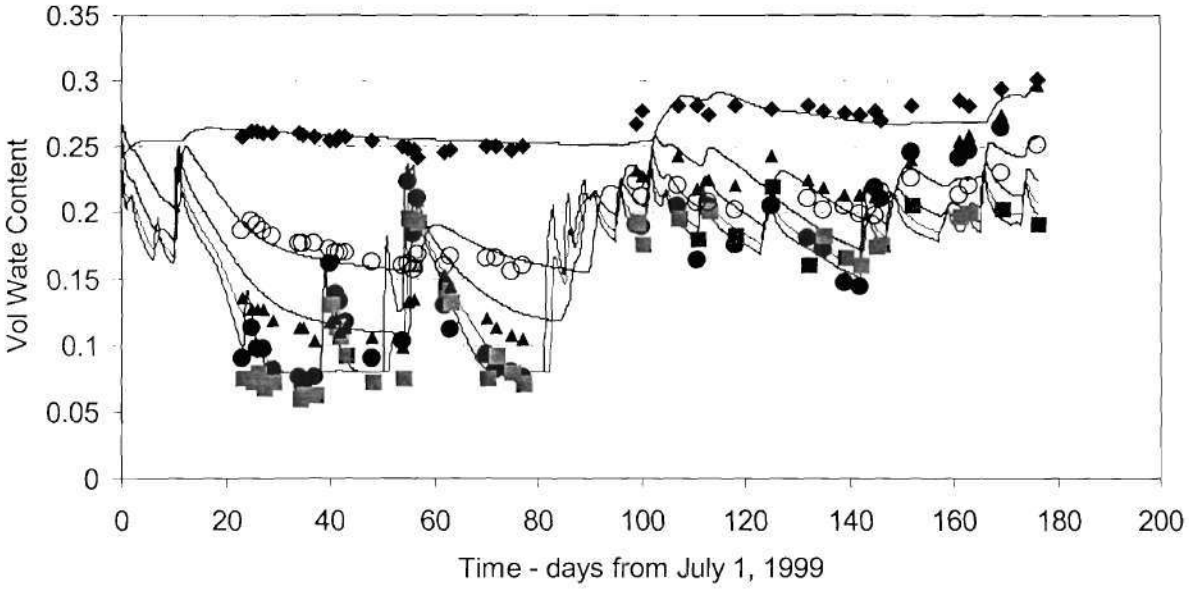

Figure 4.26 Fitted versus observed volumetric water contents, collected with the TDR from Location 4, adjacent to the spiking area. Legend: closed square – 7.5 cm; closed circle – 22.5 cm; triangle – 45 cm; open circle – 75 cm; diamond – 115 cm.

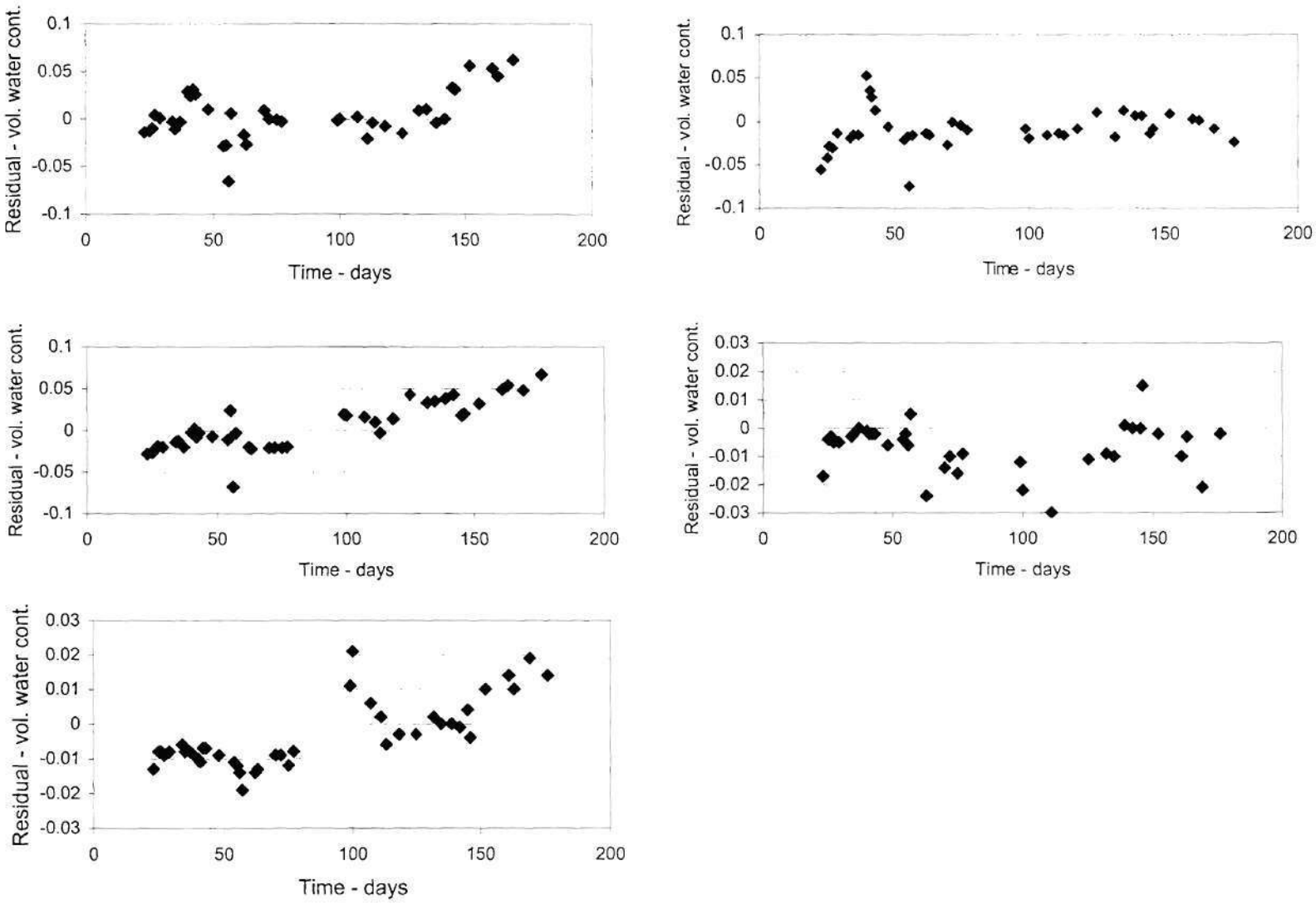

Figure 4.27 Residuals obtained from HYDRUS-1D modeling

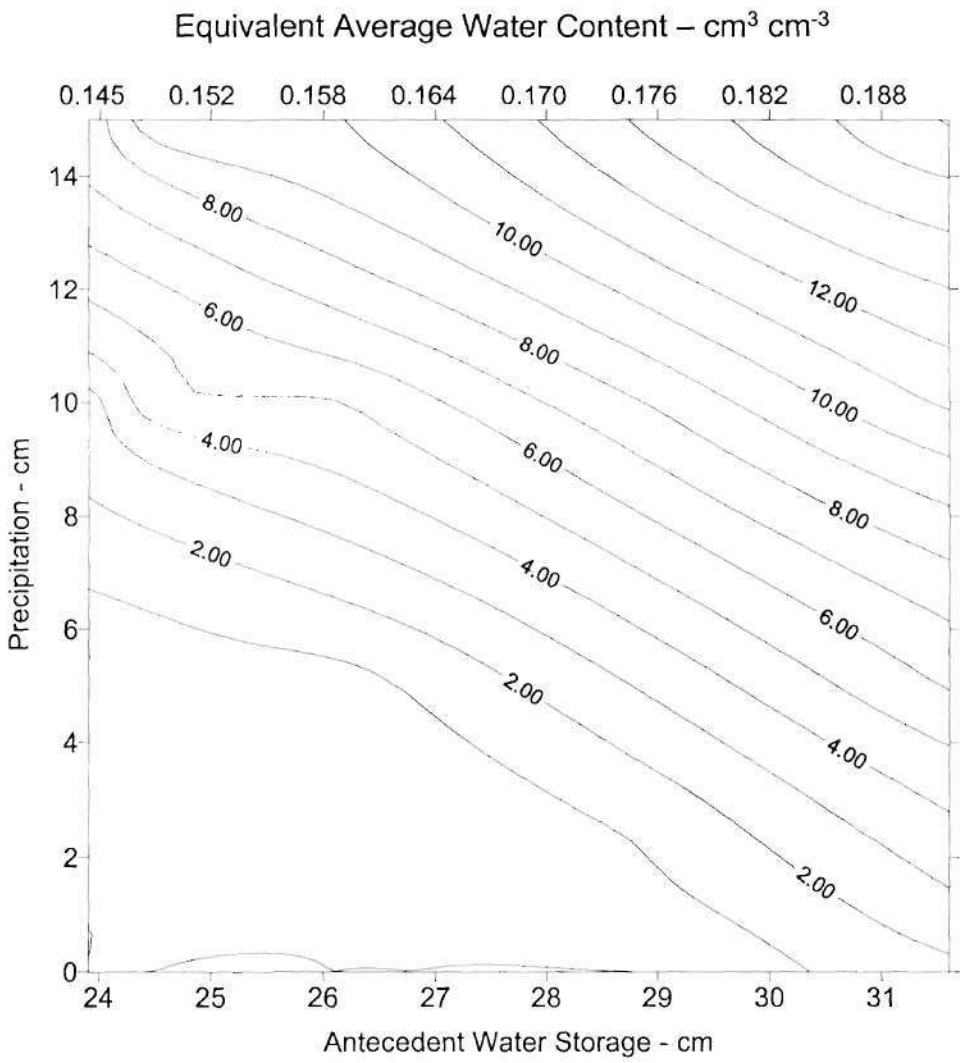

Figure 4.28 Predicted deep drainage in W2 soil profile as functions of antecedent water storage and precipitation. Water holding capacity (31.7 cm) is second y-axis. Equivalent average water content shown at top.

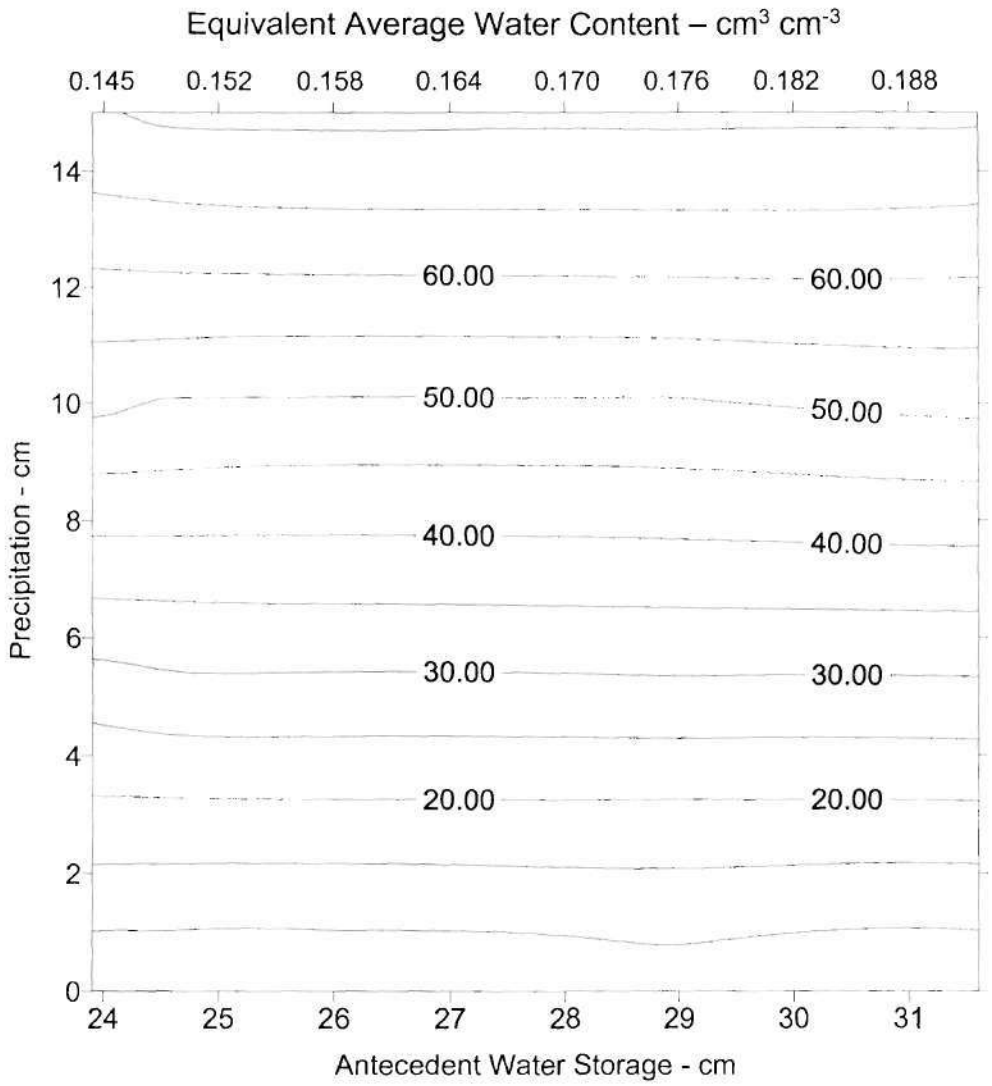

Figure 4.29 Penetration depth of peak concentration of ideal solute in W2 soil as functions of antecedent water storage and precipitation. Water holding capacity (31.7 cm) is second y-axis. Equivalent average water content shown at top.

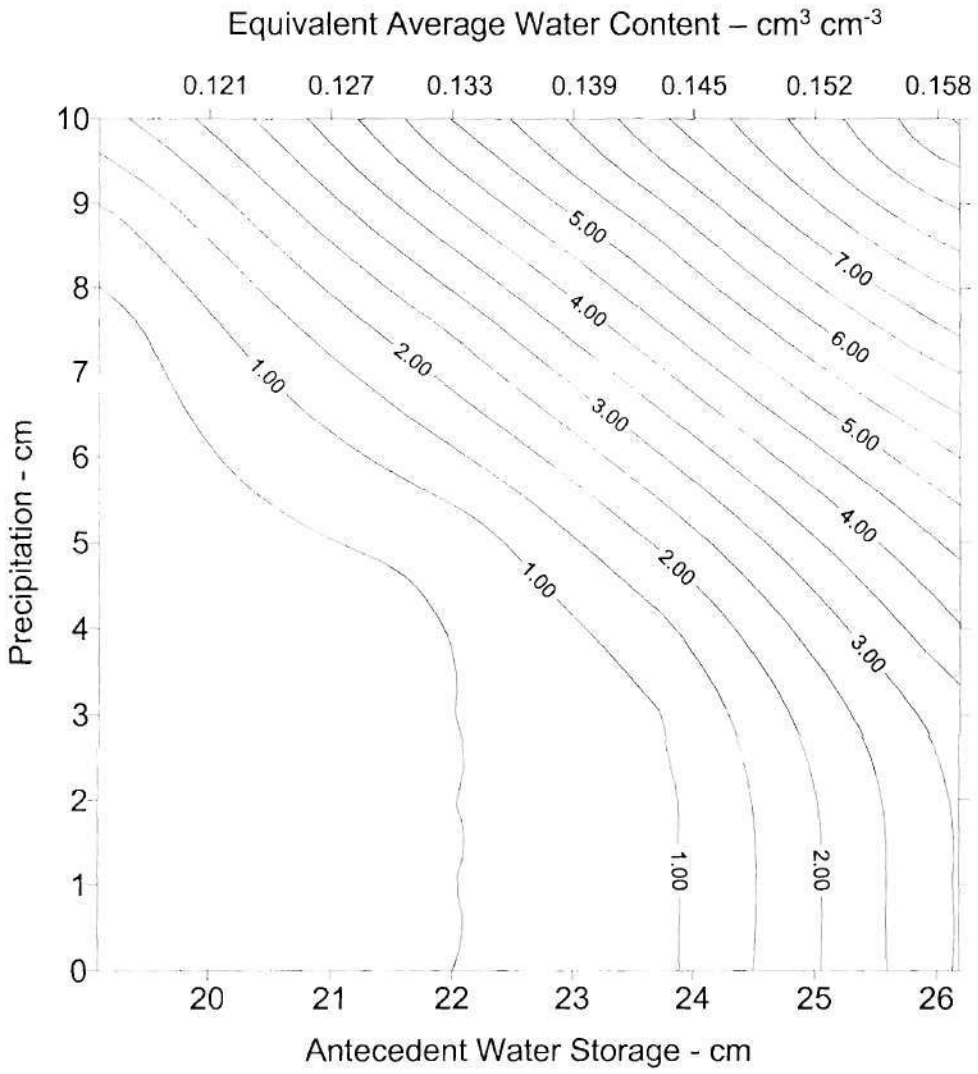

Figure 4.30 Predicted deep drainage in hypothetical silt loam – sand soil profile as functions of antecedent water storage and precipitation. Water holding capacity (26.4 cm) is second y-axis. Equivalent average water content shown at top.

CHAPTER 5
SUMMARY, CONCLUSIONS AND RECOMMENDATIONS

SUMMARY

The project is the first study to investigate the transport of a *Cryptosporidium* surrogate under field conditions. Polystyrene microspheres of similar size (4-6 μm) as *Cryptosporidium* oocysts were used to spike a defined area in a cattle grazing field site with borehole wells instrumented with zero-tension lysimeters and pressure transducers. The polystyrene microspheres were detected and counted using epiflorescence microscopy. The groundwater flow at the field site was characterized using state of the art geophysical surveys and the hydrology (rainfall, soil water, groundwater flow and evapo-transpiration) was followed for a period of approximately one year. The transport of the surrogate microspheres was followed by periodic sampling at the zero-tension lysimeters, monitoring wells and a perennial spring.

The field study was complemented by column studies in the laboratory under controlled conditions. The column studies focused on transport of surrogate microspheres through well characterized sand media and soil media from the field site. The column studies produced numerical values for parameters used for a one-dimensional transport model. The model was tested for the column configuration and the field site.

CONCLUSIONS

The major contribution and conclusions of the project are:

1. Improvements in field sampling and measurements for a surrogate used for *Cryptosporidium parvum* have been developed for field transport studies and laboratory column studies.
2. The vertical migration of polystyrene microspheres in the column studies was minimal. This suggests that migration of *Cryptosporidium parvum* oocysts through fine-textured soils is likely to be minimal.

3. Since a few microspheres were detected on a few occasions at sampling sites of the field, especially after rainfall events, the data suggests that a very small number of these surrogate particles travel through preferential flow paths at field sites.
4. The parameters measured from column studies were used as input variables in a 1-D hydrological (HYDRUS-ID) transport model, and indicated that reasonable predictions could be made on soil water content and the limited movement and depth penetration of solutes (surrogate particles) would occur based on antecedent water storage and precipitation.

RECOMMENDATIONS

Two recommendations are made

1. The single and major recommendation for further study is a validation at a field site of a watershed, whether viable or non-viable oocysts of *Cryptosporidium parvum* will be transported only through preferential flow paths.
2. Use a similar methodology combining column and field studies to validate a two (HYDRUS-2D) or three dimensional model for transport and quantitative predictions for *Cryptosporidium* transport in watersheds.

REFERENCES

Allen R.G. 1994. *Reference Evapotranspiration Calculator*. V2.15. Utah Sate University Foundation, Utah State University, Logan, UT.

Amirtharajah, A. 1988. Some Theoretical and Conceptual Views of Filtration. *Jour. AWWA*. 80(12): 36-46.

Atwill, E.R. 1996. Assessing the Link Between Rangeland Cattle and Waterborne *Cryptosporidium parvum* Infection in Humans. *Rangelands* 18:48-51.

Bruce, R.R., J.H. Dane, V.L. Quisenberry, N.L. Powell, and A.W. Thomas. 1983. *Physical Characteristics of Soils in the Southern Piedmont: Cecil*. Southern Cooperative Series Bulletin 267. USDA.

Clausnitzer, V., and J.W. Hopmans. 1995. Non-linear Parameter Estimation: LM_OPT. General-Purpose Optimization Code Base on the Levenberg-Marquardt Algorithm. Land, Air and Water Resource Paper No. 100032, University of California, Davis, CA.

Chapman, T.G. 1991 Comment on Evaluation of Automated Techniques For Base Flow and Recession Analyses, by R.J. Nathan and T.A. McMahon. *Water Resour. Res.* 27(7):1783-1784.

Driscoll, F.G. 1986. *Groundwater and Wells*. St. Paul, MN: Johnson Division.

Drozd, C. and J. Schwartzbrod. 1996. Hydrophobic and Electrostatic Cell Surface Properties of *Cryptosporidium pavum*. *Appl. and Envir. Micro.* 62: 1227-1232.

Feddes, R.A., P.J. Kowalik, and H. Zaradny. 1978. *Simulation of Field Water Use and Crop Yield*. NewYork: John Wiley and Sons.

Fisher, D.S., J.L. Steiner, D.M. Endale, J.A. Stuedemann, H.H. Schomberg, A.J. Franzluebbers, and S.R. Wilkinson. 2000. The Relationship of Land Use Practices to Surface Water Quality in the Upper Oconee Watershed of Georgia. *Forest Ecology and Management* 128:39-48.

Freeze, R.A., and J.A. Cherry. 1979. *Groundwater*. New York: Prentice-Hall.

Garrot, Jr., D.J. and C.F. Mancino. 1994. Consumptive Water Use of Three Intensively Managed Bermudagrasses Growing Under Arid Conditions. *Crop Sci.* 34:215-221.

Gilbert, R.O. 1987. *Statistical Methods for Environmental Pollution Monitoring*. New York: Van Nostrand Reinhold Co.

Hancock, C.M., J.B. Rose, M. Callahan. 1997. The Prevalence of *Cryptosporidium* and *Giardia* in U.S. Groundwaters. Int'l Symposium on Waterborne *Cryptosporidium*, Newport Beach, CA.

Harter, T., S. Wagner, and E.R. Atwill. 2000. Colloid Transport and Filtration of *Cryptosporidium parvum* in Sandy Soils and Aquifer Sediments. *Environ. Sci. Technol.* 34:62-70.

Harvey, R.W. and S.P. Garabedian. 1991. Use of Colloid Filtration Theory in Modeling Movement of Bacteria Through a Contaminated Sandy Aquifer. *Environ. Sci. and Technol.* 25:178-185.

Hayes, E.B., T.D. Matte, T.R. O'Brien, T.W. McKinley, G.S. Logsdon, J.B. Rose, B.L. Ungar, D.M. Word, P.F. Pinksy, M.L. Cummings, M.A. Wilson, E.G. Long, E.S. Hurwitz, D.D. Horowitz, A.J. K.A. Elrick, and R.C. Hooper. 1989a. A Comparison of Instrumental Dewatering Methods for the Separation and Concentration of Suspended Sediment for Subsequent Trace Element Analysis. *Hydrol. Proc.* 2:163-184.

Hayes, E.B., Matte, T.D., O'Brien, T.R., McKinley, T.W., Logsdon, G.S., Rose, J.B., Ungar, B.L.P., Word, D., M., Pinsky, P.F., Cummings, M.L., Wilson, M.A., Long, E. G., Hurwitz, E.S., Juranek, D.D. 1989b. Large Community Outbreak of *Cryptosporidiosis* Due to Contamination of a Filtered Public Water Supply. *N. Eng. J. Med.* 320: 1372-1376.

Jacobsen, O.H., P Moldrup, C. Larson, L. Konnerup, and L.W. Peterson. 1997. Particle Transport in Macropores of Undisturbed Soil Columns. *J. Hydrology.* 196(1-4):185-203.

Jewett, D.G., T.A. Hilbert, B.E. Logan, R.G. Arnold, R. Bales. 1995. Bacterial Transport in Laboratory Columns and Filters: Influence of Ionic Strength and pH on Collision Efficiency. *Water Res.* 29 (7): 1673-1680.

Johnson, W.P., K. Blue, B.E. Logan, and R.G. Arnold. 1995. Modeling Bacterial Detachment During Transport Through Porous Media as a Residence-Time-Dependent Process. *Water Res.* (11): 2649-2658.

Jury, W.A., W.R. Gardner, W.H. Gardner. 1991. *Soil Physics.* 5th Edition. New York: John Wiley and Sons.

LeChevallier, M.W. W.D. Norton, and R.G. Lee. 1991. Occurrence Of *Giardia* And *Cryptosporidium* In Surface Water Supplies. *Appl. Environ. Microbiol.* 57:2610-2616.

Lengerich, E.J., D.G. Addiss, J.J. Marx, B.L.P. Ungar, and D.D. Juranek. 1993. Increased Exposure To *Cryptosporidia* Among Farmers In Wisconsin. *J. Inf. Dis.* 167:1252-1255.

Li, S.Y., J.A. Goodrich, J.H. Owens, G.E. Willeke, F.W. Schaefer, and R.M. Clark. 1997. Reliability Of Surrogates For Determining *Cryptosporidium* Removal. *Jour. AWWA.* 89(5):90-99.

Lyne, V., and M. Hollick. 1979. Stochastic Time-Variable Rainfall-Runoff Modeling. I.E. Aust. Natl. Conf. Publ. 19/10 Inst. of Eng. Aust. pp. 89-93.

MacKenzie, W.R., N.J. Hoxie, M.E. Proctor, M.S. Gradus, K.A. Blair, D.E. Peterson, J.J. Kazmierczak, D.G. Addiss, K.R. Fox, J.B. Rose, and J.P. Davis. 1994. A Massive Outbreak In Milwaukee Of *Cryptosporidium* Infection Transmitted Through The Public Water Supply. *New Engl. J. Med.* 331:161-167.

Madore, M.S., J.B. Rose, C.P. Gerba, M.J. Arrowood, and C.R. Sterling. 1987. Occurrence Of *Cryptosporidium* Oocysts In Sewage Effluents And Selected Surface Waters. *J. Parasit.* 73:702-706.

Marquardt, D.W. 1963. An Algorithm For Least-Squares Estimation Of Nonlinear Parameters. SIAM. *J. Appl. Math.* 11:431-441.

Mau, D.P., and T.C. Winter. 1997. Estimating Ground-Water Recharge From Streamflow Hydrographs For A Small Mountain Watershed In A Temperate Humid Climate, New Hampshire, USA. *Groundwater.* 35:291-304.

McBean, E.A., F.A Rovers. 1998. *Statistical Procedures For Analysis Of Environmental Monitoring Data & Risk Assessment.* Prentice-Hall. Upper Saddle River, NJ: Prentice Hall.

McCuen, R.H. 1993. *Statistical Hydrology.* Englewood Cliffs, New Jersey, PTR-Prentice Hall.

McNeill, J.D. 1980. Electromagnetic Terrain Conductivity Measurements At Low Induction Numbers. Technical Note TN-6: Geonics Ltd., Mississauga, Ontario, Canada. 15 p.

McNeill, J.D. 1992. Rapid, Accurate Mapping Of Soil Salinity By Electromagnetic Ground Conductivity Meters. In *Advances in measurement of soil physical properties: Bringing theory into practice.* SSSA Special Publication No. 30. Soil Sci. Soc. Am., Madison, WI.

Miron et al., 1991. Calves As A Source Of An Outbreak Of *Cryptosporidium* Among Young Children In An Agricultural Closed Community. *Ped. Inf. Dis. Jour.*, 10:438-441.

Mualem, Y. 1976. A New Model For Predicting The Hydraulic Conductivity Of Unsaturated Porous Media. *Water Resour. Res.* 12:513-522.

Nathan, R.J., and T.A. McMahon. 1990. Evaluation Of Automated Techniques For Base Flow And Recession Analyses. *Water Resour. Res.* 26:1465-1473.

Ongerth, J.E., and J.P. Pecoraro. 1996. Electrophoretic Mobility Of *Cryptosporidium* Oocysts And *Giardia* Cysts. *Jour. Environ. Engr.* 122:228-231.

Pontius, F.W. 2001. Regulatory Update for 2001 and Beyond. *Jour. AWWA.* 93(2):66-80.

Powelson, D.K. and C.P. Gerba. 1995. Fate and Transport of Microorganisms in the Vadose Zone. In *Handbook of Vadose Zone Characterization and Monitoring.* Edited by L.G. Wilson, L.G. Everett, S.J. Cullen. Boca Raton, Fla.: Lewis Publishers.

Rajagopalan, R., and C. Tien. 1976, Trajectory Analysis of Deep-Bed Filtration With Sphere-in-a-cell Porous Media Model. *AIChE Jour.* 22(3): 523-533.

Rose, J.B. 1988. Occurrence And Significance Of *Cryptosporidium* In Water. *Jour. AWWA.* 80(2):53-58.

Schaap, M.G., and W. Bouten. 1996. Modeling Water Retention Curves Of Sandy Soils Using Neural Networks. *Water Resour. Res.* 32:3033-3040.

Schaap, M.G., F.J. Leij, and M.Th. van Genuchten 1998. Neural Network Analysis For Hierarchical Prediction Of Soil Water Retention And Saturated Hydraulic Conductivity. *Soil Sci. Soc. Am. Jour.* 62:847-855.

Sheets, K.R, and J.M.H. Hendrickx. 1995. Noninvasive Soil-Water Content Measurement Using Electromagnetic Induction. *Water Resour. Res.* 31:2401-2409.

Šimůnek, J., K. Huang, M. Šejna, and M. Th. van Genuchten. 1998. The HYDRUS-1D Software Package For Simulating The One-Dimensional Movement Of Water, Heat, And Multiple Solutes In Variably- Saturated Media. Version 1.0. IGWMC - TPS - 70, International Ground Water Modeling Center, Colorado School of Mines, Golden, Colorado, 162pp.

Šimůnek, J., M. Šejna, and M. Th. van Genuchten. 1999. HYDRUS-2D/MESHGEN-2D Software For Simulating Water Flow And Solute Transport In Two-Dimensional Variably Saturated Media. Version 2.0. IGWMC - TPS – 53C, International Ground Water Modeling Center, Colorado School of Mines, Golden, Colorado, 227pp.

Stanridge, J. 1999. Personal Communication.

Thompson, M. L., and R. L. Scharf. 1994. An Improved Zero-Tension Lysimeter To Monitor Colloid Transport In Soils. *Jour. Environ. Qual.* 23:378-83.

Toride, N., F.J. Leij, and M.Th. van Genuchten. 1995. The CXTFIT Code for Estimating Transport Parameters from Laboratory or Field Tracer Experiments, Version 2.0. Research Report No. 137, U.S. Salinity Laboratory, Agricultural Research Service, USDA, Riverside, CA. pp. 121.

U.S. Department of Agriculture. 1979. *Field Manual for Research in Agricultural Hydrology. Agricultural Handbook 224*. Washington, D.C.

U.S. Environmental Protection Agency. 1986. *RCRA Ground-water Monitoring*, Technical Enforcement Guidance Document. OSWER-9950.1.

van Genuchten, M.Th. 1980. A Closed-Form Equation For Predicting The Hydraulic Conductivity Of Unsaturated Soils. *Soil Sci. Soc. Am. Jour.* 44:892-898.

van Genuchten, M. Th., F. J. Leij, and S. R. Yates. 1991. The RETC Code For Quantifying The Hydraulic Functions Of Unsaturated Soils, Version 1.0. EPA Report 600/2-91/065, U.S. Salinity Laboratory, USDA, ARS, Riverside, California.

Vogel, T. 1987. SWMII – *Numerical model of two-dimensional flow in a variably saturated porous medium*, Research Rep. No. 87, Dept. Hydraulics and Catchment Hydrology, *Agric.* University, Wageningen, The Netherlands.

Page intentionally left blank

ABBREVIATIONS

A	filter area
ARS	Agricultural Research Service
As	Happel's flow field factor
a	the area of each subarea
b(z)	normalized water uptake function at depth, z
C	measured solute concentration (mg/L)
C_0	influent solute concentration (mg/L)
C*	the relative solute concentration (mg/L)
c	aqueous (liquid) phase solute concentration (M/L^3)
D_H	the hydrodynamic dispersion coefficient (cm^2/hr)
D_k	dispersion coefficient for the liquid phase (L/t)
d_c	mean grain size
ESWTR	Enhanced Surface Water Treatment Rule
ET	evapotranspiration
FTC	flow-through centrifuge
f	the fraction of solid phase in contact with the mobile water
f_k	the interflow response at time, k
GPR	ground penetrating radar
GT	Georgia Tech
GW	groundwater
ΔGWS	change in ground water storage
H	total head (L)

IF	interflow, or shallow subsurface water flow
i	an iteration counter
i subscripts	depth
j subscripts	location
K	the hydraulic conductivity (L/t)
K_D	the linear distribution coefficient (mL/g)
K_d	linear distribution or partition coefficient (L^3/M)
K_{ij}^A	components of a dimensionless anisotropy tensor
K_s	saturated hydraulic conductivity (L/t)
k	chemical species being modeled
L	the column length (cm)
L_z	rooting depth of the plants
m_q	number of different sets of measurements
N	the total number of microspheres
N_G	gravitational number (settling velocity/pore water velocity)
N_{Lo}	London—van der Waals constant
N_R	size group (particle diameter/mean particle diameter)
n	pore size distribution parameter
n_{qj}	number of measurements in a particular measurement set
P	precipitation
Pe	the Peclet number
P_i	precipitation that varies from 0 to 15 cm/d
pv	dimensionless pore volumes

q	Darcy velocity (L/t)
$q_j^*(z,t_i)$	specific measurements at time t_i for the jth measurement set at location $z(z,t_i)$
$q_j(z,t_i,b)$	corresponding model predictions for the vector of optimized parameters
R_F	the retardation factor
R_m	the retardation factor for the mobile water
RMSE	root mean square error
R_T	the total (equilibrium) retardation factor
r subscripts	residual volumetric water contents
S	sink term that represents water loss through plant root uptake (L^3/L^3t)
SAR	sodium adsorption ratio
SRI and SRO	surface runon and runoff, respectively (both assumed zero)
ΔSWS	change in soil water storage
s	sorbed (solid) phase solute concentration (M/M)
S_p	potential water uptake rate [1/T]
T_p	potential transpiration rate [L/T]
t	time (t)
VES	vertical electrical sounding
v_j and $w_{i,j}$	weights associated with a particular measurement set or point, respectively
v	the pore water velocity
w and *s*	subscripts corresponding to the aqueous (water) phase and the solid phase concentration, respectively
X	dimensionless distance
x	distance along the column (cm)

x_i	spatial coordinates (i=1,2)
y	the total springflow
ZTL	zero-tension lysimeter
z	depth of measurement
α	filter parameter that controls attenuation of the signal
α_e	empirical constant called the collision efficiency
α_l	the longitudinal dispersivity (L) ($\alpha_l = D_k/v_z$)
α_m	the solute mass transfer coefficient between mobile and immobile water (1/hr)
Φ_m	the ratio of mobile water to immobile water
Θ	relative volumetric water saturation
θ	volumetric water content (cm^3/cm^3)
θ_m	volumetric content of mobile water (cm^3/cm^3)
λ	filter coefficient
η	single collector efficiency
σ	apparent electrical conductivity (ECa)
ρ_b	soil bulk density (M/L^3)
ρ_s	soil particle density (M/L^3 assumed at 2.65 g/cm^3)
ψ	soil water potential (L)
$\psi_i(z)$	initial soil water potential